Characterizing Large Storage Systems: Error Behavior and Performance Benchmar ks

by

Nisha Darshi Talagala

B.S. (Wayne State University) 1991
M.S. (Wayne State University) 1992

A dissertation submitted in partial satisfaction of the

requirements for the degree of

Doctor of Philosophy
in

Computer Science

in the

GRADUATE DIVISION

of the

UNIVERSITY OF CALIFORNIA, BERKELEY

Committee in Charge:

Professor David Patterson, Chair
Professor Randy Katz
Professor George Shanthikumar

Fall 1999

Report Documentation Page

Form Approved
OMB No. 0704-0188

1. REPORT DATE	2. REPORT TYPE	3. DATES COVERED
1999		**00-00-1999 to 00-00-1999**

4. TITLE AND SUBTITLE	5a. CONTRACT NUMBER
Characterizing Large Storage Systems: Error Behavior and Performance Benchmarks	5b. GRANT NUMBER
	5c. PROGRAM ELEMENT NUMBER
6. AUTHOR(S)	5d. PROJECT NUMBER
	5e. TASK NUMBER
	5f. WORK UNIT NUMBER
7. PERFORMING ORGANIZATION NAME(S) AND ADDRESS(ES) **University of California at Berkeley,Department of Electrical Engineering and Computer Sciences,Berkeley,CA,94720**	8. PERFORMING ORGANIZATION REPORT NUMBER
9. SPONSORING/MONITORING AGENCY NAME(S) AND ADDRESS(ES)	10. SPONSOR/MONITOR'S ACRONYM(S)
	11. SPONSOR/MONITOR'S REPORT NUMBER(S)

12. DISTRIBUTION/AVAILABILITY STATEMENT
Approved for public release; distribution unlimited

13. SUPPLEMENTARY NOTES

14. ABSTRACT

This dissertation characterizes two causes of variability in a large storage system: soft error behavior and disk drive heterogeneity. The first half of the dissertation focuses on understanding the error behavior and component failure characteristics of a storage prototype. The prototype is a loosely coupled collection of Pentium machines; each machine acts as a storage node, hosting disk drives via the SCSI interface. Examination of long term system log data from this prototype reveals several interesting insights. In particular, the study reveals that data disk drives are among the most reliable components in the storage system and that soft errors tend to fall into a small number of well defined categories. An in-depth study of hard failures reveals data to support the notion that failing devices exhibit warning signs and investigates the effectiveness of failure prediction. The second half of the dissertation, dealing with disk drive heterogeneity, focuses on a new measurement technique to characterize disk drives. The technique, linearly increasing strides, counteracts the rotational effect that makes disk drives difficult to measure. The linearly increasing stride pattern interacts with the drive mechanism to create a latency vs. stride size graph that exposes many low level disk details. This micro-benchmark extracts a drive's minimum time to access media, rotation time, sectors/track, head switch time, cylinder switch time, number of platters, as well as several other pieces of information. The dissertation describes the read and write versions of this micro-benchmark, named Skippy, as well as analytical models explaining its behavior, results on modern SCSI and IDE disk drives, techniques for automatically extracting parameter values from the graphical output, and extensions.

15. SUBJECT TERMS

16. SECURITY CLASSIFICATION OF:			17. LIMITATION OF ABSTRACT	18. NUMBER OF PAGES	19a. NAME OF RESPONSIBLE PERSON
a. REPORT **unclassified**	b. ABSTRACT **unclassified**	c. THIS PAGE **unclassified**	**Same as Report (SAR)**	**174**	

Standard Form 298 (Rev. 8-98)
Prescribed by ANSI Std Z39-18

Abstract

Characterizing Large Storage Systems: Error Behavior and Performance Benchmarks

by

Nisha Darshi Talagala

Doctor of Philosophy in Computer Science

University of California, Berkeley

Professor David Patterson, Chair

This dissertation characterizes two causes of variability in a large storage system: soft error behavior and disk drive heterogeneity. The first half of the dissertation focuses on understanding the error behavior and component failure characteristics of a storage prototype. The prototype is a loosely coupled collection of Pentium machines; each machine acts as a storage node, hosting disk drives via the SCSI interface. Examination of long term system log data from this prototype reveals several interesting insights. In particular, the study reveals that data disk drives are among the most reliable components in the storage system and that soft errors tend to fall into a small number of well defined categories. An in-depth study of hard failures reveals data to support the notion that failing devices exhibit warning signs and investigates the effectiveness of failure prediction.

The second half of the dissertation, dealing with disk drive heterogeneity, focuses on a new measurement technique to characterize disk drives. The technique, linearly increasing

strides, counteracts the rotational effect that makes disk drives difficult to measure. The linearly increasing stride pattern interacts with the drive mechanism to create a latency vs. stride size graph that exposes many low level disk details. This micro-benchmark extracts a drive's minimum time to access media, rotation time, sectors/track, head switch time, cylinder switch time, number of platters, as well as several other pieces of information. The dissertation describes the read and write versions of this micro-benchmark, named Skippy, as well as analytical models explaining its behavior, results on modern SCSI and IDE disk drives, techniques for automatically extracting parameter values from the graphical output, and extensions.

Professor David Patterson
Dissertation Chair

DEDICATION

To my parents, Rohana and Punya

TABLE OF CONTENTS

LIST OF TABLES

LIST OF FIGURES

ACKNOWLEDGEMENTS

Many people have helped and guided me through my time at Berkeley. The foremost of these people is my advisor David Patterson. I am extremely lucky to have been able to work with him. Dave helped me focus the direction of my research, while allowing me the freedom to pursue my interests. His advising has been a great combination of technical guidance, encouragement, and general good advice on all professional matters.

I would also like to thank my other readers, Randy Katz and George Shanthikumar, for their advice during both my qualifying exam and dissertation. Randy Katz has always been an inspiring influence, and has given me very good advice whenever I have interacted with him. I was also fortunate to take a great course in Stochastic Processes from George Shanthikumar.

I also owe thanks to Terry Lessard-Smith, Bob Miller, and Kathryn Crabtree, who have saved me on many occasions in everything from registration matters to equipment.

Many thanks also to my fellow office mates in 477 Soda Hall, Remzi Arpaci-Dusseau and Satoshi Asami. I have learned a great deal through working with each of them, and I'd like to thank them for insightful comments, many fun discussions, and in all a friendly, and memorable office environment. Thanks also to my other friends, in particular, Sumudi, Rachel, and Manosha, who have been there for me throughout.

My husband, Amit, has been an essential background figure in this dissertation. In addition to giving me technical feedback and advice, he has been incredibly patient and given me much emotional support and encouragement throughout my final years at Berkeley.

I owe a great debt to my parents. They instilled in me the importance of learning; they have devoted their energy and made numerous personal sacrifices to enable me to study in the United States. This dissertation would not have been possible without them.

This research was funded by DARPA Grant N00600-93-K-2481, donations of equipment from IBM and Intel, and the California State Micro Program.

1 Chapter 1: Introduction

The past decade has seen several fundamental changes in the field of I/O and storage systems. One of these changes was the invention of Redundant Arrays of Inexpensive Disks (RAID) in 1988. The RAID work fueled a new class of disk-based storage systems containing multiple disk drives with built in data redundancy. These innovations made it possible to construct large, multiple disk storage systems to serve I/O limited applications such as video service. In 1999, eleven years later, RAID is a ten billion dollar industry, with more than 50 companies making RAID-based subsystems. Storage systems research during this time has also developed ways to improve the performance of RAID arrays, as well as storage system designs for improving reliability.

However, modern applications, especially those derived from the web, require storage infrastructures that are much larger than a simple disk-tape hierarchy containing a single RAID system backed up by a single tape robot. Although stand-alone storage systems range in capacity from hundreds of gigabytes to a few terabytes, large commercial installations contain terabytes to petabytes of data. This data is contained many storage arrays on different hosts, many interconnected via switched networks. One of the largest unsolved

problems for such installations is not simply performance or reliability, but *manageability*. Studies show that management of storage costs between twice to twelve times the cost of the storage itself. Although management has traditionally been the task of system administrators, modern storage installations, with storage in thousands of disk drives, are far too complex for human management.

Automated storage management is a large umbrella, covering everything from maintenance, error reporting and diagnostics, to performance tuning. Solving these problems requires that the storage system be *adaptive*, reacting correctly to the widely varying states that the system will experience during its lifetime. A large part of an adaptive solution is understanding and reacting to storage system *variability*. Even with a fixed architecture and configuration, a storage system experiences considerable variability during its lifetime. This variability can result from a number of factors, including failures, component and software upgrades, and so on.

1.1. Thesis Goal

The goal of this thesis is to assist the development of automated storage management by characterizing storage system variability. In particular, the study focuses on two factors that contribute to storage system variability, unexpected errors and heterogeneity in disk drives.

(i) Error Behavior: Although much work has been done on designing storage systems to tolerate failures of any component and combinations of components, not much work has

been done to characterize error behavior. Failures, however, are not binary events. Storage systems exhibit a range of soft and hard errors, some leading to failure and some not. These errors constantly change the state of the system, affecting both its performance and availability.

(ii) Disk Heterogeneity: Although a large system may be shipped with identical disk drives, the disks in the infrastructure become more and more heterogeneous over time. There are several reasons for this. First, as drives fail, they will be replaced by newer drives that are considerably different. Second, the drive market evolves fast; a new disk appears every nine to twelve months. Third, even if the drive mechanics remain unchanged, firmware revisions appear every three to six months. Finally, a large installation is constantly incrementing its storage by adding new subsystems. As a result, at any time, the installation will contain many generations of disk drives, often from different manufacturers, and hence will result in a heterogeneous system with disks of varying capacity and performance.

1.2. Thesis Outline

This thesis characterizes the above two causes of storage system variability in the following ways.

1.2.1. Characterizing Error Behavior

The first half of the thesis, chapters 2 through 4, deals with error behavior in a large storage system. A terabyte capacity storage system prototype is described; the prototype contains

disks and supporting hardware such as SCSI controllers, network controllers and so forth. The soft error and failure behavior of this prototype are then characterized, using system logs and maintenance records gathered over six months of operation. The results reveal the common types of errors that occur, the correlations between errors, and their effects on the operating system and applications. The study also examines the events leading up to component failure, as well as the distinction between transient errors and errors leading to failure.

Chapter 2 describes the storage system architecture used in this study. The prototype, built by the Tertiary Disk group of the Network of Workstations (NOW) project, is a 3.2 TB system built from commodity hardware. The prototype contains 396 disks hosted by 20 PC and interconnected by a switched ethernet network. The application for this storage system is a web server for high resolution art images. The collection, by far the largest in the world, contains over 80,000 images and is available to users 24 hours a day, 7 days a week at *http://www.thinker.org/*.

Chapter 3 describes the soft error behavior of the prototype. Six months of system logs from the nodes of the prototype are analyzed to determine the types of errors that occur. The analysis reveals some interesting insights. The data disks drives were among the most reliable components in the system. Even though they were the most numerous component, they experienced the lowest failure rate. Also, the study finds that all the errors observed in six months can divided into eleven categories, comprising disk errors, network errors and SCSI errors. The data supports the notion that disk and SCSI failures are predictable, and suggests that partially failed SCSI devices can severely degrade performance.

Chapter 4 deals with failures in more detail. The chapter examines failure cases of disk drives and SCSI hardware. Each case shows a noticeable increase in error messages before replacement. The chapter also evaluates the effectiveness of a failure detection algorithm developed by other researchers. The evaluation reveals that the algorithm tend to be over-zealous, often reporting failures where none exist: transient errors can be labeled as failures by such an algorithm. However, the type of message can be used to detect which events are actually hardware failures and which are not.

1.2.2. Characterizing Disk Drives

The second half of the dissertation, chapters 5 through 7, presents a novel method for extracting critical parameters from modern disk drives. The technique uses small disk accesses, arranged in linearly increasing strides. The linearly increasing stride pattern interacts with the disk mechanism in such a way that the resulting latency vs. stride size graph explicitly illustrates many disk parameters. This micro-benchmark extracts a drive's minimum time to access media, rotational latency, sectors/track, head switch time, cylinder switch time, and the number of platters.

Chapter 5 describes the write and read versions of the basic linear stride micro-benchmark, named *Skippy*. The expected behavior of each version of the benchmark is described using an analytical model. The analytical model verifies the technique and illustrates how drive parameters can be extracted from the result graph. Measured results are presented on a series of modern SCSI and IDE disk drives. The results show that the write version of the benchmark is effective in extracting all the expected parameters, in all cases to within 3%

of values gathered from manufacturer specifications. The read version extracts the same parameters with similar accuracy, and also provides some insight into how the drive handles read ahead.

Chapter 6 describes an technique for automatically extracting the required parameters from the result graph. This method is useful since it makes it possible for a higher level software infrastructure, such as an adaptive storage system, to make use of the *Skippy* extraction technique. The chapter describes the automated extraction tool and tests it on the results from chapter 5. In most cases, the automatically extracted values are within 10% of their manually extracted counterparts.

Chapter 7 presents extensions to the basic *Skippy* technique. Two additional algorithms, *Zoned* and *Seeker* are presented. *Zoned* uses a bandwidth measurement to capture details of the drive's recording zones. *Seeker* shows how the linear stride technique can be used to measure seek times. In addition, the chapter also presents how *Skippy* can be extended by changing the transfer size and the stride size increment. With a larger transfer size, *Skippy* can be used to measure the drive's transfer rate. With larger stride size increments, the same parameters can be extracted with fewer strides and in less time. Finally, the chapter presents a read backwards stride micro-benchmark that retains the advantages of reads without encountering read ahead effects.

1.3. Thesis Contributions

This dissertation makes the following contributions:

(i) Presents the first public, in-depth, analysis of soft error data from a terabyte-sized storage system. The insights provided by this analysis are useful for any designer of a reliable storage system.

(ii) Presents an in depth look at how devices fail. This type of data, again, is very hard to come by, and is useful in the design of reliable storage systems. Evaluates the effectiveness of failure prediction algorithms on large scale storage systems.

(iii) Presents a novel technique for extracting low level disk drive parameters using a simple measurement that requires no a prior knowledge of the disk drive being measured. This technique is also a good match to the rotational nature of the disk, a feature that makes many other micro-benchmarks unsuitable for disk drives.

(iv) Presents extracted parameter values and performance data for a range of modern SCSI and IDE disk drives. This data, and the measurement technique that generated it, and the way the data is presented, are useful to the research community for parametrizing simulators and understanding modern disk drives from a new perspective.

2 The Storage System

2.1. Introduction

This chapter describes the storage system prototype used in this thesis. The prototype, built by the Tertiary Disk group of the Network of Workstations (NOW) project, is a 3.2 TB system built from commodity hardware. The prototype contains 368 disks hosted by 20 PCs that are interconnected by a switched ethernet network. The main application for this system is a web server for high resolution art images. The collection, by far the largest in the world, contains over 80,000 images and is available to users 24 hours a day, 7 days a week at *http://www.thinker.org/*.

Commodity storage systems, like the TD prototype, have several advantages over custom designed disk arrays. For one thing, the cost/megabyte of disk arrays increases with capacity and, in most cases, is higher than the cost/megabyte of the underlying disks. Disk array costs are high because they contain custom designed hardware. In 1999, disks cost as little as 5 cents per megabyte, close to the cost of tape libraries [Grochowski96, IDEMA97]. Although disk prices are falling by 50% every year, the cost/megabyte of disk arrays is not falling as quickly. Secondly, performance of disk arrays is limited by the bandwidth of the link to the host machine. Finally, incremental expansion in a disk array is possible only

until all available disk slots are filled. For these reasons, a commodity storage system made up of relatively independent nodes is a plausible alternative to custom designed disk array. The node-based design makes adding disks and nodes easier. The cost/megabyte of the system stays relatively constant even as the capacity grows. The nodes also provide multiple connections to the outside world, improving performance and availability. The prototype proves by example that storage systems using commodity hardware can be built for a small extra cost over the underlying disks and provides a basis for the studies on error behavior that make up the first part of the thesis.

This chapter covers the prototype's architecture and application. This information is useful as perspective for the chapters that follow. Section 2.2 describes the prototype hardware in detail. The next section covers the hardware configuration, designs of nodes, interconnections and power scheme. Section 2.4 describes the application, including data layout and user activity. Finally section 2.5 concludes with a summary.

2.2. Prototype Hardware

Table 2-1 describes the components used in the prototype. All components are the state of the art as of 1996, when work on the prototype first began. The twenty PCs that host the storage are interconnected using a switched Ethernet network. In addition, there is a separate serial network that is use for management, connecting PCs, disk enclosures and UPS units. Each PC has four PCI expansion slots on the motherboard (most PCs available at the time of this writing contain three or four PC expansion slots). The PCI slots contain two

twin-channel Fast-Wide SCSI adapters and an Ethernet card. Power and cooling for the disks is provided by disk enclosures. All the enclosures, host machines, and network components are housed in a series of racks. Power to the system is supplied through Uninterruptible Power Supply (UPS) units.

Component type	Number Used in Prototype	Description
Host machines	20	Pentium Pro 200 MHz, 96 MB main memory, 1 GB SCSI hard drive, PCI bus, 4 PCI expansion slots, 3 ISA slots.
SCSI Disks	368	IBM Ultrastar XP, 8 GB, 7200 RPM, SCSI
IDE Disks	20	Seagate ST32140A 2GB 5400RPM IDE
SCSI Controllers	40	Adaptec 3940 Twin Channel UW SCSI
Disk Enclosures	48	Sigma Trimm Model SA-H381, Dual power supplies. Each enclosure holds 7-8 disks.
Uninteruptible Power Supplies	6	Powerware Prestige 6000 Units
Ethernet Controller	20	3Com Fast Etherlink PCI 10/100 BASE-T Adapters
Ethernet Hub	2	
Serial Port Hub	2	Bay Networks 5000 Hub
Other equipment	-	Miscellaneous Cables (SCSI, Ethernet, Serial), SCSI Terminators

Table 2-1. Components Used in Storage Prototype

The main components are the disks, SCSI controllers, host machines, disk enclosures, network hardware and uninteruptible power supplies. This table gives the model numbers and other information for each main components.

The Pentium Pro machines were chosen over other alternatives (such as SPARCStation-5s and UltraSPARCs) because PCs are naturally well equipped for hosting disks. The main system bus, PCI, has a peak bandwidth of 132 MB/s, compared to 90 MB/s for the Sbus, which was the main alternative available at the time. PCs also have more expansion slots than either the SPARCStation 5 or the UltraSPARC: three or four compared to two in each

of the alternative machines. In addition, PCs were the most cost effective of the three choices. The PC model used in the prototype was not preferred over the other PC models for any reason. They were used because they were part of a donation by Intel.

Fast-Wide SCSI was chosen because it was the highest performance disk interconnect available at the time. Serial interconnects with higher bandwidth, 40-100MB/s compared to 20 MB/s for SCSI, had been introduced. However, disks and controllers using these interfaces were not yet widely available. Twin-channel SCSI adapters were used because each PC could host more SCSI strings with twin channel adapters than with single channel adapters; each PCI expansion slot can host two SCSI strings instead of one. Performance measurements comparing single and twin channel SCSI controllers revealed no noticeable performance losses when using twin channel controllers.

Power and cooling for the disks is provided by the disk enclosures. Each enclosure hosts up to seven disks. All enclosures are connected through a serial port hub. This way, any enclosure can be accessed remotely, and the status of all enclosures can be monitored from a remote location. The serial port interface supports a small set of commands; Table 2-2 lists the commands supported by our enclosures. The commands return the status of the enclosure (power supplies, disks an so on) and control the LEDs above each disk slot. When a disk needs to be replaced, the enclosure can be programmed to turn the LED above the failed disk to red, making it easier for the disk to be identified. The enclosures are the only components that are not strictly commodity. The serial port interface and other features, like dual power supplies, were included because they make maintenance and monitoring easier. The additional features make the enclosures a special order item, and not

Command Name	Command Description	Command Characters	Result/Return
Hello	Start of communications	Ctrl-A	Acknowledgment by chassis
Inquiry	Request for identification	Ctrl-E	Acknowledgment followed by the enclosure model number and firmware revision.
Status	Request for status	S	Acknowledgment followed by 8 data bytes of status information
Change Drive LEDs	Change the status of an LED to indicate failed drives	D, 1 data byte	Acknowledgment from chassis, the LED of the specified drive is changed in color (red to green or vice versa)
I/O control	Control the mute-button capture latch (can be used to detect when an operator is standing by)	I, 1 data byte	Acknowledgment from chassis
SCSI Bus Reset	Assert/Release the SCSI bus reset line	R, 1 data byte	Acknowledgment from chassis; the requested reset/release action takes place
N/A	Misunderstood character sequences	All other character combinations	Negative acknowledgment from chassis

Table 2-2. Disk Enclosure Commands

These commands are used to communicate with the disk enclosure over a serial port. More details are available in [Sigma97]; the encoding of the status bytes and the data bytes is described there. The mute button is a special button on the enclosure that stops the alarm from sounding. The mute button capture latch catches all mute button presses and is used to detect an operator standing by an enclosure.

strictly commodity. However, standard disk enclosure models are also available by companies like Sigma/Trimm.

The Uninteruptible Power Supplies provide 10 minutes of backup power to the nodes. This feature is useful both for surviving short power glitches and for allowing time for safe shutdown on power failure. The UPS units also provide a serial interface that can be polled to detect power failure events.

2.3. Hardware Configuration

This section describes the hardware configuration of the storage system, beginning with a description of the storage node architecture and ending with a discussion of the interconnection and power schemes.

2.3.1. Node Design

The prototype has two types of nodes, which from now on will be called *light* nodes and *heavy* nodes. The prototype has sixteen light nodes and four heavy nodes. Each light node contains 16 disks on 2 SCSI strings while each heavy node has 28 disks on 2 SCSI strings. There are cost and performance trade-offs in changing the disks/host ratio, as well as additional problems with large numbers of disks. The light nodes have a higher cost and better performance than the heavy nodes. As the disks/host ratio is increased, the cost/megabyte of the node becomes closer to the cost/megabyte of the disks, making the heavy nodes more cost-effective.

Figure 2-1 shows the internal hardware architecture of a storage node. For clarity, the figure shows only one SCSI string. In the heavy nodes, the 14 disks on each string are housed in two disk enclosures of 7 disks each; in the light nodes, each SCSI string has 8 disks housed in a single enclosure. Disks plug directly into the enclosure's backplane, which contains the SCSI bus, a design that reduces the SCSI cable length within the disk enclosure. The SCSI bus is made up of the SCSI cable, starting at the SCSI controller and ending as the enclosure backplane. Each enclosure is powered by two power supplies and cooled with a single fan. Each machine also contains a single Ethernet card and a cable

connecting the machine to the switched network. Inside the host PC is a 2GB internal IDE disk.

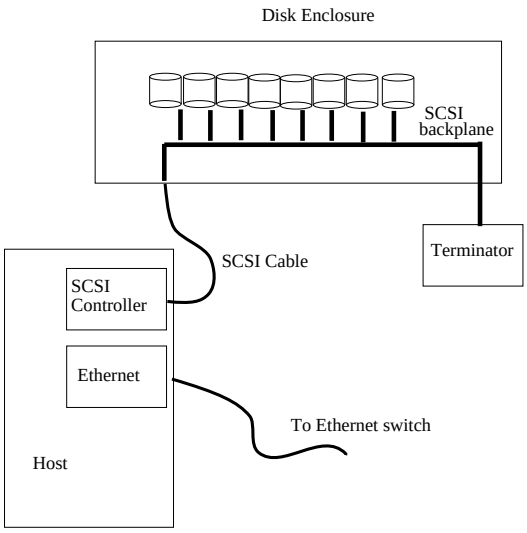

Figure 2-1. Storage Node Architecture

For the sake of clarity, the figure only shows one SCSI string. The SCSI bus is made up of two parts: a cable between the controller and the disk enclosure, and the enclosure's back-plane. The disk canisters plug directly into this backplane.

2.3.1.1. Performance Trade-offs of Varying the Disks/Host Ratio

Figure 2-2 illustrates the performance of different disks/host ratios. The figure show the read bandwidth possible through the raw disk interface and the throughput for 8KB, 64KB, and 256KB requests. The performance for 8KB requests scales with the number of disks up to 32 disks, leveling off at about 20 MB/s. Performance for 64KB and 256KB requests increase to about 65MB/s and then levels off. The bottleneck in this case is the SCSI bus. For this workload, having more than 32 disks per host will not increase performance if the

requests are small. However, for larger requests, the disks per host ratio can be increased up to 42 disks before the host becomes a bottleneck.

Different levels of performance should be expected with different disks/host ratios. Both the light and heavy nodes can support small requests without the host or SCSI subsystem limiting performance. However, for larger requests, the shared SCSI bus limits performance for both types of nodes. These results can change further for reads and writes using the file system. The prior experiment used the raw disk interface because the performance through the raw interface is similar across different operating systems.

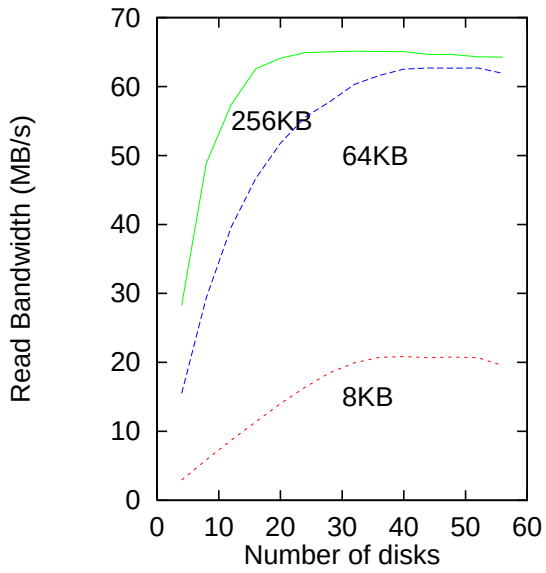

Figure 2-2. Performance Trade-Offs of Varying the Disks/Host Ratio

This figure shows the read bandwidth possible from a single host using the raw disk interface. The throughput for 8KB reads scales up to 32 disks, and then levels off at about 20 MB/s. For the larger requests (64KB and 256KB), the throughput levels off at around 65MB/s. Since four SCSI buses are used, each bus is delivering around 16MB/s, close to the normal observed peak of 17MB/s.

2.3.1.2. Problems with high Disk/Host Ratios

Since PCs are not normally required to support such a large number of disks, unexpected problems may crop up when the disk/host ratio becomes larger. A few problems that we encountered are listed below:

(i) Operating system and firmware bugs: Since most PC operating systems were not designed to host large numbers of disks, increasing the disks/host ratio can expose undiscovered problems in operating system and disk controller software. While developing our prototype, we ran across several such problems. Windows NT, for instance, supports only 31 disks through its Disk Administrator GUI. Versions of Solaris x86 that we experimented with had problems with more than 7 disks on a SCSI string. We also discovered an Adaptec firmware bug that did not allow 15 disks on both strings of a twin channel SCSI adapter. More details on these issues are available in [Talagala96].

(ii) SCSI Limits: Since the maximum length of a Fast-Wide SCSI string is about 9 feet, if a SCSI string is longer, time-outs and other problems can occur. If the string is not properly terminated, these problems can happen with shorter buses as well. We were able to keep the string length short inside an enclosure by having the SCSI bus on the enclosure backplane. If the SCSI bus is not on the enclosure backplane, cabling between disks inside the enclosure can add to the total string length. Differential SCSI allows longer cable lengths (up to almost 80 feet), making string length less of a problem. Serial interconnects will also allow very long strings [Schwarderer96].

(iii) Host Machine Limits: Most PCs have at most four PCI slots, placing a limit on the number of disks that can be connected to it. In this case PCI-PCI bridges can be used to extend the host PCI bus.

Because of such problems, we were not able to reliably connect more than 56 disks to a single node. As the prior section indicated, increasing the disks/host ratio beyond this limit also makes the host and SCSI subsystem a performance bottleneck.

2.3.2. Ethernet and Serial Interconnection

All nodes are connected via 100Mbit Switched Ethernet. Figure 2-3 shows the Ethernet and Power Switch topology for the prototype. The subnet contains two Ethernet switch hubs. The host machines are named *m0-m19*; each machine has its own ethernet address. The heavy nodes are *m0-m3* and the light nodes are *m4-m19*. The subnet contains four additional machines. Two of these machines provide NFS, home directories, and naming services for the storage cluster. The last two machines, namely *ackbar* and *tarkin*, are front ends for the image server application. Their use is discussed further in section 2.4. Finally, each remotely controlled power switch also occupies an ethernet address.

In addition to Ethernet, all machines are also connected via serial lines that provide an alternative way to access the machines for easier management. For simplicity, all serial connections are routed through a single serial port concentrator. This concentrator has four 24 port serial terminal servers, each with its own ethernet connection. This single hub is a possible point of failure; however this is not much of a problem since the serial lines are intended only for monitoring and management, not for data transfer. The disk enclosures and UPS (Uninteruptible Power Supply) Units are also interconnected with serial lines.

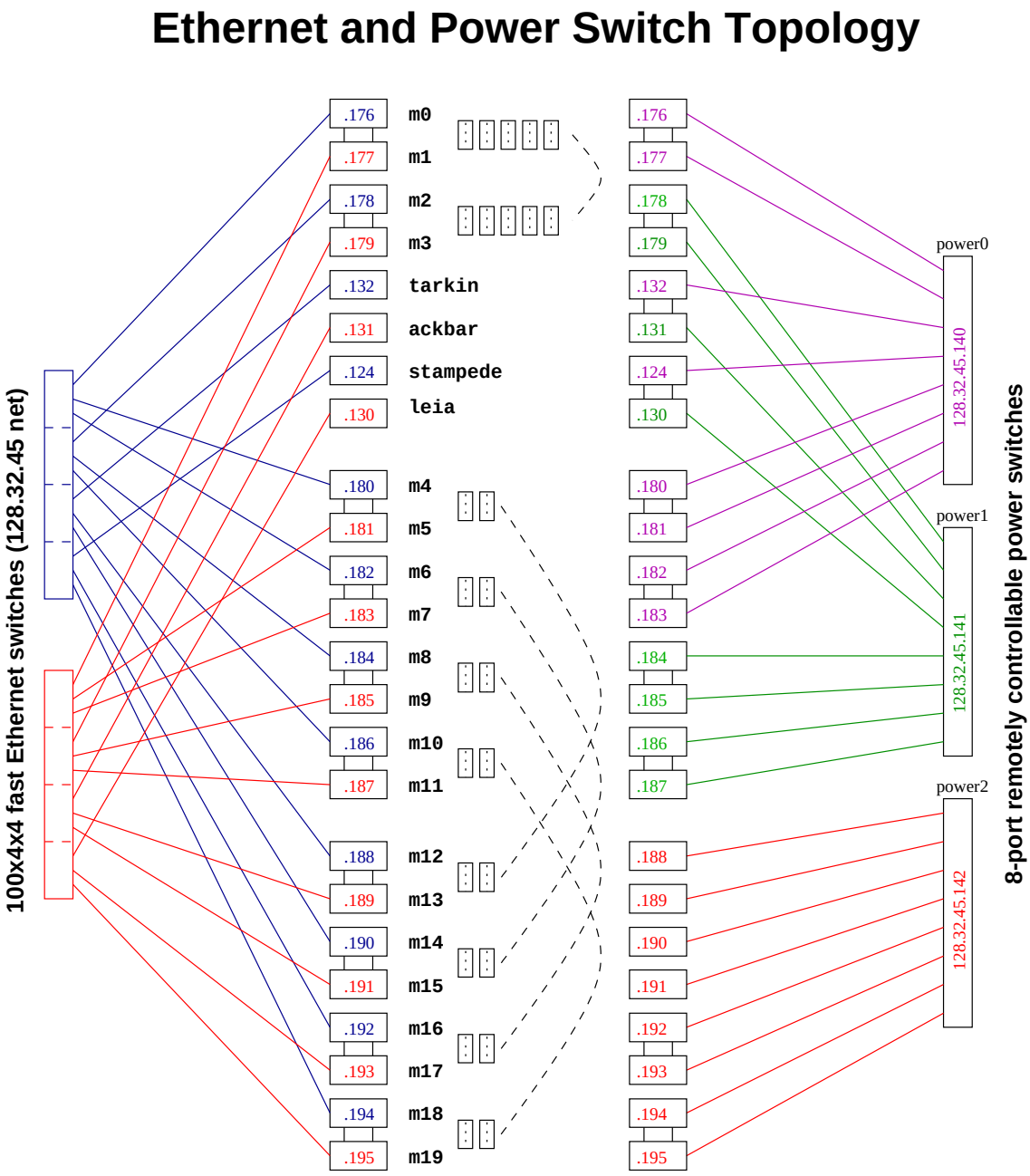

Figure 2-3. Interconnection and Power Topologies

Each machine, serial port switch, and remote power switch is accessible via ethernet. Three remote power switches (powered via UPS) control power to the machines and disk enclosures. The machines *ackbar* and *tarkin* are the front ends for the image server application and *stampede* provides NFS services to all nodes.

2.3.3. Power Scheme

Figure 2-3 also shows how power is routed to the cluster. Each disk enclosure contains two power supplies. In addition, power protection is provided for the entire cluster via the six UPS units. The power scheme is completed by the remotely controllable power switches that enable automatic hard resets of each machine.

2.3.4. Redundancy

The data served by the image server is mirrored across the nodes. The dotted lines in figure 2-3 identify pairs of mirror nodes. As the figure shows, the configuration strives to provide independent network paths and power paths to node in a mirrored pair.

2.4. Application: A Web-Accessible Image Server

The storage cluster hosts a web-accessible image server. This service, called *The Zoom Project*, has been available to users since March 1st 1998. This site, a collaborative effort between UC Berkeley and the Fine Arts Museums of San Francisco, provides a database of over 80,000 high resolution images of art work. Each image is available at resolutions of up to 3072x2048 pixels. It is by far the largest on-line art collection in the world.

2.4.1. Application Overview

Figure 2-4 shows how the site works. The front end, at *http://www.thinker.org/*, is hosted by the Fine Arts Museum. Each image is searchable by title, artist, time period, and other

descriptive keywords. This search database contains only the image attributes, not the images themselves. Within the database, each image is identified by a 16 digit key. The storage prototype host the larger versions of the images. When a user wishes to view an image, the image is requested from the storage servers using this key. This request is passed down to the storage front end, which forwards the request to a storage server with a copy of the image. From then on, all image data transfer occurs between the storage server and the client. Note: We have two front ends because the database and the storage server portions of the site are at different geographical locations. The second front end eases management by creating a level of indirection between the search engine and the storage servers. This way, we are able to reconfigure the storage system component without modifying the search database.

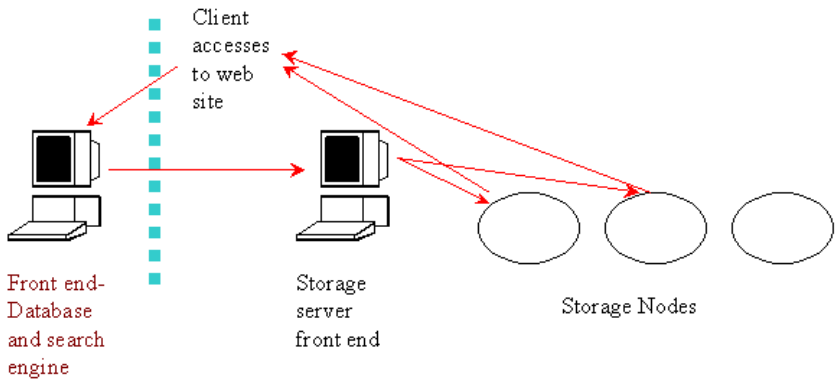

Figure 2-4. Image Server Operation

This figure shows how the site works. Clients access images through a keyword search at the front end. Once an image is selected, tiles are transferred to the client from a storage server that is holding the image. The storage servers are managed by a storage front end. The vertical line separating the database and storage system indicates that these two servers are in different geographical locations

The storage front end is implemented by the machines *tarkin.cs* and *ackbar.cs* that back each other up using IP aliasing. All requests are directed to the canonical address *gpx.cs.berkeley.edu*. When *tarkin.cs* is up and running, it handles all requests to this address. *tarkin.cs* is constantly monitored by *ackbar.cs*. If *tarkin.cs* goes down, then secondary takes over by assuming the *gpx.cs.berkeley.edu* address. Once *tarkin.cs* comes back up, *ackbar.cs* gives up the *gpx* address. The front ends maintain a directory of image IDs and storage servers. In addition, the front ends periodically monitor the storage servers and maintains lists of non-responding servers. When a storage server goes down, all image requests are forward to the server with the mirror copy of the image.The requests are forwarded from the front ends to the storage servers using HTTP-redirect. Each host in the prototype serves its local images using the Apache Web Server.

Unlike prior file-service based storage systems architectures, this failover design does not attempt to mask failures for client connections that are already in progress. This decision reflects the design principle that for this type of web-based application, Fix-By-Reload is the necessary level of availability. Studies have shown that the when internet users experience slowdowns, the problem is far more likely to be the connection to the web server than the server itself [Manley97]. Since the user's only means of access is through a slow and unreliable link, they are capable of retrying requests that time-out or fail. Therefore, for users coming over the web, the only availability requirement that the system must meet is to recover within enough time to satisfy the request retry. In particular, it is not necessary to mask all failures at the site. In many cases, no matter how reliable the web server, the internet will generate failures that are visible to the user. Prior work on smart clients has shown that it is possible for the client browser to do fault tolerance by switch-

ing between several sites that are offering the same service [Yoshikawa97]. This idea can also be used to build an automatic retry mechanism into the browser so that the user does not even have to click reload when a failure occurs.

Once the user specifies a screen size, a 12.5% resolution version of the image appears inside a zoom window. Figure 2-5 shows Picasso's *Still Life with Skull, Leeks and Pitcher* in zoom windows at 12.5% and 50% resolutions. We can see the Picasso signature by zooming into a corner of the painting. Once the image becomes too large to fit in the window, scrollbars appear. Users can zoom in up to 1600% resolution, 16 times the art work's full size.

2.4.2. File Format and User Interface

The images are stored in a tiled format called GridPix [Asami98], similar in concept to the FlashPix standard [Kodak97]. Both formats have the notions of tile-based images and multiple image resolutions within a single file. The difference is that GridPix is a simpler format designed only for storing tiled images, while FlashPix is a more generalized format designed with many different uses in mind. A GridPix file contains a header structure, an index of offsets, and a sequence of JPEG encoded image tiles in resolutions from 12.5% to 100%. Tiles for resolutions higher than 100% are generated on the fly from the 100% resolution tiles. The GridPix file format and associated software is discussed in more detail in [Asami98].

The viewer is implemented by two CGI programs; one creates the graphical viewer and the second retrieves each tile. The viewer places the tiles adjacent to each other in the HTML page to create the full image. All images are initially displayed at 12.5% resolution. At this

Figure 2-5. GridPix Viewer

Pablo Picasso's *Still Life with Skull Leeks and Pitcher* at 12.5% and 50% resolution within the GridPix viewer. At 50% we can see the artist's signature at the lower right hand corner of the image.

size, most images fit entirely within the window. Once the image becomes too large for the viewing area, the user can scroll up/down or left/right by clicking on the scrollbars. As the user navigates, the necessary tiles are extracted from the GridPix file and sent to the user. We do not describe the application further in this thesis; a more detailed description of workload and user access patterns is available in [Talagala99].

2.4.3. Disk Usage

In addition to the GridPix images, the prototype also contains images in TIFF format; the GridPix images are on average 1.2MB, while the TIFF images are on average 12MB in size. Only the GridPix images are served by the site; the TIFF images are needed because the GridPix images cannot be modified. At times, the images are displayed with incorrect orientations and less than perfect color. In these cases, the corrections are performed on the TIFF counterpart and a new GridPix image is generated. Note: other tile-based image formats, like FlashPix, do allow editing. If such a format is used, it may not be necessary to

keep other formats around. However, in our experience, a large and constantly evolving image database will contain images in several formats.

Each disk is divided into three key partitions. The first is a 32KB partition that contains start-up scripts for each disk. These scripts are to identify the disk at boot time; they are described in more detail in [Asami99]. The second partition is 1GB and is used for various experiments. The third partition occupies the bulk of the disk, 7GB, and is used for image storage. On each storage server, the third partition of all the disks are organized as a striped disk array using the CCD (Concatenated Disk Driver) pseudo device driver. The GridPix image files are stored on a BSD Fast-File System (BSD FFS) on this striped disk array [BSD96].

The 2GB internal drive contains the operating system and swap area for each node. In addition, each node mounts shared NFS filesystems from the infrastructure servers. These file systems contain software tools and home directories for the system's users.

2.5. Summary

This chapter described the storage system prototype and its application. The prototype consists of a group of relatively independent nodes interconnected by a switched network. Directed by a front end, the nodes collectively form a web-accessible image database for the high resolution art images of the Fine Arts Museums of San Francisco. The prototype is used to study the soft error behavior in a large storage system; these studies are described

in the next two chapters. In addition, the prototype's disks are used in the studies on disk performance variability in chapters 5 and 6.

3 Characterizing Soft Failures and Error Behavior

3.1. Introduction

This chapter presents data on the soft failure characteristics of the prototype. We analyze system error logs from the storage system described in Chapter 2. We describe the soft error behavior of disks and SCSI components, the effects of component failures on the operating system of the host machine, and the effects of network failures. We also correlation between soft errors on different storage nodes.

The analysis leads to some interesting insights. We found that the SCSI disk drives were among the most reliable components in the system. Even though they were the most numerous component, they experienced the lowest failure rate. Also, we found that all the errors observed in six months can divided into eleven categories, comprising disk errors, network errors and SCSI errors. We also gained insight into the types of error messages reported by devices in various conditions, and the effects of these events on the operating system. Our data supports the notion that disk and SCSI failures are predictable, and sug-

gests that partially failed SCSI devices can severely degrade performance. Finally, we observed the disastrous effects of single points of failure in our system.

The rest of the chapter is organized as follows. Section 3.2 outlines related work. Section 3.3 describes the statistics on absolute failures for the prototype over 18 months of operation. Absolute (or hard) failures are cases where the component was replaced. These statistics provide a useful perspective for the study on soft errors that makes up the rest of the chapter. Section 3.4 describes the logs used to gather soft error information. Section 3.5 describes the results obtained from studying these logs. Section 3.6 discusses the results and their implications. Finally Section 3. 7 concludes with a summary.

3.2. Related Work

There has been little data available on the reliability of storage system components. An earlier study [Tsao83] suggested that system error logs can be used to study and predict system failures. This work focused on filtering noise and gathering useful information from a system log. The authors introduced the “tuple concept”; they defined a tuple as a group of error records or entries that represent a specific failure symptom. A tuple contains the earliest recorded time of the error, the spanning time, an entry count, and other related information. The work described a Tuple Forming Algorithm, to group individual entries into Tuples, and a Tuple Matching Algorithm to group tuples representing the same failure symptom. The study did not attempt to characterize the failure behavior of devices, and was not specifically targeted at storage systems. Follow up work characterized the distri-

butions of various types of errors and developed techniques to predict disk failures [Lin90]. In this study, the system was instrumented to collect very detailed information on error behavior [Lin90]. The DFT algorithm, a failure prediction algorithm developed in this work, is used in the next chapter as part of a study of device failures.

A second study associated with the RAID effort [Gibson88] [Shulze89] presented factory data on disk drive failure rates. This study focused on determining the distribution of disk drive lifetimes. The authors found that disk drive lifetimes can be adequately characterized by an exponential distribution. A third study, an analysis of availability of Tandem systems was presented in [Gray90]. This work found that software errors are an increasing part of customer reported failures in the highly available systems sold by Tandem.

Most recently, disk companies have collaborated on the S.M.A.R.T (Self, Monitoring, Analysis and Reporting Technology) standard [SMART99]. SMART enabled drives monitoring a set of drive attributes that are likely to degrade over time. The drive notifies the host machine if failure is imminent.

3.3. Failure Statistics

We begin with statistics on absolute hardware failures for eighteen months of the prototype's operation (from March 1997 to August 1998). Table 3-1 shows the number of components that failed within this one and a half year time frame. For each type of component, the table shows the number in the entire system, the number that failed, and the percentage failure rate. Since our prototype has different numbers of each component, we cannot

directly compare the failure rates. However, we can make some qualitative observations about the reliability of each component.

Component	Total in System	Total Failed (Absolute Failures)	% Failed
SCSI Controller	44	1	2.3%
SCSI Cable	39	1	2.6%
SCSI Disk	368	7	1.9%
IDE Disk	24	6	25.0%
Disk Enclosure	48	13	28.3%
Enclosure Power	92	3	3.26%
Ethernet Controller	20	1	5.0%
Ethernet Switch	2	1	50.0%
Ethernet Cable	42	1	2.3%
Total Failures		34	

Table 3-1. Absolute Failures over 18 Months of Operation.

For each type of component, the table shows the total number used in the system, the number that failed, and the percentage failure rate. Note that this is the failure rate over 18 months (it can be used to estimate the annual failure rate). Disk enclosures have two entries in the table because they experienced two types of problems, backplane integrity failure and power supply failure. Since each enclosure had two power supplies, a power supply failure did not affect availability. As the table shows, the SCSI data disks are among the most reliable components, while the IDE drives and SCSI disk enclosures are among the least reliable. Note that this table does not show the same number of components as Table 2-1 since it lists the total number of components used over the 18 month time frame.

Our first observation is that, of all the components that failed, the data disks are the most reliable. Even though there are more data disks in the system than any other component, their percentage failure rate is the lowest of all components. The enclosures that house these disks, however, are among the least reliable in the system. The disk enclosures have two entries in the table because they had two types of failure, power supply problems and SCSI bus backplane integrity failures. The enclosure backplane has a high failure rate while the enclosure power supplies are relatively more reliable. Also, since each enclosure

has two power supplies, a power supply failure does not incapacitate the enclosure. The IDE internal disks are also one of the least reliable components in the system, with a 25% failure rate. The unreliability of the IDE disks could be related to their operating environment. While the SCSI drives are in enclosures specially designed for good cooling and reduced vibration, the IDE drives are in regular PC chassis. Overall, the system experienced 34 absolute failures in eighteen months, or nearly two absolute failures every month.

We note that Table 3-1 only lists components that failed over eighteen months (Table 2-1 lists all hardware components in the prototype). Some components had no failures at all in this time frame. These components include the PC internals other than the disk (the motherboard, power supply, memory modules, etc.), serial hardware, UPS units an so on.

3.4. Logs and Analysis Methodology

The operating system reports error messages, boot messages, and other status messages to the internal system log. The kernel, system daemons, and user processes can contribute to this log using the *syslog* and *logger* utilities [FreeBSD97]. These logs are located at `/var/log/messages` in our configuration of FreeBSD 2.2. We studied these logs to gather information about soft failure behavior.

We began by filtering out messages that reported status and login information. To this end, we removed all messages from *sshd* (secure shell logins), *sudo* messages, other login messages, and all boot messages. This preprocessing reduced the size of the logs between 30%

and 50%. The messages that remained were primarily from the OS kernel and network daemons.

```
Feb 6 08:09:21 m2 /kernel: (da1:ahc0:0:1:0): SCB 0x85 - timed out while
idle, LASTPHASE == 0x1, SCSISIGI == 0x0
```

Figure 3-1. A Sample Line from Syslog Showing a SCSI TimeOut

Figure 3-1 shows a sample error message from a system log that is reporting a timeout on the SCSI bus. This log line has seven pieces of information. The first three fields contain the date and time. The fourth field is the machine name, in this case *m2*. The fifth field lists the source of the message; in this case the operating system kernel is reporting the error. The sixth field specifies the device on which the timeout occurred. The first two subfields of the sixth field specify the disk number and SCSI bus number within the system; in this case, the error is on the disk *da1* that is attached to SCSI bus *ahc0*. The remainder of the message describes the error; the value of the SCSI Control Block is 0x85, and the device timed out while in the idle phase of the SCSI protocol.

We use the following terms in the rest of the chapter to describe the analysis results:

Error Message: An error message is a single line in a log file, as in Figure 3-1.

Error Instance: An error instance is a related group, or tuple, of error messages. The notion of error tuples has been described in detail in [Tsao83]. We used a very

simple grouping scheme; error messages from the same error category that were within 10 seconds of each other were considered to be a single error instance.

Error Category: By manually examining the logs, we identified eleven categories of errors. For example, the message above fell into the category “SCSI Timeout”. These categories are described in detail in Section 3.5.1. We separated the messages from each category by searching for keywords in each message.

Error Frequency: An error frequency is the number of error instances over some predefined time period. Section 3.5.2 presents results on error frequencies.

Absolute Failure: An absolute or hard failure occurs when a component is replaced. An absolute failure is usually preceded by many error instances reported in the log. Absolute failures are explored in more depth in Chapter 4.

3.5. Results

In this section we present the results of the system log analysis. Section 3.5.1 lists and defines all the error categories, the types of error messages that we encountered in the logs. These definitions are used in the remainder of Section 3.5. Sections 3.5.2-3.5.4 report results on six months of log data for 16 of the 20 machines in the prototype. We were not able to include four nodes in the study because they did not have six months worth of log data. The storage nodes are labeled 1 through 16; nodes 1 through 4 have 28 disks each, and all other nodes have 16 disks each. Section 3.5.2 describes the frequencies of each error

category, within and across machines. The effects of these errors, in particular their relationship to machine restarts, is discussed in Section 3.5.3. Section 3.5.4 discusses the correlation between errors.

At this point it is useful to say something about the load levels on each machine. Intuition tells us that there is a relationship between a machine's load level and the number of reported errors on it. By consulting with system administrators and users, we learned that, during the six month period, the machines that received the most load were 1,3 and 8-12. Machines 13-16 had very little load during this time.

3.5.1. Error Types

We now define all the error categories that we observed in the logs. Table 3-2 lists a sample message for each type of error that we include in this study. While some errors appear as one line in the log, others appear as multiple lines. Definitions of each error category follow.

1. Data Disk Errors

Recall that the data disks are SCSI drives. An error from a data disk usually has three lines. The first line reports the command that caused the error. The second line reports the type of error and the third contains additional information about the error. The messages in the second and third line are defined in the SCSI specification [SCSI2]. Although the spec defines many error conditions, we only mention those that actually appeared in the logs.

Type	**Sample Message**

Data Disk: Hardware Failure	`May 23 08:00:20 m5 /kernel: (da45:ahc2:0:13:0): WRITE(10). CDB: 2a 0 0 29 de f 0 0 10 0`
	`May 23 08:00:20 m5 /kernel: (da45:ahc2:0:13:0): HARDWARE FAILURE asc:2,0`
	`May 23 08:00:20 m5 /kernel: (da45:ahc2:0:13:0): No seek complete field replaceable unit: 1 sks:80,3`

Data Disk: Medium Error	`Dec 13 00:55:31 m1 /kernel: (da41:ahc2:0:9:0): READ(10). CDB: 28 0 0 71 29 1f 0 0 30 0`
	`Dec 13 00:55:31 m1 /kernel: (da41:ahc2:0:9:0): MEDIUM ERROR info:712935 asc:16,4`
	`Dec 13 00:55:31 m1 /kernel: (da41:ahc2:0:9:0): Data sync error - recommend reassignment sks:80,2f`

Data Disk: Recovered Error	`Jul 24 10:40:09 m0 /kernel: (da73:ahc4:0:9:0): READ(10). CDB: 28 0 0 50 54 cf 0 0 80 0`
	`Jul 24 10:40:09 m0 /kernel: (da73:ahc4:0:9:0): RECOVERED ERROR info:505546 asc:18,2`
	`Jul 24 10:40:09 m0 /kernel: (da73:ahc4:0:9:0): Recovered data- data auto-reallocated sks:80,12`

Data Disk: Not Ready	`May 20 11:14:09 m14 /kernel: (da1:ahc0:0:1:0): WRITE(10). CDB: 2a 0 0 26 2e 6 0 0 10 0`
	`May 20 11:14:09 m14 /kernel: (da1:ahc0:0:1:0): NOT READY asc:40,80`
	`May 20 11:14:09 m14 /kernel: (da1:ahc0:0:1:0): Diagnostic failure: ASCQ = Component ID field replaceable unit: 1`

Internal Disk: Hard Error	`Aug 19 16:43:12 m13 /kernel: wd0h: hard error reading fsbn 1970460 of 1970384-1970511 (wd0 bn 3412252; cn 54162 tn 2 sn 12)wd0: status 59<rdy,seekdone,drq,err> error 40<uncorr>`
Internal Disk: Soft Error	`Aug 19 16:43:14 m13 /kernel: wd0h: soft error reading fsbn 1970461 of 1970400-1970511 (wd0 bn 3412253; cn 54162 tn 2 sn 13)wd0: status 58<rdy,seekdone,drq> error 40<uncorr>`
Internal: VM_fault	`Jul 31 12:12:37 m14 /kernel: vm_fault: pager input (probably hardware) error, PID 15211 failure`
Network Error: NIS	`Nov 20 16:22:13 m17 ypbind[95]: NIS server [128.32.45.124] for domain “td” not responding`
Network Error: NFS	`Nov 20 16:23:10 m17 /kernel: nfs server stampede:/disks/stampede/sandbox1: not responding`

SCSI: Parity	`May 12 01:10:32 m2 /kernel: (da40:ahc2:0:8:0): WRITE(10). CDB: 2a 0 0 b9 54 cf 0 0 50 0`
	`May 12 01:10:32 m2 /kernel: (da40:ahc2:0:8:0): ABORTED COMMAND asc:47,0`
	`May 12 01:10:32 m2 /kernel: (da40:ahc2:0:8:0): SCSI parity error`

SCSI TimeOut	`May 17 02:14:58 m0 /kernel: (da33:ahc2:0:1:0): SCB 0x61 - timed out while idle, LASTPHASE == 0x1, SCSISIGI == 0x0`

Table 3-2. Sample Error Messages

This table lists the categories of errors that are discussed in this chapter and includes a sample message for each type of error.

The Hardware Failure message indicates that the command terminated (unsuccessfully) due to a non-recoverable hardware failure. The first and third lines describe the type of failure that occurred.

The Medium Error indicates that the operation was unsuccessful due to a flaw in the medium. In this case, the third line recommends that some sectors be re-assigned. The line between Hardware Failures and Medium Errors is blurry; it is possible for a drive to report a flaw in the medium as a Hardware Failure [SCSI2]. A Recovered Error indicates that the last command completed with the help of some error recovery at the target. This happens, for instance, if a bad sector is discovered. Drives handle bad sectors by dynamically re-assigning the affected sector to an available spare sector [Worthington95, Schwarderer96]. The table shows such an instance. If more than one recoverable error occurs within a single request, the drive chooses which error to report. Finally, A Not Ready message means that the drive is unprepared to serve requests.

2. Internal Disk Errors

The internal disks are IDE Drives. The logs contained two types of errors for IDE drives: soft errors and hard errors. Unlike the SCSI disk errors, these messages are operating system specific. By examining the operating system source code, we learned that soft errors were operations that encountered some form of error but recovered, while hard errors were operations that were not successful after the maximum number of retries. The request information is buried within the error

message; for instance, the hard error message listed in Table 3-2 occurred while the drive was trying to read block number 1970460.

3. Internal vm_fault

This error message appears when the OS kernel attempts to read a page into virtual memory for a process. The error indicates that the read needed to satisfy the page fault did not complete successfully. This error usually causes the affected process to terminate abnormally.

4. Network Errors

Our system reported two types of network errors, those related to the naming (NIS) services and those related to network file system (NFS) services. These errors were reported whenever the system was unable to contact one of these services (i.e., the problem was not in the reporting machine).

5. SCSI Errors

The two SCSI errors are TimeOuts and Parity errors; both are self explanatory. SCSI Timeouts can happen in any of the SCSI bus phases. In our analysis, we don’t separate the SCSI Timeout errors by SCSI BUS phase. By inspecting the OS source, we found that the SCSI driver usually responds to a SCSI timeout by issuing a BUS RESET command. This operation aborts all outstanding commands on the SCSI bus. The other type of SCSI error is Parity. As Table 3.2 shows, SCSI parity error messages appear as the cause of an aborted request.

3.5.2. Error Frequencies

Now we analyze the errors that appeared in six months of system logs of 16 of the 20 host machines. These logs are for the last six months of the 18 month period referred to in Table 3-1. During this time, the system experienced three IDE disk failures and one data disk failure. As mentioned previously, we were unable to include four machines because they did not have six months of log data. Ironically, the logs of two of these machines were destroyed when the IDE internal disks failed. The machine whose data disk failed is not included in this section's data, but the failure is discussed separately in Chapter 4 with other data disk failures The data presented here are based on error instances, all groups of errors that occurred more than 10 seconds apart.

Error Type	Number	% of Total (Including Network Errors)	% of Total (Not Including Network Errors)
Data Disk: Hardware Failure	2	0.29%	0.52%
Data Disk: Medium Error	3	0.43%	0.78%
Data Disk: Recovered Error	10	1.45%	2.60%
Internal Disk: Hard Error	24	3.49%	6.23%
Internal Disk: Soft Error	4	0.58%	1.04%
Internal: VM_fault	6	0.87%	1.56%
Network Error: NFS	43	6.25%	-
Network Error: NIS	260	37.79%	-
SCSI: Parity	129	18.75%	33.50%
SCSI TimeOut	207	30.09%	53.76%
Total	688	100%	-

Table 3-3. Error Frequencies for 16 Machines over 6 Months

The table shows the percentages of each error type. Since our network errors were due to a single point of failure that can be removed, the last column shows error frequencies without including network errors.

Table 3-3 shows how frequently each error happened over all 16 machines. 688 error instances were reported; on average, almost 4 errors appeared per day. As the table shows, the network is a large source of error. Together, the NIS and NFS error messages make up over 40% of all error instances over six months. These errors happened because the storage nodes were dependent on external sources for name service and certain NFS mounted file systems. Since the source is external, these errors are also highly correlated between machines (we discuss error correlation further in Section 3.5.4). This correlation is partly why the number of network errors is so high; one external fault, if it affects all the machines, will be reported as 16 error instances. These services created single points of failure in the system. However, we do not believe that highly available storage systems will have such dependencies. In our system, they were kept only for the convenience of local users. These errors can be removed simply by removing the dependencies. For this reason, we also present the percentage frequencies of other errors without including network errors. Once the network errors are removed, the total number of errors for 6 months was 385, or an average of 2.2 error instances per day.

The largest source of errors in our system are SCSI timeouts and parity problems. SCSI timeouts and parity errors together make up 49% of all errors; when the network errors are removed, this figure rises to 87% of all error instances. Data disk errors, on the other hand, make up a surprisingly small percentage of the total error count, around 4% overall. This happens even though disks make up 90% of the components of the system. Even in these disk errors, the bulk, 3%, are Recovered Errors where the requests did complete successfully. Not all disks on the system are this reliable; IDE disk drives are responsible for over 8% of all reported errors, even though there are only 20 IDE drives in the system. This high

count of IDE errors is partly due to a failed IDE disk in machine 8. For the most part, the error percentages match the failure rates in Table 3-1; SCSI bus failures on enclosures and IDE drive failures make up the bulk of the absolute failures on the system.

Next we break the error information down by machine. Figure 3-2 shows the categories of errors that each machine experienced. Note that Figure 3-2 does not show the total number of errors reported on each machine; that data is in the accompanying table, Table 3-4. Not surprisingly, all machines had a share of network errors. Figure 3-2 shows that IDE disk errors actually appeared on only 3 machines, machines 5, 8 and 13. Data disk errors also appeared on 8 machines. The figure also shows that 11 of the 16 machines experienced SCSI timeout errors.

Table 3-4 shows that the error frequencies vary widely between machines. Ten machines reported between 10 to 30 error instances, while three of the machines reported over 90 errors in the same time frame. Machines 1, 3 and 7 reported the most errors. Figure 3 shows that, in all three cases, the bulk of the messages were all in a single category; for machines 1 and 7 the category was SCSI timeout, while for machine 3 it was SCSI parity. This data suggests an impending failure or other serious problem in each machine. We were able to trace the parity errors in machine 3 to an enclosure replacement that happened later. There were no SCSI component replacements in machines 1 and 7; this suggests that the problem may have been a loose cable that was later fixed. The SCSI errors in machine 9 also led to a later cable replacement. The only other component replacement that occurred during the six months was the IDE drive on machine 8.

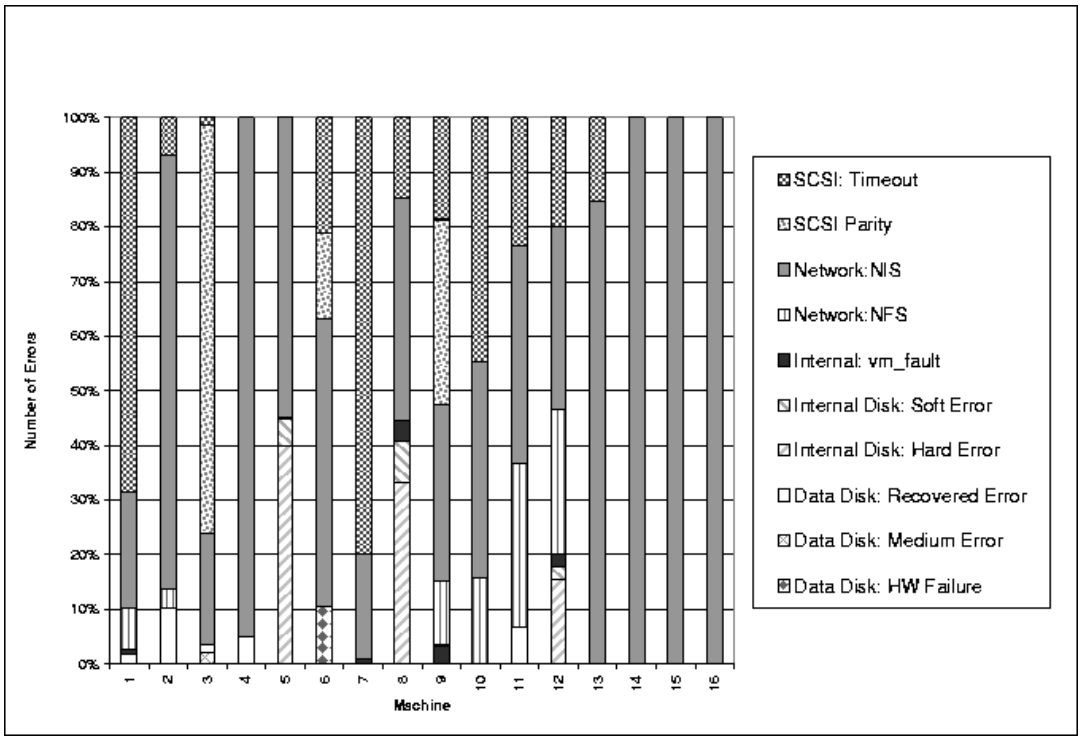

Figure 3-2. Distribution of Errors by Machine over a Six Month Period.

Each column represents a single machine; the column shows the relative percentages of each error type on that machine. The figure shows that network errors occurred on all machines, but other errors each occurred in two or three of the machines.

	1	**2**	**3**	**4**	**5**	**6**	**7**	**8**	**9**	**10**	**11**	**12**	**13**	**14**	**15**	**16**
Network	31	24	29	19	11	10	18	11	26	21	21	27	11	12	18	14
Others	77	5	113	1	9	9	76	16	33	17	9	18	2	-	-	-
Total	108	29	142	20	20	19	94	27	59	38	30	45	13	12	18	14

Table 3-4. Total Number of Errors per Machine

This table and Figure 3-3 together describe how the errors were distributed between machines. The table shows that errors are not evenly distributed; machines 1, 3 and 7 had many more error entries than the others.

We can make several other observations from this graph and table. First, all machines experienced NIS errors. This behavior is not surprising, since these errors appear when the nodes lose a connection with an external service. If the external service is down, all storage nodes will report the same error. In Section 3.5.4, we show that NIS errors are heavily cor-

related between machines. The other type of network error, NFS, does not occur on all machines. This happened because not all machines were mounting the same NFS filesystems at the same time. Second, 10 of the 16 machines reported SCSI timeouts. In this case, the cause was not external; the SCSI subsystems of the machines are independent of each other. Also, the number of SCSI timeouts is not correlated with the number of disks on a node; node 7 has a large number of timeouts even though it only hosts 16 disks. Finally, although Table 3-3 shows that SCSI parity errors have high frequency, Figure 3-2 shows that almost all of these errors appeared on a single machine, caused by an enclosure failure.

Even though the number of potential problems on a system this large is virtually unlimited, only ten different types of problems occurred over the six months. Another interesting observation is that no type of error was limited to only one machine. SCSI, IDE disk and other errors all occurred on at least two machines. This distribution suggests that even though many combinations of errors can occur in theory on a storage system, there are a small set of problems that can be expected to occur in a given architecture. We can also conjecture that if an error happens once, it may happen again on a different machine.

3.5.3. Analysis of Reboots

The prior section looked at the errors that appeared in six months of system logs. The real question is though, what are the consequences of these errors? To address this question, we looked at restarts of nodes in the prototype. For each restart that occurred, we checked the prior 24 hours of the system log for any errors that could be related to the shutdown. We

used these errors to guess the reason for the restart. After studying the causes of restarts, we classified the restarts into the following four categories:

Cold Boot: A Cold Boot is a reboot that occurred without an explicit shutdown or reboot command. All reboots or shutdown commands leave an entry in the system log. When no such entry is present, we assume that the machine was power cycled, either intentionally or because of a power outage. Normally, a machine will not be power cycled unless all attempts to login via network or serial port have failed.

Reboot: A reboot is a restart of a machine with a prior reboot or shutdown command.

Within Maintenance Reboot: This is a reboot that happened within 3 hours of a prior reboot. In this case, we assume that both reboots are part of the same maintenance session.

For Schedulable Maintenance: If an explicit shutdown occurs without any error messages within the prior 24 hours, we assume that the shutdown was for a planned maintenance activity, such as a hardware replacement or upgrade. We call this category Schedulable because we assume that the shutdown could have been moved to another time.

Table 3-5 shows the number of times that each machine was restarted, and Figure 3-3 shows the percentages of restarts from each category for each machine. This data does not include Within-Maintenance Reboots, since we consider them to have happened while the node was down. Overall, we found that all machines were restarted at least twice in the six

months. While most machines had 3-4 reboots, several had 7 to 10 each. There were 73 reboots over all 16 nodes. In addition to schedulable maintenance, we found cold boots with errors, cold boots without errors, reboots with errors, and reboots without errors.

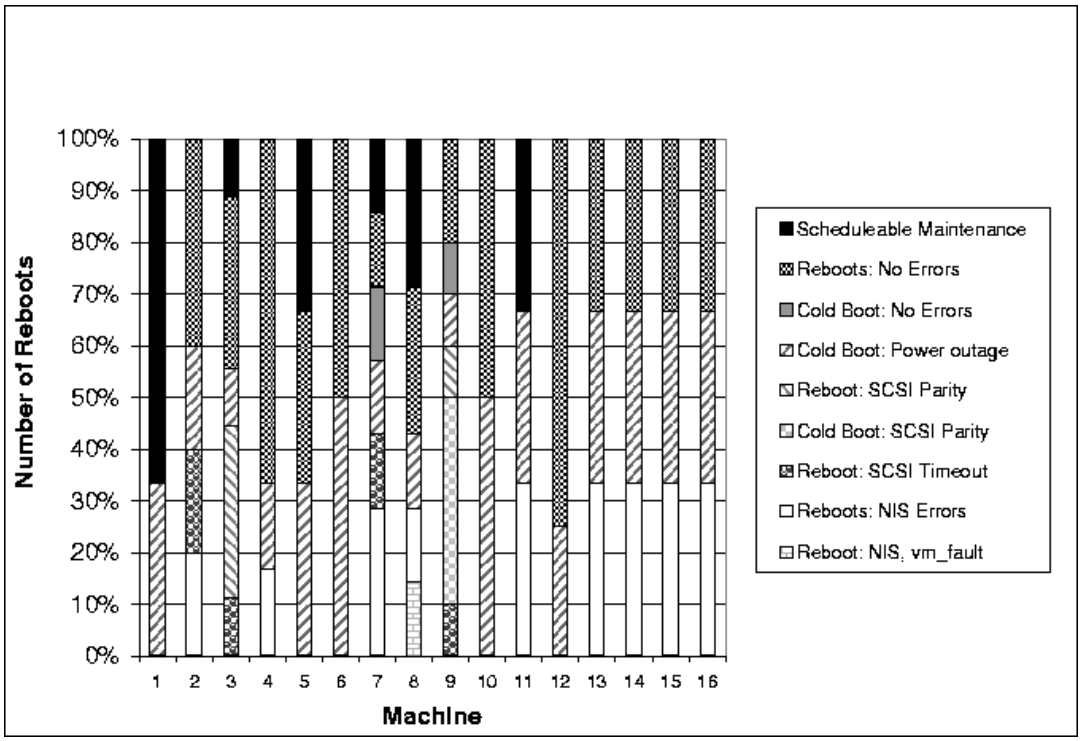

Figure 3-3. Restarts and Their Causes.

Three types of reboots are shown, Cold Boot (restart with no reboot or shutdown message), Reboot (restart with explicit shutdown or reboot message), and For Schedulable Maintenance (explicit shutdown with no error condition).

	1	**2**	**3**	**4**	**5**	**6**	**7**	**8**	**9**	**10**	**11**	**12**	**13**	**14**	**15**	**16**
Restarts	3	5	9	6	3	2	7	7	10	2	3	5	3	3	3	3

Table 3-5. Distribution of Restarts Across Machines

Most machines have been restarted between two and three times over the six months, but several machines have been restarted seven to ten times

Table 3-6 shows the frequency of each type of restart. Overall, 11% of these reboots were for schedulable maintenance; six of the 16 machines had some scheduled maintenance

Restart Type	Number	% of Total
Schedulable Maintenance	8	11.0%
Reboot: No Errors	24	32.9%
Reboot: Errors	19	26.0%
Cold Boot: No Errors	2	2.7%
Cold Boot: Errors	4	5.5%
Power Outage	16	21.9%

Table 3-6. Frequency of Each Type of Restart

The table lists breaks the Reboot and Cold Boot categories into two subcategories, those with errors and without errors. A Reboot with errors is an instance where the log data showed errors before the explicit reboot. A Cold Boot with errors is a case where the log data showed a restart, without an explicit reboot, and errors appeared before the restart occurred. As such, a Cold Boot without errors is a very unlikely occurrence.

done on them. A single power outage accounts for 22% of all restarts. Another 33% were explicit reboots with no errors in the log; these reboots could have been for software maintenance. It is very unlikely that a machine was explicitly rebooted for no good reason, however, we cannot tell from the system logs whether a software upgrade took place. All machines were rebooted without errors. Two machines also received cold boots with no error messages. Finally, the remaining 32% of restarts happened due to errors.

We found only three types of error instances that preceded reboots or cold boots; they were SCSI Timeout, SCSI parity, and NIS errors. Two machines were restarted for SCSI parity problems; one of these is machine 3 that had the failed disk enclosure. Four machines were restarted for SCSI timeout problems. By far, the main cause of reboots and cold boots was NIS errors. All the machines but one were restarted because of network problems. The reason could be that network errors are more fatal to an OS than SCSI errors. While the effects of SCSI errors can be limited to the processes that are reading or writing to the affected drives, the network errors affect all communication between the machine and the outside world.

One interesting point is that no machine restarts happened because of data disk or IDE disk errors. Even though there were hard errors on the three of the 16 system disks, these errors did not cause the operating system to crash. The OS survived hard errors on the internal disk because all of the errors occurred on a user partition that occupied around 80% of the drive.

3.5.4. Correlations

Sections 3.5.2 and 3.5.3 described aggregate data on types of errors and causes of reboots. In this section we examine the time correlation between errors, within and between machines.

Figures 3-4 and 3-5 show the time distribution of errors. The X axis is time and the Y axis shows the identification numbers of each machine. The errors for each machine over time appear on a single horizontal line. A vertical line indicates correlation of errors between machines. Figure 3-4 only shows NFS and NIS errors, while Figure 3-5 shows all other errors. It is clear from Figure 3-4 that network errors are correlated between machines. This data reiterates the need to remove all single points of failure from a highly available storage system. The bulk of the errors are NIS errors. When NFS errors occur, they also seem to be correlated with NIS errors.

Figure 3-5 shows all other forms of errors. In this case there is no reason to expect errors on different machines to be correlated; each node is relatively independent of all other nodes. However, the figure shows that even though there is no direct correlation between SCSI errors (no single source), it is possible to have several SCSI errors across different machines at the same time. For example, near August 13, 1998, several machines experi-

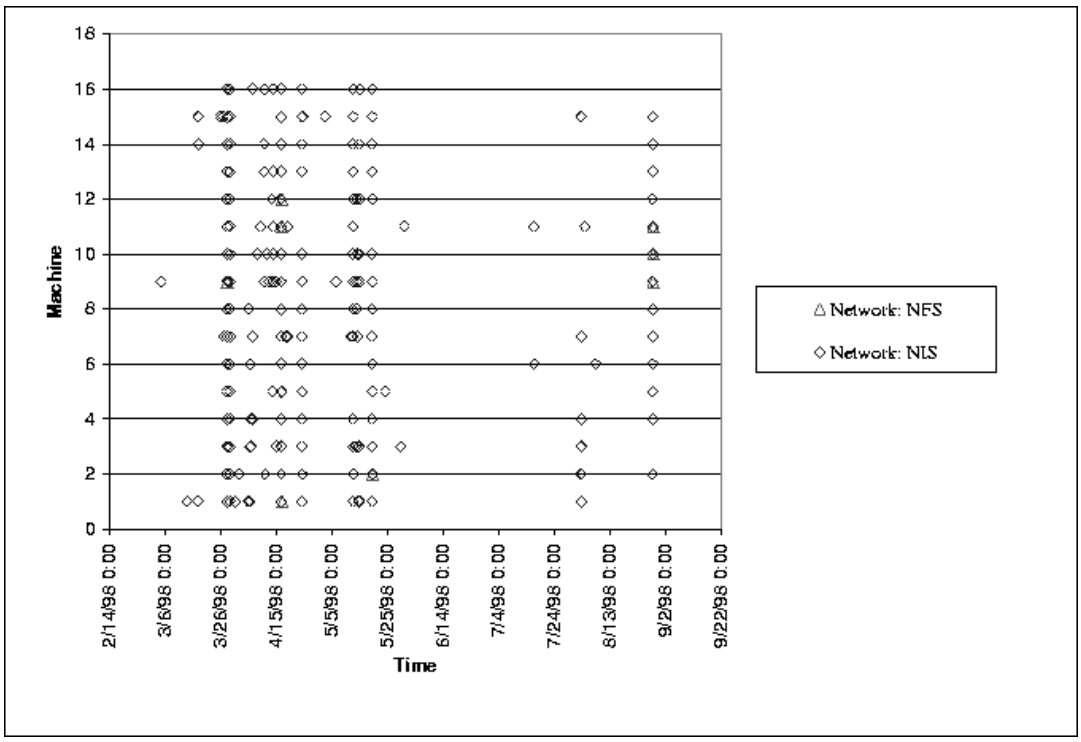

Figure 3-4. Network Errors over Time

This figure shows NFS and NIS related errors over time for all 16 machines. The X axis shows time; the errors of each machine are displayed on a horizontal line. The Y axis shows machines. The figure shows that network errors are heavily correlated over machines. This behavior is not surprising as the cause of the errors is an external service.

enced either a disk or SCSI error. The figure also suggests that SCSI failures may be predictable; machines 1, 3, and 9 show SCSI parity and timeout errors that escalated over time.

Figure 3-6 shows the time distribution of reboots. The figure indicates that there is a strong correlation between error-free reboots on different machines. This observation further suggests that these reboots were part of software maintenance or upgrade. There are two other heavily correlated groups of reboots between 5/5/98 and 5/25/98. We traced the first back

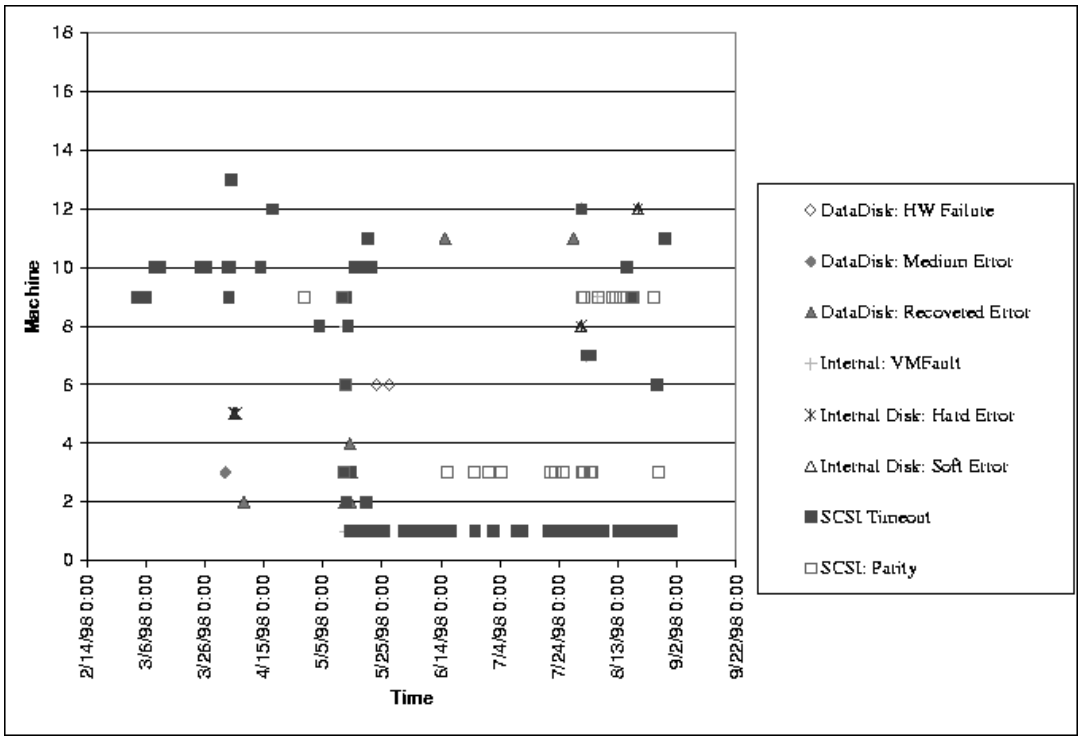

Figure 3-5. Other Errors over Time.

This figure shows the data disk, internal disk, and SCSI errors over time. Since there are no shared components between machines, we do not expect these errors to be correlated over time. The figure does show that unrelated soft errors can occur at the same time on different nodes.

to a NIS service problem. The second was due to a power outage. All other restarts (16 in total or 22% of all restarts) do not appear to be correlated.

3.6. Discussion

We can draw several conclusions from the data in Section 3.5. First, the data supports our intuition that failures are not instantaneous. The time correlation data in Section 3.5.4 showed that several machines showed bursts of SCSI errors, escalating over time. This data

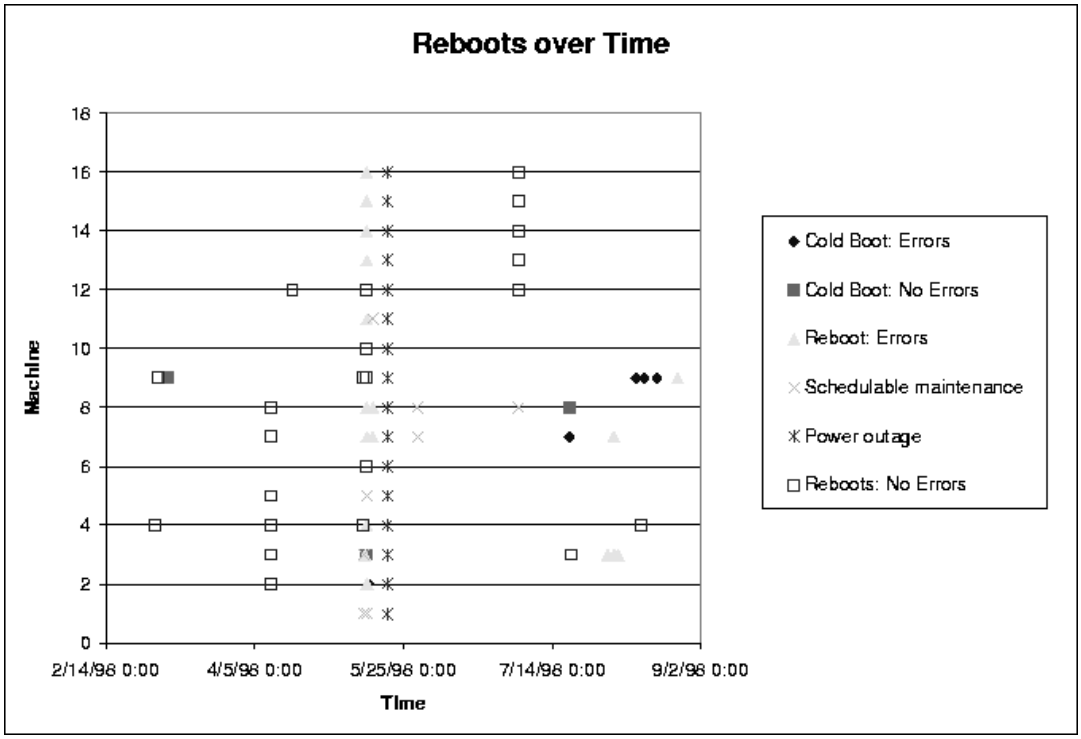

Figure 3-6. Time Distribution of Restarts

The X axis shows time; each machine's restarts are shown on a separate horizontal line. There are two time instances where nearly all machines were restarted at around the same time. The first is an external network failure. The second is a power outage. The figure also shows that Reboots with No Errors are also correlated between machines, suggesting that the restarts were part of software maintenance.

suggests that a sequence of error messages from the same device will suggest imminent failure. A single message is not enough; as Section 3.5 showed, components report hardware errors from time to time without failing entirely.

Second, SCSI errors happen often in a large storage system. Section 3.5.2 showed that over six months, SCSI errors made up almost 50% of all errors in the system. Even though the SCSI parity errors were relatively localized, appearing in only three of the 16 machines studied, the SCSI timeout errors were not. SCSI timeout errors appeared in 10 of the 16

machines. These timeouts affect system performance for two reasons. First, a timeout typically indicates that devices that wish to use the bus are not able to use it, delaying requests. Second, as the SCSI controller regains control by issuing a BUS RESET, a timeout can cause the controller to abort all active requests on the bus. When there a large number of disks on the bus and each disk has several tagged commands outstanding, a SCSI timeout can severely degrade performance. The data also suggests that failures of SCSI components are predictable. Disks already provide some warning that failure is imminent; the data in Sections 3.5.2 and 3.5.4 suggest that SCSI failures may also be predictable. Since many disks are dependent on a single SCSI bus, it would be very useful to predict the failures of SCSI buses. It may also be possible to avoid the degraded performance that occurs before a SCSI bus has an absolute failure.

Third, the data also shows that data disks are among the most reliable components in the system. Section 3.3 showed that data disks had the lowest percentage failure rate of all components that failed in one year. This data suggests that work in the literature that has focused on disk reliability [Burkhard93, Ng94] do not adequately reflect the reliability challenges of real systems.

3.7. Summary

This chapter presented an analysis of hardware errors in a large storage system. We show results from six months of system logs on 16 machines, absolute failure data for the entire prototype for eighteen months, and four case studies of disk drive failures. The data

showed that data drives are among the most reliable components in the system, while SCSI components generated a considerable number of errors. The data shows that no failure happens instantly, and that there are performance consequences when operating with degraded components.

The data also supported the idea that it is possible to predict the failure of both disk drives and SCSI components. The next chapter explores this idea in more depth. In particular, we analyze error streams that occur before SCSI and disk drive failures to determine the long term characteristics of failure events. Chapter 4 also explores the effectiveness of prediction techniques to detect and remove failing components before they can degrade the system performance and availability.

4 Characterizing Failures

4.1. Introduction

This chapter explores the failure behavior of devices in depth. In particular, we attempt to understand what outward signs accompany the failure of disks and SCSI systems. We present cases of device failure; for each case we ask the following questions: what messages appear before failure?, can these messages be used to predict failure?, how do the messages compare in type to what appears without a failure? and finally, can all this information be used to determine the best cause for action when a failure occurs? We also present some evidence of the side effects of failures.

Section 4.2 defines different types of failure events. The terms defined are used in the discussions of failures in the rest of the chapter. The remainder of the chapter focuses on understanding the nature of SCSI and disk drive failures. To do this, we begin by presenting each failure case for which system logs are available. For each case, we determine the type of messages that were reported and whether those messages increased in intensity over time. The next section, section 4.4, determines whether these failures are predictable by applying a failure prediction algorithm. Section 4.5 presents empirical data on the side effects of disk drive failure and section 4.6 concludes with a summary.

4.2. Methodology

Before we explore the nature of failures, we must define exactly what is meant by a failure. The literature uses various terms to define failure events, *transient, intermittent* and *permanent* faults. *Transient* faults, as the name implies, are errors that appear and disappear with no action needed. *Intermittent* faults tend to reoccur over time. *Transient* and *intermittent* faults differ in that intermittent faults can be removed by replacing hardware, while transient faults cannot. Once the hardware is replaced, the fault is labeled *permanent* [Lin90]. The decision to replace hardware is subjective, and is usually made by a system administrator when a component's error behavior exceeds some tolerance level. In this thesis, such faults are also called *absolute* or *hard* failures.

Chapter 3 used the system logs gathered from the prototype to determine the nature of soft failures. This chapter uses the same logs to study the nature of absolute (or hard) failures. As Figure 3-1 in Chapter 3 showed, each error message identifies the device or subsystem that is reporting the error. Using this information, we can separate the log data into per-device error streams. Studying the error streams of failing devices and comparing them with error streams of other devices reveals the nature of failures.

In addition to the types of failure outlined above, we define an extra category of errors, *Required Human Intervention*. The error data presented so far showed that recurring errors are far more common than hardware replacement. In quite a few cases, a problem that generated a series of recurring errors was solved by a hard or soft system reset. This type of problem is not transient, since the errors do not disappear with no intervention, and cannot be termed permanent or absolute since no hardware is replaced. We define such problems

as requiring human intervention. The system logs show cases where humans intervened. In particular, if the host machine was manually shutdown or rebooted several times before the error stream stopped, we assume human intervention.

4.3. A Look At Failure Cases

This section takes a more in-depth look at the failure cases of SCSI and disk drive components. SCSI failures deserve an in-depth look because the soft error data presented in Chapter 3 revealed that SCSI errors made up the largest percentage of all errors experienced by the system. Also it would be particularly useful to predict SCSI bus failures since they affect many disk drives. It is important to understand data disk failures since the data disks are the most numerous and the most important part of any storage system.

We present each failure case in turn and describe both the types of messages that preceded the failure event, and the duration of messages.

4.3.1. SCSI Cases

There were three SCSI bus failure cases for which system log data was available; Table 4-1 summarizes the cases. For each case, the table shows the types of messages that occurred, the number of messages and the duration of messages. As the table shows, all three SCSI failures displayed Parity error messages. Two of the three cases displayed Timeout messages as well. The first and third case displayed considerably more messages than the

second case; however, in all cases, the messages appeared over durations of thousands of hours.

The log data does not reveal which part of the SCSI subsystem failed, but examination of maintenance logs revealed that FSCSI-1 and FSCSI-3 were failures of the SCSI bus segment on the disk enclosure backplane, and FSCSI-2 was a failure of the bus segment in a SCSI cable.

Case	Types of Messages	Number of Messages	Duration (hours)
FSCSI-1	SCSI Parity	147	2562
FSCSI-2	SCSI TimeOut	10	2528
	SCSI Parity	6	
FSCSI-3	SCSI TimeOut	48	4033
	SCSI Parity	36	

Table 4-1. Summary: SCSI Failure Cases

This table summarizes the three SCSI bus failure cases. The cases are label FSCSI-1 through 3. For each case, the table shows the types of messages that occurred, the number of messages before replacement, and the duration of messages.

4.3.2. Disk Drive Cases

Next we look at disk drive cases. The system log data contained entries corresponding to four disk drive failures. Table 4-2 summarizes these cases. This table shows, for each failed disk drive, the primary and secondary messages that appeared before failure. The primary messages were explained in Chapter 3. The secondary messages are also defined in the SCSI specification and are fairly self explanatory. The first message, “Peripheral Device Write Fault” indicates that the device encountered a failure during a write. The message, “Diagnostic Failure” indicates that diagnostic checks indicated device failure [Merry98, Smith98]. The secondary messages in FDISK-3 and FDISK-4 are the most

Case	Primary Message	Secondary Message	Number of Messages	Duration (hours)
FDISK-1	Hardware Failure	Peripheral device write fault field replaceable unit	1763	186
FDISK-2	Not Ready	Diagnostic failure: ASCQ = Component ID field replaceable unit	1460	90
FDISK-3	Recovered Error	Failure Prediction Threshold Exceeded Field Replaceable Unit	1313	5
FDISK-4	Recovered Error	Failure Prediction Threshold Exceeded Field Replaceable Unit	431	17

Table 4-2. Summary: Disk Drive Failure Cases

This table summarizes the four SCSI disk drive failure cases. While the SCSI messages were always either Timeout or Parity, disk drives display both primary and secondary messages. The primary messages were defined in Chapter 3; the secondary messages are also defined in the SCSI specification.

interesting; the message “Failure Prediction Threshold Exceeded” indicates that the drive’s failure prediction mechanism’s have detected imminent failure [Merry98, Smith98, PFA99]. In the first and second cases, messages appeared days before replacement. In all cases, a large number of messages appeared before replacement.

4.4. Effectiveness of Fault Prediction

All the failure instances had one thing in common; all generated considerable numbers of error messages before the components were finally replaced. This behavior suggests that these failures may have been predictable. In this section, we test the predictability of such failures by applying a failure prediction algorithm, the Dispersion Frame Technique (DFT) described in [Lin90].

Since the goal of this chapter is to understand the nature of failures, including how predictable they are, we evaluate only this one fault prediction algorithm. This algorithm was

chosen for several reasons. First, it is the result of the most recent work on fault prediction that we are aware of. Second, it attempts to detect increasing intensity of error messages, a pattern noticeable in our observed failure cases. Finally, it was also originally used on, and shown effective on, operating system based error messages for a group of workstations.

The effectiveness of fault prediction is determined not just by how many failure cases the algorithm detects beforehand, but also by how few cases are incorrectly predicted. For this reason, we apply the DFT algorithm not only to the cases described in Section 4.4, but also to all error streams generated by SCSI components and data disk drives *that did not fail*.

4.4.1. The Dispersion Frame Technique

The Dispersion Frame Technique (DFT) was developed by [Lin90], a study showing that error arrival times tend to follow the Wiebull distribution. The Wiebull distribution is as follows: Both *a* and *b* are greater than 0; *a* is the shape parameter and *b* is the scale parameter. Note that when *a=1*, the distribution reduces to the exponential distribution function.

Equation 4-1. $$R(t) = e^{(-bt)^a}$$

The DFT method is a group of heuristics that determine whether the shape of the error arrival matches a Wiebull distribution. In general, it captures a convergence in error instances, i.e. when the interarrival time between errors starts to decrease. The details of how the heuristics detect matches with the Wiebull distribution are covered in [Lin90].

The DFT technique calculates two metrics, the Dispersion Frame (DF) and the Error Dispersion Index (EDI). The Dispersion Frame is the time interval between successive errors. The Error Dispersion Index is the number of error messages in half of a DF. Figure 4-1 shows an example error series illustrating frames and EDI. In the figure, when error i arrives, frame (i-3) has three errors when centered on errors (i-3) and (i-2). This behavior triggers the 3:3 rule.

The DFT technique predicts failure if one of the following events occurs:

(1) 3:3 Rule: The EDI from two consecutive applications of the same frame is greater than or equal to 3

(2) 2:2 Rule: The EDI from two consecutive frames is greater than or equal to 2.

(3) 4 Decreasing Rule: If there are four monotonically decreasing frames, and at least one frame is half the size of the prior frame.

(4) 4 in 1 rule: Four messages in 24 hours

(5) 2 in 1 rule: Two messages in 1 hour.

Rules 1, 2, and 3 attempt to capture various shapes in the error arrival processes. Heuristics 4 and 5 represented the rules of thumb commonly used at the time. We discard the last two rules because the success or failure of these two rules is heavily affected by the reporting mechanism in the system. Since the first three rules are based on a theoretical expectation of error distributions we apply these rules to error streams see how well the technique predicts failures.

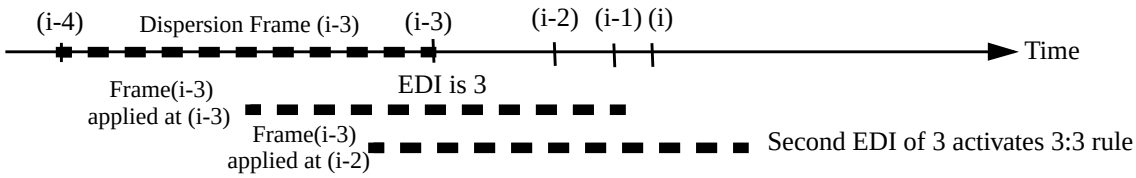

Figure 4-1. Graphical Illustration of the Dispersion Frame Technique

This figure, based on a similar illustration in [Lin90] shows how the DFT technique is applied to an error stream. A frame is calculated as half the time between the current and previous error. As each new error arrives, the algorithm updates the EDI of the frames surrounding each previous error. In the example, the interarrival time between error (i-3) and (i-4) is used to determine the length of Dispersion Frame (i-3). When error (i-1) arrives, the second half of Frame (i-3) contains 3 errors. When error (i) arrives, the same frame, centered around (i-2), also contains 3 errors. As such, the condition for Rule 3:3 is met.

4.4.2. SCSI Cases

As noted in Section 4.3, two types of SCSI errors occur before failure, Timeouts and Parity errors. We apply the fault prediction algorithm to the error streams of each SCSI subsystem that generated errors, and compare its predictions with the failures that actually occurred.

Since a minimum of four error messages are needed to activate any of the rules, we removed all cases of SCSI buses that had three errors or less of each type. (Note that no failed SCSI bus generated less than four messages.) Table 4-3 shows the DFT predictions for each case where more than four SCSI Timeouts occurred. The first two entries in the table, labeled FSCSI-2 and FSCSI-3, are the actual failure cases. FSCSI-2 was not included in this group since it did not generate any Timeout messages. The table also shows the message count and duration, the DFT prediction result, the number of messages required to

generate a prediction, and the prediction time. The table also shows which cases required human intervention.

The DFT algorithm predicted nine failures. For both cases where failure occurred, the algorithm generated a positive prediction in one hour or less. However, the algorithm did have a high false alarm rate; a positive prediction was given for seven cases where no failure occurred. Further examination of maintenance data revealed that in one of the seven cases, a component did fail around the time when the messages were generated; a disk drive attached to the SCSI bus. This event was evidence that disk failures can extend to errors on the SCSI bus. For the rest of the components, there was no replacement. It is certainly possible that these components will fail sometime in the future, however, all information to date suggests that the algorithm is over conservative.

Another way to estimate effectiveness is to compare the DFT failure predictions with instances that *Required Human Intervention*. By this metric the DFT algorithm fares much better. Of the six positive predictions where no component was replaced, the log data in four cases showed evidence of human intervention.

Of all the SCSI buses, there were only three that reported parity errors; each reported more than three messages and each was a failure case. Table 4-4 shows prediction effectiveness when the Parity error streams are used. As the table shows, two of the three failures were predicted by DFT. The algorithm did not predict the failure of FSCSI-2. This failure was predicted, on the other hand, when the algorithm was applied to the Timeout message stream.

Case	Message Count	Messages Needed for Prediction	Prediction Time (hours)	Predicted by DFT?	Actual Failure/ Replacement?	Human Intervention?
FSCSI-2	10	7	0	Yes	Yes	Yes
FSCSI-3	48	5	1	Yes	Yes	Yes
OTHR-1	39	9	690	Yes	-	Yes
OTHR-2	65	12	437	Yes	-	Yes
OTHR-3	11	5	1271	Yes	-	Yes
OTHR-4	4			-	-	-
OTHR-5	175	10	0	Yes	-	Yes
OTHR-6	14	8	416	Yes	-	-
OTHR-7	10	10	1712	Yes	-	-
OTHR-8	6			-	-	-
OTHR-9	295	6	2	Yes	(Disk)	Yes
OTHR-10	8			-	-	-
Total				9	2	7

Table 4-3. DFT Prediction for SCSI Timeout Cases

This table shows the prediction effectiveness of the DFT algorithm. As the table shows, both actual failures were predicted by DFT, but so were several false alarms. However, all but two of the cases predicted as failures by DFT did need human intervention if not actual component replacement.

Case	Message Count	Messages Needed for Prediction	Prediction Time (hours)	Predicted by DFT?	Actual Failure/ Replacement?	Human Intervention?
FSCSI-1	147	7	1280	Yes	Yes	Yes
FSCSI-2	6	-	-	-	Yes	Yes
FSCSI-3	36	13	311	Yes	Yes	Yes
Total				2	3	3

Table 4-4. DFT Prediction for SCSI Parity Cases

This table shows DFT predictions for the SCSI Parity cases. In this case, one failure (FSCSI-2) was not predicted by DFT. However, DFT did predict the same failure using the SCSI Timeout messages.

4.4.3. Disk Drive Cases

Table 4-5 shows the actual and predicted failures for data disk drives. The DFT algorithm predicted all four disk failures that occurred, but also predicted all other disk cases as fail-

ures. We do note, though, that in all the cases, the logs show evidence of human intervention before the error messages stopped. These actions ranged from reboots to short shutdowns that may have been used to readjust cables and restart disk enclosures.

Section 4.3 showed the types of primary and secondary messages generated by disk drives

Case	Message Count	Messages Needed for Prediction	Prediction Time (hours)	Predicted?	Actual Failure/ Replacement?	Human Intervention?
FDISK-1	1763	76	12	Yes	Yes	Yes
FDISK-2	1460	5	33	Yes	Yes	Yes
FDISK-3	44	6	1	Yes	Yes	Yes
FDISK-4	1313	6	1	Yes	Yes	Yes
OTHR-1	2986	5	0	Yes	-	Yes
OTHR-2	37	4	0	Yes	-	Yes
OTHR-3	8989	5	0	Yes	-	Yes
OTHR-4	2217	6	0	Yes	-	Yes
OTHR-5	23	6	1	Yes	-	Yes
OTHR-6	28	6	1	Yes	-	Yes

Table 4-5. DFT Prediction for Disk Drive Cases

This table shows the effectiveness of the DFT algorithm for predicting disk drive failures. The DFT algorithm predicted each test case as a failure, capturing all the real failures as well as many false alarms. However, each case predicted by DFT to be a failure did require human intervention.

during failure. Table 4-6 compares these messages to those generated in the cases where no disk components were replaced. Further examination of the log data revealed that cases OTHR-1 through OTHR-4 all occurred during system bootup, indicating that some component may have been incorrectly connected. As the table shows, some disk drives that are not about to fail do generate the same primary and secondary messages as those that are about to fail. In particular, cases OTHR-5 and OTHR-6 generated the “Failure Prediction

Threshold Exceeded Message". Further examination of these cases revealed that they were side effects of the SCSI bus failure FSCSI-2.

4.4.4. Discussion

The close up look at each failure case revealed the following insights:

(i) In all the failure cases that were examined, the devices generated a considerable number of soft error messages before absolute failure. These messages also tended to increase in intensity over time. As a result, the DFT algorithm was able to detect all the failure cases and issue a prediction well before the device was actually replaced.

(ii) Although DFT was good at predicting real failures, it also predicted failure in many cases where the components were not replaced. These false alarms occurred because other events also generate many error messages, with more messages as time goes by. Since the DFT prediction scheme is based entirely on detecting an increasing intensity of error messages, the algorithm cannot differentiate between these false alarm conditions and actual failures. However, each case predicted as a failure by DFT did require some form of human intervention. Therefore, the DFT appears to do better as a detector of cases where human intervention is needed, rather than a failure prediction algorithm.

(iii) The few SCSI failure cases available for analysis suggest that failing SCSI bus hardware tends to generate both timeout and parity errors. All the false alarm cases generated timeout errors but none generated parity errors. This observation matches intuition; a failing SCSI device is likely to have the types of integrity problems that generate parity errors.

Graph	Primary Message	Secondary Message
FDISK-1	HARDWARE FAILURE	Peripheral device write fault field replaceable unit
FDISK-2	NOT READY	Diagnostic failure: ASCQ = Component ID field replaceable unit
FDISK-3	RECOVERED ERROR	Failure prediction threshold exceeded field replaceable unit
FDISK-4	RECOVERED ERROR	Failure prediction threshold exceeded field replaceable unit
OTHR-1	NOT READY HARDWARE FAILURE	Logical unit not ready, initializing command required Internal target failure field replaceable unit
OTHR-2	NOT READY HARDWARE FAILURE	Logical unit not ready, initializing command required Internal target failure field replaceable unit
OTHR-3	NOT READY HARDWARE FAILURE	Logical unit not ready, initializing command required Internal target failure field replaceable unit
OTHR-4	NOT READY HARDWARE FAILURE	Logical unit not ready, initializing command required Internal target failure field replaceable unit
OTHR-5	RECOVERED ERROR HARDWARE FAILURE	Failure prediction threshold exceeded field replaceable unit Diagnostic failure: ASCQ = Component ID field replaceable unit
OTHR-6	RECOVERED ERROR HARDWARE FAILURE	Failure prediction threshold exceeded field replaceable unit Diagnostic failure: ASCQ = Component ID field replaceable unit

Table 4-6. Primary and Secondary Disk Error Messages

This table compares the primary and secondary messages generated by disks in failure conditions to those generated by disks not in failure conditions. As the table shows, in some cases, drives that are not in failure conditions can generate the same types of messages as those in failure conditions.However, note that these messages appeared on drive connected to a SCSI bus that failed.

This distinction may be useful to separate failure cases from the cases that only need human intervention.

(iv) SCSI failures can masquerade as disk failures and vice versa. Table 4-3 shows a case where a large number of SCSI timeout messages are generated by a failing disk. We examine this case further in the next section. Table 4-6 shows a case where a single SCSI failure generated error streams on two disks on the bus.

4.5. Side Effects of Disk Drive Failures

Figure 4-2 shows disk error and SCSI timeout events in one disk failure case. This is the case labeled FDISK-1 Table 4-2 and the SCSI case labeled OTHR-9 in Table 4-3. The figure shows that the failing disk generated a large number of SCSI Timeouts. The other disks on the bus also generated some timeouts. As the intensity of the disk error messages increased, so did the intensity of the timeout messages.

In this case, the failing disk did interrupt (though it did not halt) the activities of other devices on the bus. The BSD SCSI driver responds to a SCSI timeout condition by issuing a BUS RESET command to regain control of the SCSI bus. The BUS RESET has the side effect of aborting all outstanding commands on the BUS. These commands must be issued again. Both the timeout and its resulting BUS RESET several handicap the performance of all devices on the bus. The figure is evidence that it is possible for failing disks to hold on to the interconnect, causing timeouts and resulting in resets to reclaim the bus.

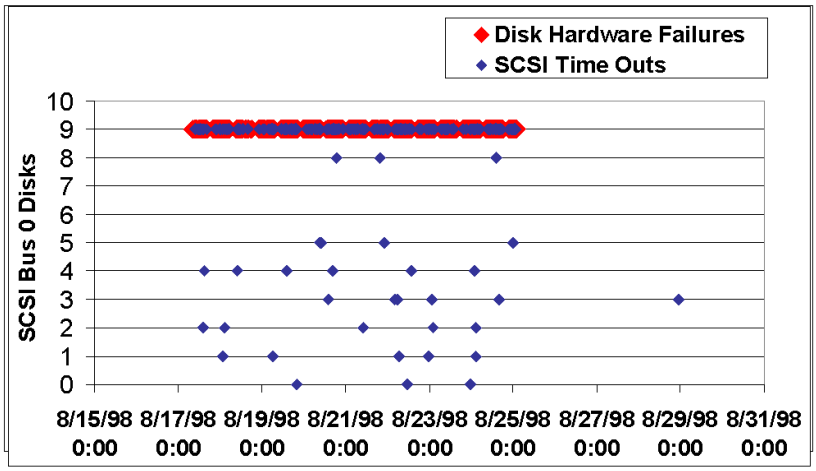

Figure 4-2. Side Effects of Disk Failure

This figure shows the failure process of the drive in case FDISK1. The X axis shows time, the Y-axis shows each disk on the shared bus. As the figure shows, the failing disk drive generated many SCSI Timeout messages. Also, while the drive was failing, neighboring drives also generated Timeout messages. These messages appear to be side effects of the failure, since they no longer appear after the failing drive is removed.

4.6. Summary

This chapter explored the failures of devices in depth. The analysis revealed some interesting insights. Devices that are about to fail generate a large number of error messages, increasing in intensity over time. This behavior makes it possible to use fault prediction algorithms to predict these failures. However, other events such as transient failures also behave in a similar way. These events are also often predicted as failures. The analysis suggests that failure prediction algorithms are far more effective if they are assumed to detect events that require human intervention, rather than events that require component replacement.

5 The Skippy Linear Stride Benchmark

5.1. Introduction

The past two chapters focused on soft error behavior of large scale storage systems. This chapter, and the two that follow, describe the second portion of this dissertation, addressing disk drive heterogeneity. The primary contribution towards this goal is the development of a new technique for characterizing disk drives. This technique of linear strides, named Skippy, is useful in that it is simple, it is an excellent match to the rotational latency of a disk drive, it allows many parameters to be extracted with a simple, fast and portable experiment, and in that it requires no prior information about the drive being measured. This chapter presents the basic technique. The two following chapters describe techniques for automatically extracting parameters from the Skippy graphical result and extensions of the basic benchmark.

The Skippy experiment uses single sector reads and writes through the raw (character) disk interface. The benchmark strides through the disk, increasing the step size between accesses with each iteration. The resulting latency vs. step size curve has a distinctive saw-

tooth shape from which we extract the following parameters: sectors/track ratio, rotation time, minimum time to access media, disk head positioning time, head switch time, cylinder switch time, and the number of recording surfaces.

The rest of the chapter is organized as follows. Section 5.2 covers background on disk drives and related work on modern disk measurement. Section 5.3 describes the write benchmark; we outline the algorithm and use an analytical model to illustrate the behavior that we expect. This section also presents the graphical results for a synthetic disk and for the IBM UltraStar XP SCSI drive described in Chapter 2. After comparing the synthetic disk's results to the IBM disk's results, we refine our analytical model further in Section 5.4. Section 5.5 presents measurement data on other SCSI and IDE disk drives. Section 5.6 presents the read version of the benchmark and results on the synthetic and IBM disks. Section 5.7 contains read results for the remaining disks and Section 5.8 summarizes the chapter.

5.2. Background and Related Work

Before describing the benchmark, we provide some background on disk drives and define the terms that are used in the rest of the paper. We only provide the disk background that is necessary to understand the benchmark. References [Schwarderer96], [Worthington95] and [Ruemmler91] describe disk internals in more detail. We also outline related work in disk drive measurement.

5.2.1. Disk Background

Figure 5-1 shows a disk drive's internal structure. There are several rotating disks coated on both sides with magnetic media. Each rotating disk is called a *platter;* each side is called a *recording surface.* Data is stored on each recording surface on concentric circles called *tracks*. Each track is divided into *sectors*; a sector is the minimum unit of data that can be accessed from the disk media. Typical modern disks have 512 byte sectors. The tracks from each surface that are equidistant from the center form a *cylinder*. Most disks use *Zoned Bit Recording (ZBR)* (not shown on figure); the outer cylinders have a higher sectors/track ratio than the inner cylinders.

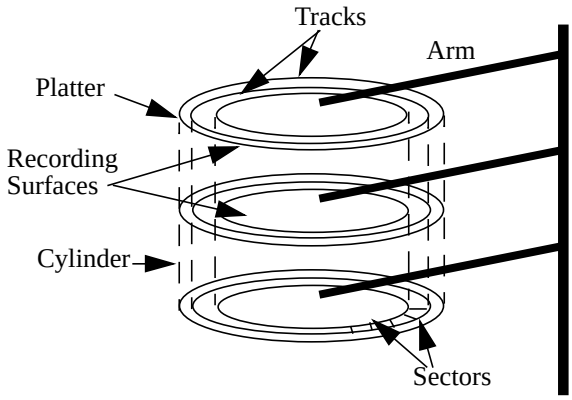

Figure 5-1. Disk Drive Basics

This figure illustrates *recording surfaces, platters, tracks,* and *sectors*. A disk drive contains a stack of rotating platters coated on one or both sides with magnetic media. Each magnetically coated surface is called a recording surface. Each platter contains concentric tracks; the tracks on each platter equidistant from the disk form a cylinder. Data is stored on a track in units of sectors.

The disk controller masks these details from the outside world. The operating system sees a disk as an array of blocks. Read and write requests address the disk by *Logical Block Address (LBA)*; the drive translates this *LBA* into the *CHS (Cylinder, Head, Sector)*

address. Logical block numbering starts with the outermost tracks and continues inward with each successive cylinder. Therefore, the sector after the last of any given track is the first of the next track in the same cylinder.

Each recording surface has its own read head and write head. The heads are ganged together on the disk arm. The time to move the arm to the right track is called *Seek Time* and the time for the required sector to rotate under the head is called *Rotational Latency*. The time to transfer the data from the media is called *Transfer Time*. In modern disks, only one head is active at any time. When an access spans two tracks, the disk must complete the portion on the first track, switch heads, and continue on the second track. The sector mappings on consecutive tracks are skewed to allow for this *Head Switch* time. Switching heads requires a short repositioning time; the skew prevents a request that crosses track boundaries from missing the next logical block and having to wait a full rotation. Similarly, if an access spans two cylinders, the disk arm has to seek forward one cylinder. Consecutive cylinders are skewed to allow for this *Cylinder Switch Time*.

5.2.2. Related Work

Saavedra [Saavedra92, Saavedra94] introduced a simple, yet powerful, mechanism to extract performance characteristics from a multi-level memory hierarchy. The benchmark repeatedly executes a loop of reading memory locations in a fixed size array at a given stride. Surprisingly, almost all the characteristics of the memory hierarchy, including number of caches, their capacity, associativity, block size, and access times, can be extracted by changing the size of the array and the length of the stride. This technique,

unfortunately, cannot be applied directly to disk drives. The complex interaction between mechanical and electronics functions makes the results much more unpredictable and difficult to decipher than the those that occur when the benchmark is run on a memory hierarchy.

Ganger and Worthington [Worthington95] described partially automated tools for extracting parameters from SCSI disk drives. They used a twofold approach, interrogative and empirical extraction. Interrogative extraction uses a library of SCSI access functions to read the disk's Mode Pages. The mode pages describe disk parameters like the sectors/track ratio, prefetch buffer size, and so on. The information extracted from the mode pages is used to construct test vectors for the empirical extraction process. They measured the minimum time between requests (MTBRC) of various kinds. By comparing the MTBRCs of different test vectors, they calculate switching times and other parameters.

The main disadvantage of this approach is that the user needs to know about the SCSI subsystem. In particular, the user must be able to send low level SCSI commands to the disks, requiring in turn that each drive manufacturer support the required commands. If the disk is not SCSI, but IDE, then the user would need access to low level IDE commands. Also, each parameter requires a separate group of test vectors. The ideal benchmark would combine the simplicity and elegance of the Saavedra solution to the accuracy of the Ganger and Worthington approach.

5.3. The Write Benchmark

This section describes the write version of the Skippy benchmark. We present the algorithm and use a simple analytical model to illustrate the behavior that we expect. We parametrize this analytical model with a synthetic disk and show the expected graphical result. Next, we present the results on an actual disk, the IBM Ultrastar XP. Finally, we extract the IBM disk's geometry and switching latencies from the result graph and compare them to the manufacturer specified values.

5.3.1. The Algorithm

The benchmark does a sequence of single sector writes and seeks through the raw device interface; Figure 5-2 shows the pseudocode. By using the raw device interface, we can bypass file optimizations activities like caching, buffering, and read ahead. The benchmark writes one sector to the disk, seeks and writes again. At each iteration, the seek distance (or StepSize) increases by one.

```
int i;
open (raw disk device);
for (i=0; i< Number of Measurements;i++)
{
            Read start time
       lseek(raw device, i);
       write(1 sector)
}
close (raw device);
```

Figure 5-2. Pseudocode for the Write Version of Skippy.

At this point, it is important to distinguish between the algorithm's notion of seeks (or steps) and the traditional definition of seeking. As mentioned in the prior section, *Seek Time*, in the disk context, means the time to move the disk arm to the correct track. In the operating system context, an *lseek* causes the operating system to change the current position in the device file. Lseek calls have no direct relationship to actual disk seeks. In this benchmark, we limit the step sizes between requests to less than a cylinder. Therefore, the benchmark does not cause the disk arm to move further than a cylinder switch. To maintain the distinction between benchmark steps and disk seeks, we refer to the distance between two benchmark accesses as the *Step Size*, not *Seek Distance*.

The terms used in the analytical model are defined below. These terms are used in the rest of this chapter and the following two chapters. whenever possible, we use the full name of each term, rather than the abbreviation.

Tl: *Transfer Time*. The time to read data from or write data to the surface.

Mtm: *Minimum Time To Media*. This is the minimum time access data on the disk surface. A disk request completes in *Mtm+Tl* when it incurs no rotational or seek latency.

s: *Step Size* in sectors between the last request position and the current request position. (the value of the second argument to *lseek*).

t: *Sectors/track ratio*.

p: *Position of the last access* relative to the start of the current track.

Rl: *Time for one full rotation.* We call this *Full Rotation Time*. *Rotational Latency*, on the other hand, is the time that a given request spends waiting for the required sector to rotate under the head. The *Rotational Latency* can vary anywhere between zero and the *Full Rotation Time*.

Hsw: *Head Switch Time.*

Csw: *Single Cylinder Switch Time*

Stm: *Number of sectors that the disk rotates in Minimum Time to Media*. Equation (1) defines *Stm* in terms of *Mtm*, *t*, and ***Rl***, as

Equation 5-1. $$Stm = \frac{MinimumMediaTime \times SectorsPerTrack}{FullRotationTime}$$

Note that equation 5-1 assumes a linear relationship between the latency and the number of sectors rotated. It is well known that seek time does not increase linearly with seek distance. However, as we stated earlier, the step sizes used do not generate any arm movement; the delay is purely rotational. Since the disk rotates at a fixed speed, the delay increases linearly with the number of sectors rotated.

Figure 5-3 shows the expected sequence of events for two single sector writes labeled *W1* and *W2*. We assume that the step size between the writes is small enough that the two requests will be on the same track. The figure shows five stages that each write goes through; the disk rotates a few sectors between each stage. *W1*, starts at time *W1Start*. By time *W1atDisk*, the OS and SCSI subsystem have processed the request and the command has reached the disk. By time *W1atSurface*, the disk has positioned the head on the neces-

sary track. By time *W1underHead*, the required sector is under the disk head. The difference between *W1atSurface* and *W1underHead* is the *Rotational Latency* for *W1*. By *W1End*, the write system call has returned. Some short time later, the second write begins. The figure does not explicitly show transfer time, but *W1End-W1atSurface* includes the transfer time, *Tl*. By *W2atSurface*, the disk has already rotated some distance forward. In the illustration, the step size *s* is greater than this distance; the required sector is still up ahead and the second request can be served in the same rotation.

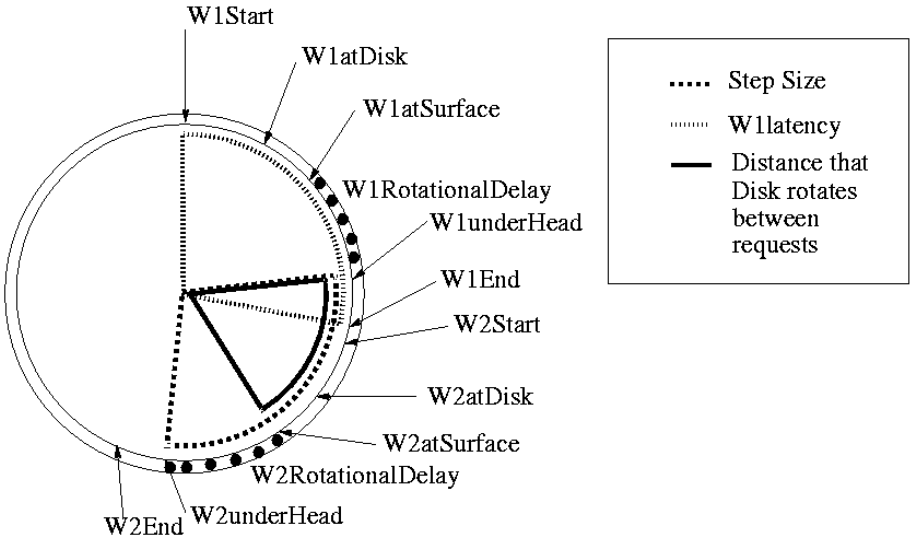

Figure 5-3. Sequence of Events for Two 1 Sector Writes

This figure shows the expected sequence of events for two 1 sector writes to the disk media. The writes are labeled W1 and W2.

The time between *W1End* and *W2Start* is the time to start the next loop iteration and execute the *lseek* call; this time is negligible compared to the disk access times. In our system, it is on average 7-8us, while the entire write takes between 2000-10000 us. If we assume that the time between *W1End* and *W2Start* is negligible, we can make some interesting observations:

(i) As the rotational delay approaches zero, *W2End-W2Start* becomes *MinimumMedia-Time+TransferTime*.

(ii) When the rotational delay is eliminated, *W2atSurface-W1atSurface* is also *Minimum-MediaTime*. Therefore, the disk rotates for approximately *Mtm* time, or over *Stm* sectors, between any two requests. In other words, if *StepSize < Stm, W2* will need an extra rotation. If *StepSize>Stm, W2* can complete in the same rotation as *W1*.

Using the above logic, we can model the latency of the second write request. If the access is on the same track as the prior access, (i.e *p+StepSize < Sectors/Track*), and *StepSize > Stm*, the request can be satisfied in the current rotation and the latency is

Equation 5-2. $$Latency = \frac{(StepSize - Stm) \times FullRotationTime}{SectorsPerTrack} + MiminumMediaTime + TransferTime$$

This latency is the minimum time to media plus the time to rotate the remaining sectors. Substituting equation 5-1 into 5-2 gives us a simpler term for the latency:

Equation 5-3. $$Latency = \frac{StepSize \times FullRotationTime}{SectorsPerTrack} + TransferTime$$

As the equation shows, the latency is a linear function of the step size. If *StepSize<Stm*, the request is satisfied in the next rotation, and the latency is given by equation (4):

Equation 5-4.

$$Latency = \frac{(SectorsPerTrack + StepSize - Stm)}{SectorsPerTrack} \times FullRotationTime + MinimumMediaTime + TransferTime$$

Equation 5-4 can also be simplified by substituting 5-1, giving equation 5-5:

Equation 5-5. $$Latency = \frac{StepSize \times FullRotationTime}{SectorsPerTrack} + FullRotationTime + TransferTime$$

When *StepSize*<*Stm*, the latency is still linear in *StepSize* with the fixed vertical offset equal to *FullRotationTime*. If the step puts the new request on a different track (*p*+*StepSize* > *Sectors/Track)*, then the request incurs an extra head switch delay. Since the tracks are skewed, a head switch does not cause the disk to have to wait a full rotation. In this case, the latencies can be calculated as in equations 5-6 and 5-7, When *StepSize*>*Stm*:

Equation 5-6.

$$Latency = \frac{(StepSize - Stm) \times FullRotationTime}{SectorsPerTrack} + MinimumMediaTime + HeadSwitch + TransferTime$$

When *StepSize*<*Stm*:

Equation 5-7.

$$Latency = \frac{(SectorsPerTrack + StepSize - Stm)}{SectorsPerTrack} \times Rl + MinimumMediaTime + HeadSwitch + TransferTime$$

The equations for a cylinder switch are similar, with *CylinderSwitchTime* in place of *Head-SwitchTime*.

Note that all these equations assume that there are no long distance seeks going on. This model and the benchmark are not intended to for step sizes that cause seeks greater than a single cylinder. After that point, there is significant arm movement and the latency does not scale linearly with step size.

5.3.2. Graphical Result

Now we evaluate the above equations using a synthetic disk whose parameters are listed in Table 5-1. The synthetic disk is 7200 RPM, with 15 recording surfaces containing 150 sectors per track. The minimum time to access media is 2.0 ms, and the head and cylinder switch times are 0.7 ms and 2.1 ms respectively. Since the benchmark does not create long distance seeks, we do not specify a seek profile.

Parameter	Value
Sectors/Track	150
Full Rotation Time	8333.33 us
Minimum Media Time	2000 us
Number of Heads	15
Head Switch Time	700.00 us
Cylinder Switch Time	2100.00 us

Table 5-1. Parameters for Synthetic Disk Drive

This table lists the parameters for a synthetic disk drive. These parameters are used in this section and section 5.6 to illustrate the expected graphical results for the write and read versions of the benchmark.

Figure 5-4 shows the expected graphical result; the accompanying illustrations, Figures 5-5(a-d), show what happens at points (1) through (4) in the graph. Each illustration shows two writes; the second write shows the request pattern at the marked point in the graph. Each track is shown as two concentric circles; the rotational delay for Write1 is marked on the outer circle and the rotational delay for the Write2 is marked on the inner circle. The illustrations do not show *Transfer Time*; since we are focusing on single sector accesses, the transfer time is nearly negligible. We will discuss *Transfer Time* further when we extract parameters in the next section and when we deal with larger transfer sizes in the next chapter.

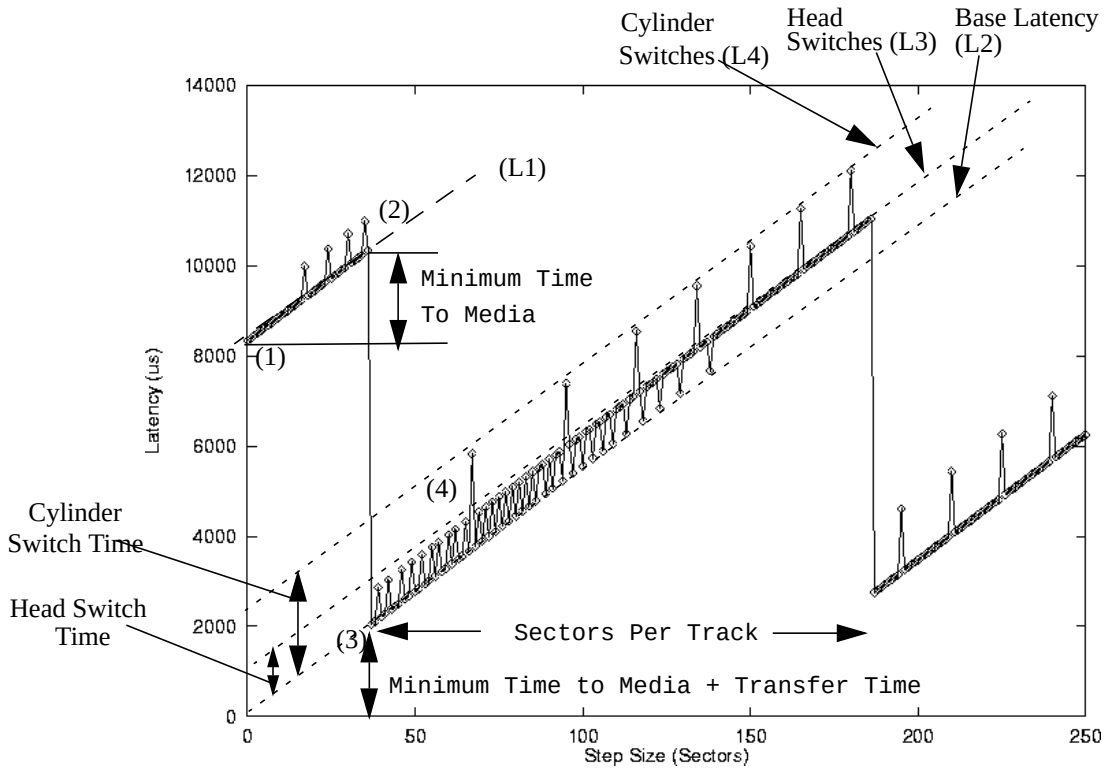

Figure 5-4. Expected Skippy Result

This figure shows the expected result for the Skippy benchmark, derived by evaluating the analytical model using the synthetic disk parameters. The X axis shows step size in sectors, and the Y axis shows write latency in microseconds.

As the step size increases linearly, the latency follows a sawtooth pattern. At point (1), (Figure 5-5(a)) StepSize is zero, causing a large rotational delay for Write2 and making W2Latency equal to the Full Rotation Time *Rl*. As *StepSize* increases, the latency increases linearly as in equation 5-4. When *StepSize* approaches *Stm*, equation (4) shows that the latency approaches *MinimumMediaTime+FullRotationTime*. At point (2) (Figure 5.5(b)), *StepSize* is almost *Stm*. By the time the disk head is lowered on the track, the required sector has just been missed and a full rotation takes place. The latency is therefore the *Full Rotational Time* plus *MinimumMediaTime* overhead.

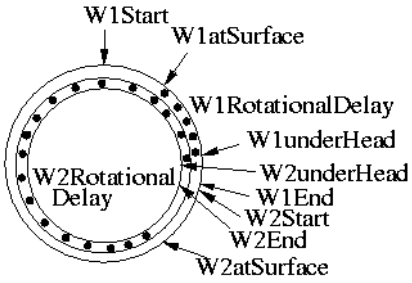

Figure 5.5(a)

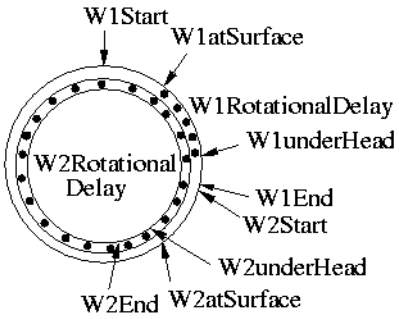

Figure 5.5(b)

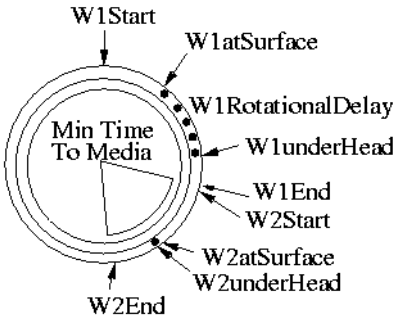

Figure 5.5(c)

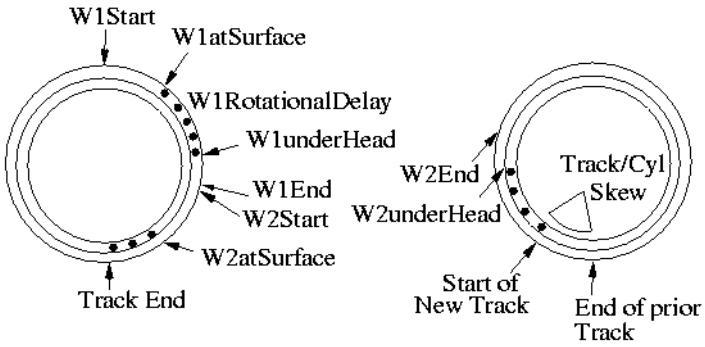

Figure 5.5(d)

Figure 5-5. Illustrations of Behavior in Skippy Result

Figures 5(a) and (b) show the request patterns at points (1) and (2) in the graph. At point (1), step size is close to zero, causing a large rotational delay for W2. W2's latency is equal to the Full Rotation Time. At point (2), the required sector is just missed, making the latency the Full Rotation Time plus Mtm overhead.Figure 5.5 (c) and (d) show the behavior at points (3) and (4) in the graph. At point (3) the required sector is available exactly when the head is positioned; there is no rotational latency. Figure (d) shows what happens when a head or cylinder switch occurs

A few steps later, we reach point (3) (Figure 5-5(c)), where *StepSize* is slightly larger than *Stm.* In this case, the disk head is lowered just in time and there is no rotational latency. The latency therefore becomes *MinimumMediaTime*. From then on, as *StepSize* increases, the latency increases linearly as in equation 5-2. The graph has a sawtooth shape; the transition happens at *StepSize=Stm*.

The graph also shows a series of upward spikes that correspond to head and cylinder switches. Point (4) (Figure (5-5(d)) illustrates a head switch. In this case, the rotational latency is increased by *HeadSwitchTime* as specified by equation 5-6. The smaller spikes correspond to head switches and the larger spikes correspond to cylinder switches.

5.3.3. Extracting Parameters

Figure 5-4 exposes many useful disk details. The X coordinate of point (3) is *Stm* and the Y coordinate is *MinimumMediaTime+TransferTime.* Since the transfer time is very small for a single sector, the Y coordinate of point (3) is a good estimate for *MinimumMediaTime*. *Mtm* is also the difference between the Y coordinates of points (1) and (2). *FullRotationTime Rl* is the latency at step size 0 and the height of the transition at the *MinimumMediaTime* point.

Using this information, we can calculate the number of sectors per track. Since we know that the *MinimumMediaTime* point is reached when *StepSize=Stm*, we can reverse equation 5-1 to calculate the Sectors/Track ratio *t*:

Equation 5-8. $$SectorsPerTrack = \frac{Stm \times FullRotationTime}{MinimumMediaTime}$$

Note that we can only calculate the sectors/track ratio for the region that was written. Most modern disks employ Zone Bit Recording; outer cylinders have more sectors per track than inner cylinders. To get the Sectors/Track ratio of other regions in the disk, we will need to run the benchmark on those regions as well.

As *StepSize* increases, the latencies form three distinct lines with the same slope and different offsets. Figure 5-4 shows four lines labeled L1 through L4. L1 conforms to equation 5-4 and L2 conforms to equation 5-2. By taking the difference in offsets between these two lines, we can calculate the rotation time. The slope of each line is *FullRotationTime/SectorsPerTrack*. Once *FullRotationTime* is known, we can extract the Sectors/Track ratio from the slope value.

Each point on L3 represents a head switch and the latencies conform to equation 5-6. Hence, the vertical offset between the L3 and the L2 is *HeadSwitchTime*. Each point on L4 corresponds to a cylinder switch; the vertical offset between the third line and L2 is *CylinderSwitchTime*.

Finally, while the step size is less than the number of sectors per track, we can get the number of recording surfaces by counting the number of head switches between two cylinder switches. We can also calculate the number of recording surfaces from the total step distance between two cylinder switches. Since the benchmark moves forward with each step, the distance between the sectors accessed at step sizes *s1* and *s2* is not simply *s2-s1*. If we assume that the benchmark started by writing sector 0, the address of the sector written at step size *s1* is the sum of *s1* iterations of the arithmetic progression starting at 0 with increment 1. This sum is

Equation 5-9. $$\frac{s1 \times (s1+1)}{2}$$

We can calculate the address of the sector written at step *s2* in the same way. Taking the difference between these two addresses gives us the actual step distance between the measurements at step sizes *s1* and *s2*. The total distance between the two accesses is

Equation 5-10. $$StepDist = \frac{(s2-s1)}{2} \times (2s1 + (s2-s1))$$

Since we already know the number of sectors per track, the number of recording surfaces is

Equation 5-11. $$RecordingSurfaces = \left\lceil \frac{StepDist}{SectorsPerTrack} \right\rceil$$

As the step size gets larger, the number of steps between successive head and cylinder switches decreases. As figure 5-4 shows, after *StepSize* is greater than *SectorsPerTrack+Stm*, every step causes a head switch.

5.3.4. A Sample Result

The prior section showed how all the parameters in Table 5-1 can be extracted from Figure 5.4. Now we apply these techniques to the IBM UltraStar XP disk drive [UltraStar96]. From the manufacturer specifications we learn that this disk is 7200 RPM (8.33 ms rotational latency), with 9 platters (18 recording surfaces) and 8 recording zones, the outermost of which has 184 sectors per track. The head and cylinder switch times are 0.85 ms and 2.17 ms respectively.

Figure 5-6 shows the result of running the benchmark on this disk; the figure is quite similar to the model result in Figure 5-4. The result follows the behavior predicted by equations 5-1 through 5-6. Equation 5-7, however, does not completely explain the result of head and cylinder switches while *StepSize*<*Stm*. In Figure 5-4, head switches always cause upward latency spikes consistent with 5-7; figure 5-6 shows upward spikes for small *StepSize* and also some downward spikes as *StepSize* approaches *Stm*. This variation does not affect our ability to extract the necessary parameters, but it does require a refinement of the analytical model. We refine the model in Section 5-4; for now, we focus on extracting parameters from Figure 5-6.

Following the parameter extraction techniques described earlier, we get the following measured values. *FullRotationTime* from the Y coordinate at point (1) is 8.39ms; the actual latency is 8.33ms and the error is 0.73%. If we use the height of the sawtooth wave to estimate *Rl*, we get 8.30ms. In this case, the error is 0.43%. Both techniques for estimating *Rl* yield extremely accurate results.

The X coordinate value of point (3) is 47 and the Y coordinate value is 2.20ms. As equation (2) states, the offset of L2 is the *Transfer Time*; this value is 0.06ms. Since we are writing only 512 bytes, the transfer time is very small. By subtracting *Transfer Time* from the Y coordinate value at point 3, we estimate *MinimumMediaTime* to be 2.1 ms. In fact, since the transfer time is so small, its effect on the *Mtm* value is virtually indistinguishable from measurement noise and the Y coordinate value is itself a good estimate of *Mtm*. On the other hand, if we estimate Mtm as the difference between the Y values at points (1) and

(2), we get 1.87ms. *Mtm* is a system specific value and has no counterpart in the specification. It is however, an important estimate of file system overhead.

The sectors/track ratio is 181.9; since the actual sectors per track is 184, the error is 1.1%. The measured head switch time is 0.87 ms, a 2.3% error compared to the specification. Similarly, the measured cylinder switch time is 2.19ms, a 0.9% error compared to the specification. Finally, by counting the number of head switches between cylinder switches, we find that the disk has 18 recording surfaces. This value matches the disk specification. For this disk drive, the extracted values are very close to the actual values. In all cases, the error rate is less than 3%.

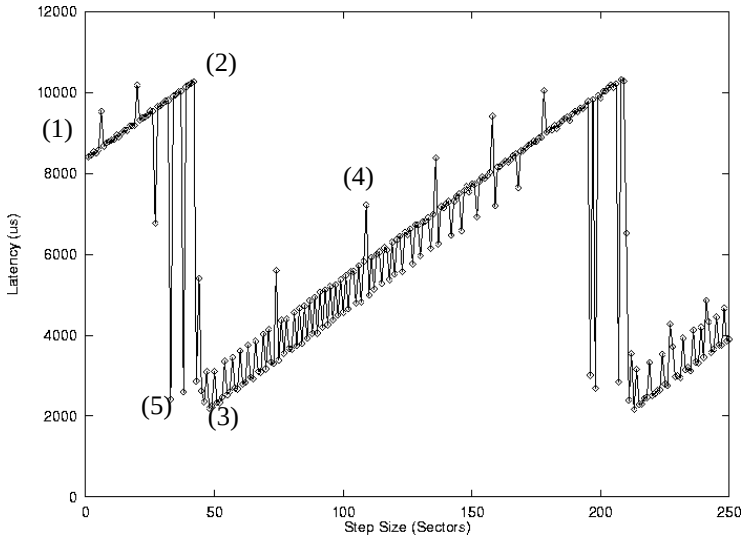

Figure 5-6. Skippy Write Result for IBM UltraStar XP disk drive

For the most part, the graph is similar to the expected graph in Figure 5-4. The one exception is that labeled in point (5). The graph shows some extra downward transitions right before the *Mtm* point. These transitions occur when a head switch happens when *StepSize* is close to *Stm*. This effect is explored further in section 5.4.

5.4. A Refined Analytical Model For Writes

Figure 5-6 showed that the simple model is inadequate for describing some parts of the benchmark behavior. In particular, the graph shows some downward spikes in the region *StepSize*<*Stm* that are not explained by equation 5-7. In this section, we present a refinement to the initial model to explain these effects.

In Figure 5-6, the downward spikes near point (5) happen when a head switch occurs while *StepSize* is close to *Stm*. In normal circumstances, when there is no head switch, the mechanics of equation 5-4 apply; there is not enough time to position the head and service the write in the same rotation as the prior write. When a head switch occurs, however, the track skew gives the disk head slightly extra time, enabling the disk to service some writes without waiting an extra rotation. These writes can complete with latencies close to *Mtm*. Figure 5-6 shows that these downward spikes actually extend L3, the head switch line, to the left of the *Mtm* point. This observation confirms our hypothesis that the spikes are caused by head switches.

To refine the model, we need to break *Mtm* down into two parts:

Mov: The sum of operating system, SCSI and disk electronics overheads to process the request.

Sov: The number of sectors the disk rotates in time *Mov*.

Mdp: The disk positioning time. This is the minimum time needed for the disk to position the arm over the required track.

Mov is the minimum time between the disk's completing the first request and *receiving the second request.* Any request where *StepSize*<*Sov* is not serviceable within the current rotation whether it includes a head switch or not. The gray area is when *Sov* <*StepSize* < *Stm*. Equation 5-12 gives the write latency when *Sov*< *Size* < *Stm*, *p*+*StepSize* > *SectorsperTrack* and a head switch occurs:

Equation 5-12.

$$Latency = \frac{(StepSize - Sov) \times FullRotationTime}{SectorsPerTrack} + Mov + HeadSwitchTime + TransferTime$$

Once again, the latency when a cylinder switch occurs can be calculated by replacing *HeadSwitchTime* in equation 5-8 with *CylinderSwitchTime*.

To evaluate the refined model, we need to add two parameters for the synthetic disk's profile in Table 5-1 We assume that *Mov* and *Mdp* are each 1.0 ms. Figure 5-7 shows the refined model parametrized for the synthetic disk.; the refined model shows the downward spikes as expected. We can use the step size at which the first downward spike occurred to estimate the value of *Mdp*, and hence *Mov*. Therefore, we can get finer estimates of operating system/interconnect overheads as well as estimates of disk positioning time.

In Figure 5-6, the result for the IBM disk, the first downward spike happened at step size 33. The *Mtm* point was at step 47. Therefore, we can estimate *Mdp* as the time taken to rotate 47-33, or 14 sectors. This time is 634 us. Since *Mdp* and *Mov* add to *Mtm, Mov* is 1565 us.

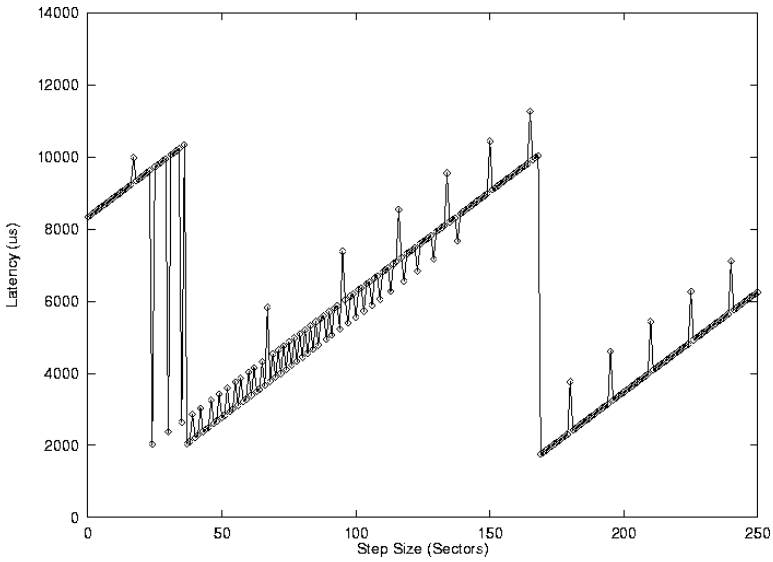

Figure 5-7. Refined Model Result for Synthetic Disk

The refined model is much closer to the actual result in Figure 5-6 than the initial model. In particular, it shows several downward spikes before the main transition, much like the sample result.

5.5. Write Measurements

The section describes how the benchmark can be used to extract parameters from a range of modern SCSI and IDE drives. Table 5-2 lists the drives that we measured; the table gives each drive's year, interface, capacity, dimension, RPM, Full Rotation Time and the number of recording surfaces. The remaining details, like head and cylinder switch times, were available only for the IBM UltraStar XP drive [UltraStar96]. For the rest, the table contains all the information that we were able to gather from the manufacturer's specification sheets [Seagate99, Micropolis99, IBM99, Quantum99]. We measured five SCSI disk drives and two IDE disk drives.

Model #	Year	Interface	Capacity (GB)	Dimension	RPM	Full Rotational Latency (ms)	Recording Surfaces
Seagate ST32430W (Hawk)	1994	SCSI	2	3.5in, LP	5411	11.1	9
Seagate ST15150W (Barracuda)	1995	SCSI	4	3.5in, HH	7200	8.3	21
MicroPolis 3391 SS	1996	SCSI	8	3.5in, HH	7200	8.3	22
IBM (UltraStar XP)	1996	SCSI	8	3.5in HH	7200	8.3	18
IBM 9ZX	1998	SCSI	8	3.5in HH	10020	6.0	12
Quantum Fireball EX 3.2A	1998	IDE	2	3.5in LP	5400	11.1	2
IBM-DTTA-351010	1997	IDE	9.6	3.5in, LP	5400	11.1	6

Table 5-2. Description of the Disks in the Testbed.

These disks are between 1 and 4 years old and range from 5400 RPM to 10020 RPM. We only have detailed specifications for the IBM UltraStar XP disk drive. The table contains all the relevant information that we were able to gather for the other disk drives from their on-line specification sheets. All drives are 3. 5 in; HH and LP mean Half Height and Low Profile respectively.

5.5.1. SCSI Disk Drives

Figures 5-8 through 5-11 show the results for the SCSI drives on the write version of the benchmark. The graphs are ordered in increasing RPM, from the 5411 Hawk to the 10020 RPM 9ZX drive. Table 5-3 summarizes the measurement numbers for each disk. The UltraStar XP's numbers are included in the table for comparison.

In all four cases, *FullRotationTime* is clear from the height of the sawtooth wave. For the 5400 RPM Hawk, the wave is about 11.22 ms high; the error rate is 0.9%. For the 7200 RPM Barracuda disk, it is about 8.43 ms; the error rate is 1.2%. The estimated rotation time for the Micropolis disk is 8.41ms; the error rate is 0.9%. Finally, the rotation time of the 10,000RPM 9ZX is 6.06ms, giving an error of 1.0%.

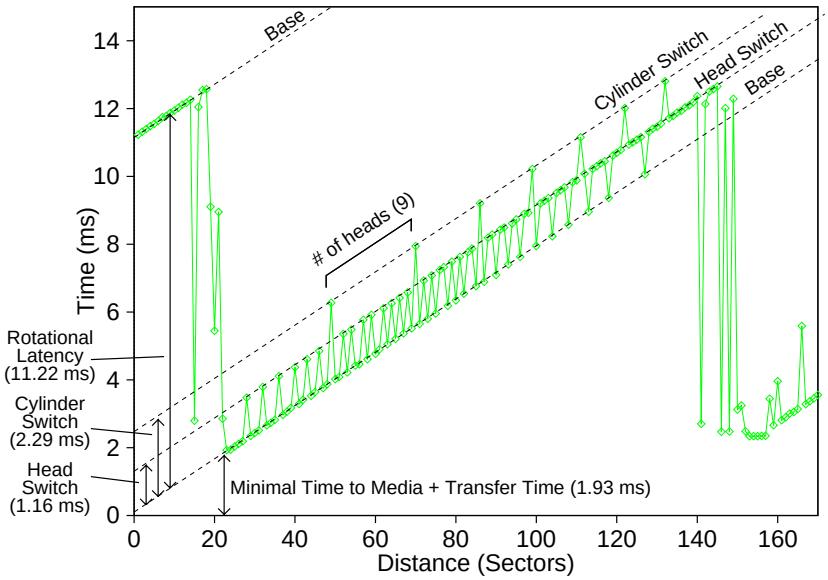

Figure 5-8. Skippy Write Result for 5400 RPM Seagate Hawk

The result shows the characteristic sawtooth shape. For a slightly older disk drive, the head and cylinder switch times are quite good. The disk also has an odd number of recording surfaces, typical of Seagate drives.

The measurements show that *MinimumMediaTime* can vary somewhat between disks of the same RPM and generation. The Hawk's average MTM is 1.9 ms, while the *Mtm* for the 7200 RPM disks ranged from 1.8ms to 3.8ms. The lowest, 1.8 ms, was the Seagate Barracuda, while the highest, 3.8 ms, was the Micropolis drive. Finally, the latest disk, the 10000 RPM 9ZX, had the lowest *Mtm* value of 1.4 ms. Since these disks were measured on the same testbed, we can assume that the operating system and SCSI overheads are similar. Therefore, the results show that the IBM drive has the lowest overhead to access media, with the Seagate Hawk and Barracuda drives not far behind. Interestingly, the Seagate Hawk, which is considerably older than the 7200 RPM drives, still has a better *Mtm* than both the IBM Ultrastar and the Micropolis drive.

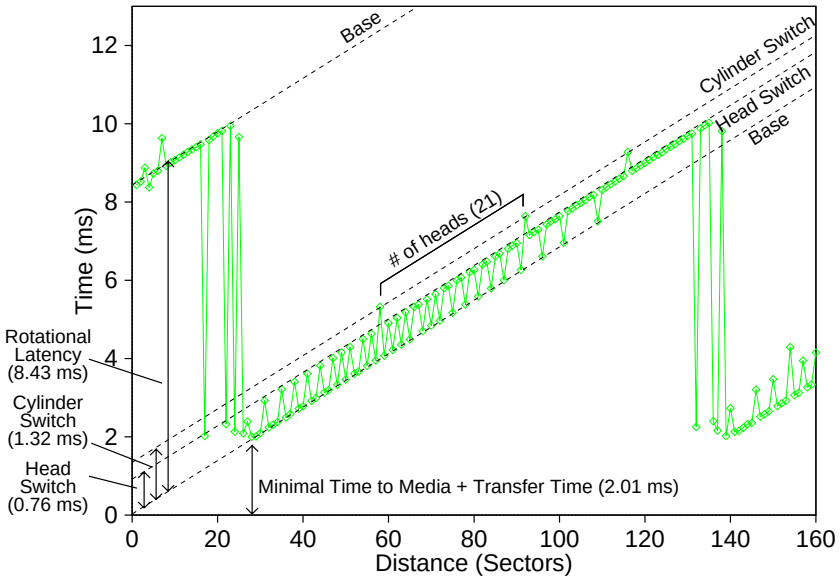

Figure 5-9. Skippy Write Result for 7200 RPM Seagate Barracuda

Like the previous figure, the Barracuda result shows very good switching times and an odd number of recording surfaces, typical of Seagate disk drives.

Since all of the measured drives employ Zone Bit Recording, we extract the Sectors/Track ratio for the outermost zone of each drive. The Hawk has around 142 sectors per track, the Barracuda about 123, the UltraStar 186, the Micropolis 201, and the 9ZX about 224. Finally, we compare the head and cylinder switch times. As the graphs show, the Seagate Barracuda drive has the lowest head and cylinder switch times. The Hawk's cylinder switch time is comparable to that of the UltraStar XP, even though the Hawk is an older drive.

By counting the number of head switches between cylinder, we learn that the Hawk has 9 recording surfaces, the Barracuda has 21, the Micropolis has 22, and the 9ZX has 12. The numbers for the Hawk, Barracuda and 9ZX match the specification data in Table 5-2.

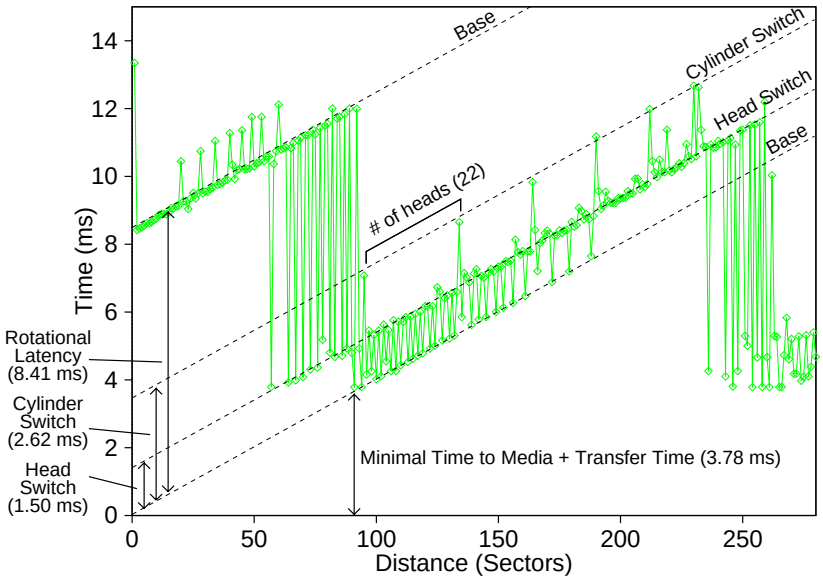

Figure 5-10. Skippy Write Result for 7200 RPM Micropolis Drive

The Micropolis drive is the worst performer in the SCSI group, with high switching times and extremely high minimum time to media. The result itself has more noise than the Skippy results of the other SCSI drives.

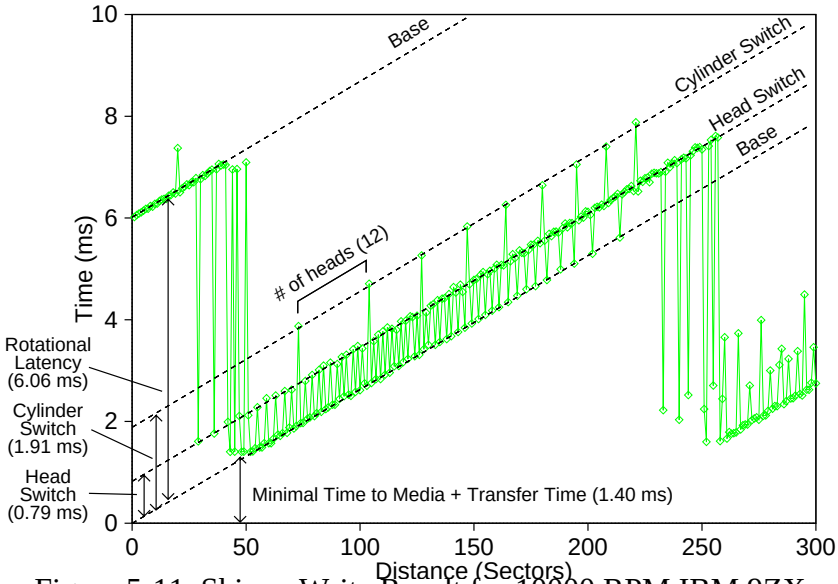

Figure 5-11. Skippy Write Result for 10000 RPM IBM 9ZX

This is the most recent drive in the collection. As a result, it has very good switching times and lowest minimum media time of all SCSI drives.

Disk	Full Rotational Latency (ms)	Minimum Time to Media (ms)	Sectors/ Track (outermost)	Number of Recording Surfaces	Head Switch Time (ms)	Cylinder Switch Time (ms)
Hawk (5400)	11.22	1.93	142.37	9	1.16	2.29
Barracuda (7200)	8.43	2.01	123.35	21	0.76	1.32
Micropolis (7200)	8.41	3.78	201.72	22	1.50	2.62
UltraStar (7200)	8.39	2.19	186.15	18	0.85	2.20
9ZX (10020)	6.06	1.40	224.69	12	0.79	1.91

Table 5-3. Extracted Parameters for SCSI Disk Drives

Table 5.3 lists the extracted parameters from each SCSI disk drive. The parameters for the IBM UltraStar XP disk are included for comparison.

5.5.2 IDE Disk Drives

Figures 5-12 and 5-13 show the write behavior for the Quantum and IBM IDE disks. These graphs show caching activity at the lower step sizes. In fact, it appears that the drives write to the buffer cache for several requests, and then empties the cache as additional requests are received. This behavior causes the entire result graph to shift to the right.

Although the graphs are slightly shifted, we can measure the rotational latency as the height of the transition at the *MinimumMediaTime* point. The measured *Full Rotation Time* is a 11.4ms, a 3% error over the specification value of 11.1 ms. The graph shows that the Quantum disk has only two recording surfaces, consistent with the disk specifications in Table 5.3. The Quantum drive also has a head switch time of 2.19ms and a cylinder switch time of 2.89ms.

The measured rotation time of the IBM disk is 11.04ms, a 0.7% error compared to the specification. The sectors per track ratio is 330.01 and the disk has 6 recording surfaces. The

head switch time is 1.93ms and the cylinder switch time is 3.81ms. This disk's *Mtm* value is 1.02ms.

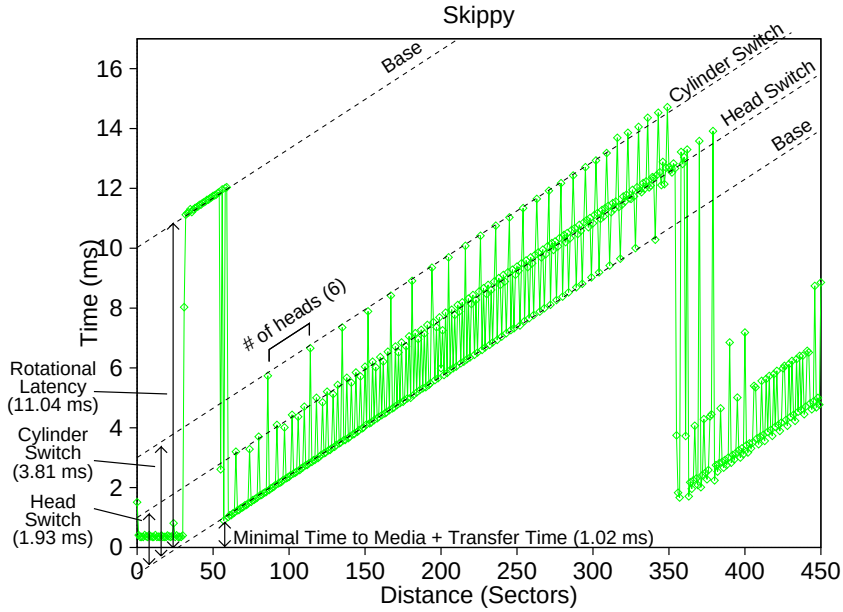

Figure 5-12. Skippy Write Result for 5400 RPM IBM IDE Drive

This IDE drive shows evidence of write caching at the smaller step sizes. The head and cylinder switch times are considerably higher than those of the SCSI drives, although the minimum time to media is lower.

5.5.2. Discussion

We can make several interesting observations from these measurements. First, we see that *MinimumMediaTime* can vary widely, even between the same generation of disk drives. Among the 7200RPM SCSI disks, the Barracuda has the lowest *Mtm*, while the Micropolis drive has the highest. In general, the Micropolis drive has the worst mechanical latencies of all the SCSI disks; its head and cylinder switch times are also much higher than those of any other SCSI drive. The Seagate drives appear to have the best mechanical latencies; the

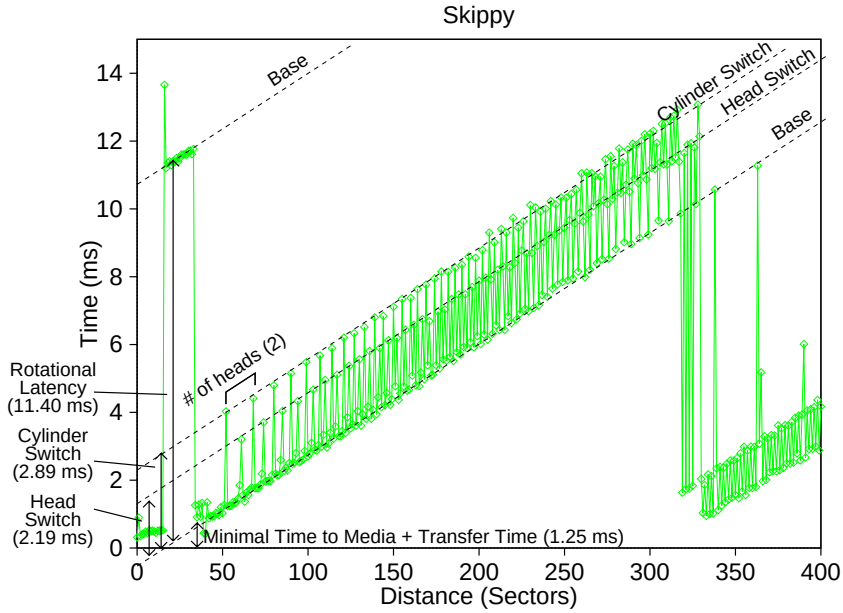

Figure 5-13. Skippy Write Result for 5400 RPM Quantum Fireball IDE Drive

Like the previous IDE drive, this result also shows evidence of write caching, higher switch times, and lower minimum time to media.

Barracuda's switching times are lower than the 9ZX, even though the 9ZX is a newer disk. Even the 5400 Hawk's switching times are comparable with the 7200RPM drives.

Second, the number of recording surfaces varies widely between disks. In general, the number of recording surfaces increases with capacity and decreases over time. For instance, the IBM 9ZX has the same capacity as the Barracuda and UltraStar, but has less recording surfaces because it is a newer disk, most likely with a higher areal density. The results also show that some disks have an odd number of recording surfaces. When we first took these measurements, we were surprised to find an odd number of heads, since it implies that one side of one of the platters is not used.

Finally, if we compare the SCSI and IDE disk results, we see that the IDE disks have a much lower *MinimumMediaTime* than the SCSI disks. Both IDE disks also show buffering activity at the smaller step sizes, something we did not see with any of the SCSI disks. The switching times of the IDE disks are also considerably higher than the SCSI disks.

5.6. Read Benchmark

The prior sections explored the benchmark's behavior when the accesses are single sector writes. Now we look at what happens if reads are used instead. The main advantage of using reads is that the benchmark can be run on a disk without damaging its contents. However, reads are more complicated than writes because many disks employ read ahead optimizations. The disk maintains a prefetch buffer; after the current sector is read, the disk reads the next few sectors into this buffer. If the request pattern is sequential, the next desired sector could be in the prefetch buffer before the request arrives. Each disk manufacturer has its own algorithm for read ahead. As we will see in the next few sections, such optimizations can make read results widely different between disks of different manufacturers.

In this section, we explore the read behavior by creating an analytical model and parameterizing it with our synthetic disk. This way, we illustrate how the graphs will look under different read ahead policies. We also describe how to extract parameters from read graphs. We round out this section by presenting the result for the IBM UltraStar XP disk.

5.6.1. Expected Behavior

We begin, as we did in section 5.3.1, by outlining the expected result of the benchmark. Unlike the write experiment, where all requests are handled in the same way by the disk, each request in the read benchmark falls into one of three distinct categories. A request's category defines what the disk needs to do to service the request and hence determines the request latency. The three categories are:

(i) In Prefetch Buffer: In the time between when the prior request completed and the current request arrived at the disk, the sector had been read into the prefetch buffer. In this case, the disk's task is very simple, return the sector from the prefetch buffer.

(ii) Immediately Ahead In Read Path: The required sector is not in the prefetch buffer but is immediately ahead in the read path. The disk chooses to read all sectors between the current sector and the requested sector. Hence, the disk does not have to reposition the head, merely wait till the required sector rotates under the head.

(iii) Far From Read Path: In this case, the required sector is far away from the sector currently being read. The disk will stop the ongoing read process and reposition the head to serve the new request.

Each disk's will have a different read ahead algorithm. Therefore, the transitions between the above three categories will occur at different step sizes in different disks. Where the transitions occur determines the shape of the result curve. We use the following terms to define the transition points in our initial model:

Mbuffer*:* Minimum time to read a sector's worth of data that is in the read-ahead buffer.

Sbuffer: Number of sectors read into the disk buffer in time Mbuffer. This is also the number of sectors that the disk rotates in time Mbuffer.

Sreposition: The value of *StepSize* at which the transition between categories (ii) and (iii) occurs.

For small values of *StepSize*, the required sector will already be in the prefetch buffer when the request arrives. The latency for category (i) requests is *Mbuffer*. Since the disk can read *Sbuffer* sectors between successive category (i) requests, the number of sectors in the prefetch buffer increases by *Sbuffer* at each step. In other words, by step *s*, there are *SBuffer*s* sectors in the prefetch buffer. The transition between categories (i) and (ii) occurs when the required sector is not in the prefetch buffer. For the moment, we assume that any sector read into the prefetch buffer us not replaced by incoming sectors before it is read. Using equation 5-9 to specify the address read at step s, we can calculate that the transition will happen when

Equation 5-13. $$\frac{StepSize \times (StepSize + 1)}{2} \geq Sbuffer \times StepSize$$

In other words, when the sector to be read is ahead at step *s* is ahead of all sectors read by step *StepSize*.

While the request is in category (ii), the disk will chose to not to reposition the head and will wait for the required sector to rotate under the head. Therefore the latency for requests

in category (ii) is given by the minimum overhead to access a sector without positioning the head, plus whatever rotational delay is incurred by each request. This latency is given by:

Equation 5-14. $$Latency = \frac{(StepSize - Sov) \times FullRotationTime}{SectorsPerTrack} + Mov + TranferTime$$

Note that in this case, the time between successive requests is *Mov*, during which the disk rotates *Sov* sectors.

The transition between categories (ii) and (iii) occurs when the required sector is far enough away that disk chooses not to read all the sectors in between. Hence, the disk repositions the head near the requested sector. In different disks, this transition will take place at different values of *StepSize*. The transition point could be related to the size of the prefetch buffer in some disks. We define the step size where the transition occurs as *Sreposition*. After this point, the read requests behave in much the same way as the write requests. If *StepSize*>*Stm*, where *Stm* is the number of sectors that the disk rotates in *MinimumMediaTime*, then the request will complete in the same rotation. If *StepSize*<*Stm*, then the request will need one extra rotation. As before, if there is a head or cylinder switch in either a category (ii) or category (iii) request, the head/cylinder switch time is added to the read latency.

We can now use this model to explore the types of result curves we are likely to see in various conditions. We use the synthetic model profile from Sections 5.3 and 5.4. We also assume that *Mbuffer* is 0.5 ms. Figure 5-14 shows the graphical result for *Sreposition=30*. The accompanying illustrations in Figures 5-15 (a-c) explain the behavior at points (1)

through (3). In the horizontal part of the graph, from *StepSize=1* to *StepSize=17*, all requests are satisfied from the prefetch buffer (category (i)) and the latency is *Mbuffer*. When *s>17*, the requests fall into category (ii) and the latency increases linearly with the step size. At *StepSize=30*, we transition into category (iii) and the disk repositions the head on each request. Between *StepSize=30* and *StepSize=37*, this repositioning makes it impossible to satisfy the request in the current rotation (i.e., *StepSize*<*Stm*), and we see an abrupt increase by about *FullRotationTime*. After *StepSize>37*, we see the same type of downward transition as we have already seen in the write results. After this, the read results are similar to the writes, with a sawtooth wave transitioning at intervals of approximately 150 sectors.

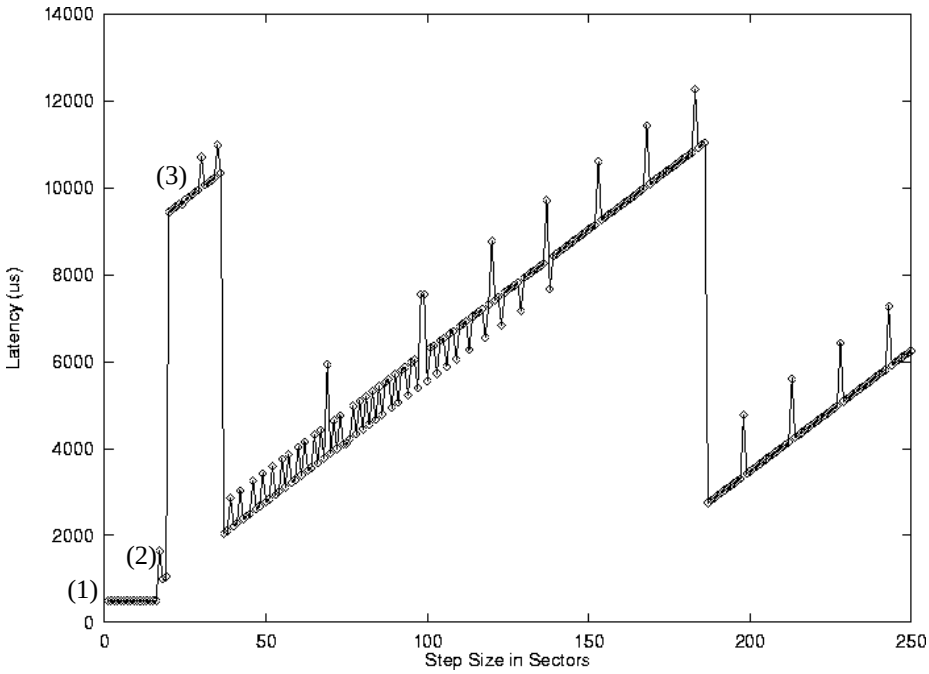

Figure 5-14. Read Model Result

This figure shows the expected behavior under reads when *Sreposition=30.*

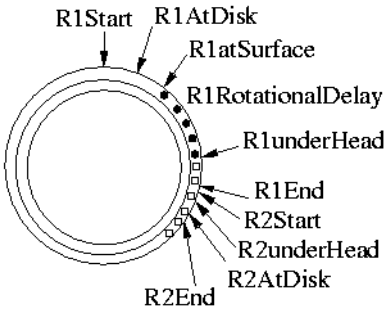

Figure 5-15(a)

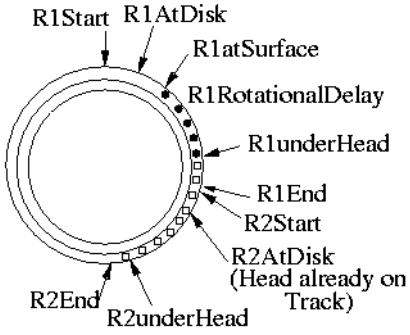

Figure 5-15(b)

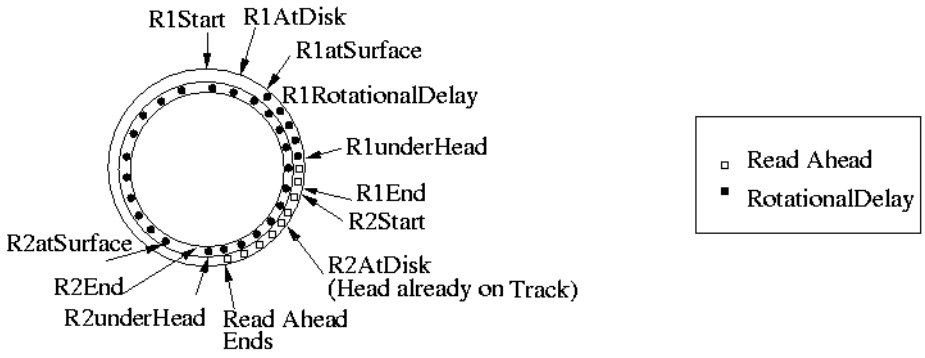

Figure 5-15(c)

Figure 5-15. Illustrations of Request Behavior

Figure 5-15 (a) and (b) show the request behavior at points (1) and (2) in Figure 5.10.

Since the read behavior is considerably more complex than the write behavior, this model is particularly useful to show how the shape of the curve is likely to change with small differences in the read ahead policy. Figures 5-16 (a) and (b) show the expected behavior for *Sreposition* values 100 and 1000. In Figure 5-16 (a), by the time the disk decides to reposition the head on each request, *StepSize* is already greater than *Stm* and none of the requests incur an extra rotation. Therefore, the latency increases linearly with *s* the initial downward transition takes place.

Figure 5-16 (b) shows an extreme case where Sreposition is set at 1000. In this case, the disk does not reposition the head for any request shown on the graph. As long as the head is kept on the surface, the disk will read all sectors between that under the head and the required sector. Each time a head switch happens; the latency will increase by *HeadSwitch-Time*. We see that in this case the latency can become arbitrarily large. Although this seems to be an extreme case, in the next section we will encounter a disk that shows exactly this behavior.

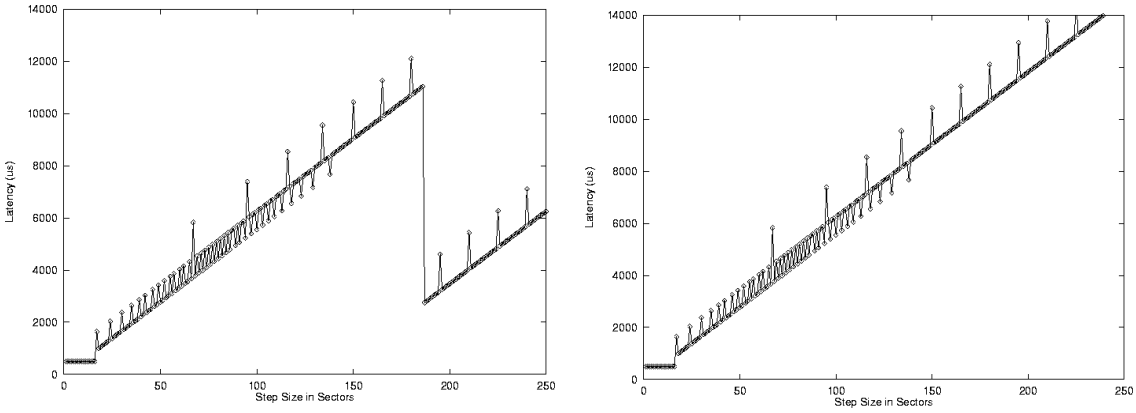

Figure 5-16. Other Possible Read Results

Figure 5-16 (a) and (b) show the expected results for Sreposition values 100 and 1000.

5.6.2. Extracting parameters.

Although the read graphs are considerably more complex than the write graphs, most of the parameters explicit in the write graphs can also be extracted from the read graphs. In this section we examine this extraction process, beginning with figure 5-14.

The latency value of the horizontal portion is *MBuffer* (500 us). Using equation 5-13 and substituting the X values before and after the transition point (1), we can estimate *Sbuffer*.

The height of the sawtooth wave is *FullRotationTime*. As in the write case, we can use the slopes of the lines to find *Sectors/Track*. The head switch time, cylinder switch time, and number of heads, are all determined in the same way as in the write graphs.

The main difference between graphs 5-14 and 5-15 (a) is that *MinimumMediaTime* is not obvious in the early part of figure 5-15 (a). We can, however, determine both *Mtm* and *FullRotationTime* from the sawtooth transition near *StepSize=175*. The height of the transition is still *Rl*; if a head switch has occurred, the Y coordinate at the bottom of the transition could be *MinimumMediaTime+HeadSwitchTime+TransferTime*. Since *HeadSwtchTime* is known, we can estimate *MinimumMediaTume* as before. We can also get *MinimumMediaTime* by subtracting *FullRotationTime* from the highest Y value in the wave.

Finally, in the third graph, Figure 5-16(b), we have lost all the information embedded in the transitions. We can still determine *Mbuffer, HeadSwitchTime, CylinderSwitchTime* and the number of heads. However, without knowing *FullRotationTime*, we cannot find *Sectors/Track*.

5.6.3. A Sample Result

Figure 5-17 shows the UltraStar XP's result on the read benchmark. This result is similar to Figure 5-14. Using the techniques outlined in the last section, we can extract the following parameters:

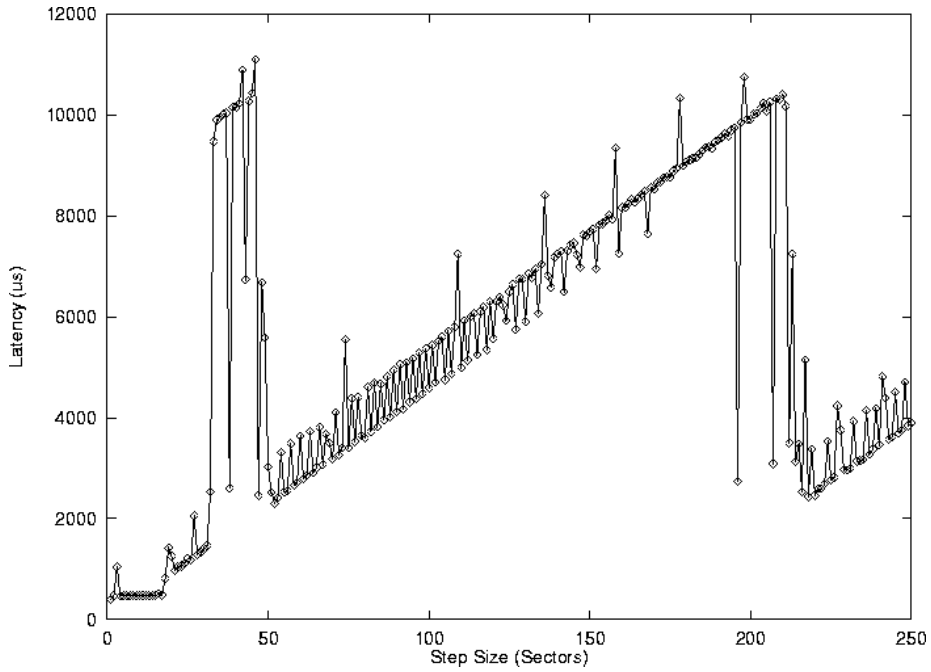

Figure 5-17. Read Result for IBM UltraStar XP

The sample read result matches the shape of the model result in Figure 5-14.

(1) *MBuffer* is approximately 470 us. The transition between categories (i) and (ii) happens between *StepSize=17 and StepSize=18*. Therefore, the estimated value of *Sbuffer* is 9.25.

(2) The *MinimumMediaTime* point is reached at *StepSize=47*; the value of *Mtm* is 2.46 ms.

(3) The height of the drop at the *Mtm* point, or the value of *FullRotationTime*, is 8.63 ms. Compared with the specification value that is 8.33ms, the error rate is 3.6%.

(4) The measured *HeadSwitchTime* is 0.84ms, a 0.6% error. The measured *Cylinder-SwitchTime* value is 2.23ms, a 1.6% error.

(5) The slope of the base line, *FullRotationTime/SectorsPerTrack,* is 45.59; using the above estimate for *FullRotationTime*, we can calculate *Sectors/Track* to be 189. Since the actual value is 184, the error rate is 2.7%.

(6) Finally, counting the number of head switches between cylinder switches gives us 18, the correct number of recording surfaces.

The parameters extracted from the read graph are also very accurate; the maximum error rate is 3.6%. As expected, we see that there is a slight difference between the read *MinimumMediaTime* value and the write *MinimumMediaTime* value.

5.7. Read Measurements

Now we examine the read results for the remaining disks in Table 5-2. Figures 5-18(a-d) show the read results for the SCSI disks and figures 5-19(a and b) show the results for the IDE disks. Figure 5-20 shows that each disk behaves quite differently. The X and Y scales are the same for all graphs except 5-18(b), the Seagate Barracuda drive.

5.7.1. SCSI Disk Drives

Table 5-4 contains the parameters extracted from Figures 5-18(a-d). The UltraStar XP's parameters are also included for comparison. We begin with the Seagate Hawk. This drive has the expected sawtooth behavior, the curve differs from its write counterpart at the smaller step sizes where the read ahead activity comes into play. The Hawk's read behavior differs from the UltraStar XP in one important respect; Figure 5-18(a) does not show the latency increase similar to that in point (3) of Figure 5-17. In the Hawk's case, the transition between categories (i) and (ii) happens well past the *MinimumMediaTime* point, and the read curve is similar to the model result in 5-16(a). We see that the transition between categories (i) and (ii) happens between *StepSize*=18 and *StepSize*=19. Therefore, *Sbuffer* is

between 9.5 and 10, averaged out to 9.75. *MBuffer* is 866 us. The measured *FullRotation-Time* is 11.05 ms, an error of 0.5% compared to the specification. The head switch time is 1.15 ms and the cylinder switch time is 2.34 ms. The Sectors/Track ratio is 140.54, and there are 9 recording surfaces. There is some difference between the measured values in the read and write experiments. In all cases, however, the difference is less than 3%.

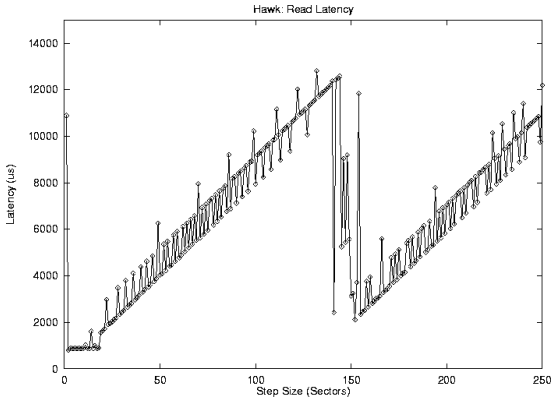

Figure 5-18(a)

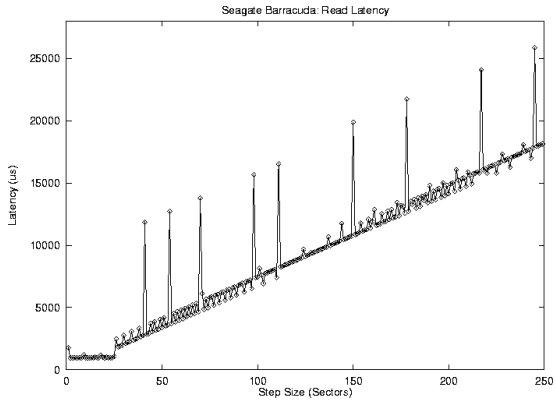

Figure 5-18(b)

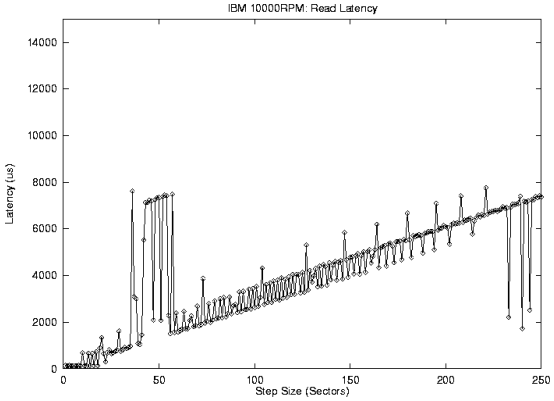

Figure 5-18(c)

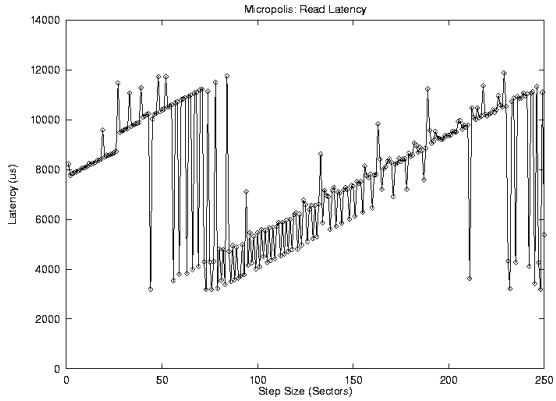

Figure 5-18(d)

Figure 5-18. Read Results for SCSI Disk Drives

Figures 5-18 a, b, c, and d (numbered in row major order) show the results of the read benchmark for the disks listed in Table 5-2

The Seagate Barracuda's result in Figure 5-18(b) is similar to model 5-16(b). Even though Figure 5-16(b) illustrates an extreme case, we see that it can actually occur in disk drives. Although Figure 5-16(b) shows only step sizes up to 250, we ran the experiment up to step size 5000. The Barracuda chose to read all sectors between the current and the requested sector. This causes the read latency to increase rapidly; even at step size 250, the latency is already around 18 ms. The measured *Mbuffer* value is 970 us. The averaged *Sbuffer* value is 12.75. The graph also shows occasional spikes caused by rotational misses. Even though we could not extract *FullRotationTime* from Figure 5-18(b), we can find it from the Barracuda result because of the rotational misses. The measured *Rl* value is 8.34 ms, a 0.1% error from the specification. The Sectors/Track ratio is 125. The head switch time is 0.73 ms. The graph does not show any noticeable cylinder switches, therefore we cannot measure the cylinder switch time or the number of recording surfaces.

Disk	**MBuffer (ms)**	**Full Rotational Latency (ms)**	**Minimum Time to Media (ms)**	**Sectors/ Track (outermost)**	**Number of Recording Surfaces**	**Head Switch Time (ms)**	**Cylinder Switch Time (ms)**
Hawk (5400)	0.87	11.05	2.11	140.54	9	1.15	2.34
Barracuda (7200)	0.97	8.34	-	125.04	21	0.73	-
Micropolis (7200)	-	8.40	3.19	206.66	22	1.31	2.97
UltraStar (7200)	0.47	8.44	2.46	182	18	0.84	2.23
9ZX (10020)	0.13	5.96	2.76	227.22	12	0.60	1.72

Table 5-4. Parameters Extracted from Read Benchmark

Table 5.4 lists the extracted parameters from each SCSI disk drive. The parameters for the IBM UltraStar XP disk are included for comparison. The *MinimumMediaTime* of the Seagate Barracuda cannot be determined because of its abnormal result.

Figure 5-18(c) shows that the 9ZX's read behavior is similar to that of the UltraStar XP. The *MBuffer* value is 130 us; the *Sbuffer* value averages out to 11.75. The measured rotation time is 5.96 ms, a 1.7% error compared to the specification. The sectors/track ratio is 227, and the head and cylinder switch times are 0.6 ms and 1.7 ms respectively. The number of recording surfaces is 12.

Finally, Figure 5-18(d) shows the read behavior of the Micropolis disk. This drive does not seem to benefit from read ahead the way that the other drives do It's read behavior is quite similar to its write behavior. The measured rotation time is 8.40 ms, a 0.8% error compared to the specification. The sectors/track ratio is 206.7, and the head and cylinder switch times are 1.31 ms and 2.97 ms. The graph also shows that the disk has 22 recording surfaces.

5.7.2. IDE Disk Drives

Next we look at the read results for the IDE drives. Figure 5-19(a) shows the read result for the IBM IDE drive; the graph is similar to model 5-16(a). *MBuffer* is 392 us and *SBuffer* is 11.25. The measured *FullRotationTime* is 11020.15 us, a 0.8% error compared to the specification. The measured values of *HeadSwitchTime* and *CylinderSwitchTime* are 1891.38 us and 3812.52 us respectively. The Sectors/Track ratio is 329.84 and the disk has 6 recording surfaces.

Figure 5-19(b) shows the result for the Quantum IDE drive; the graph matches the model result in figure 5-14. The measured *FullRotationTime* is 11.35, a 2.3% error compared to the specification. The Sectors/Track ratio is 360, and the head and cylinder switch times are 2.14 ms and 2.84 ms respectively. The graph also shows that the disk has only two recording surfaces.

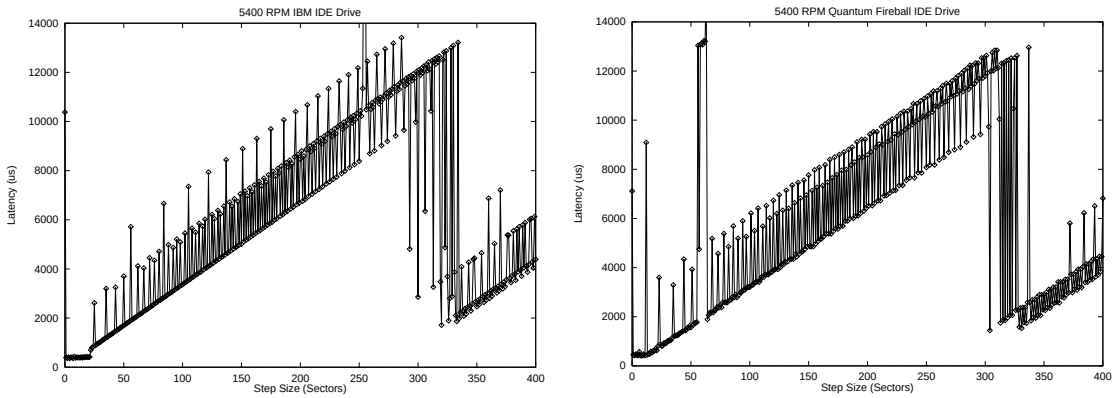

Figure 5-19. Read Results for IDE Disk Drives

Figures 5-19 (a) and (b) show the read results for the IBM and Quantum disk drives. Although the sawtooth transition is not visible in the graph, it does occur in each case at a higher step size. The IBM disk's result is similar to model 5-16(a), and the Quantum disk's result is similar to model 5-14

5.7.3. Discussion

Of the five SCSI disks and three IDE disks, we found three whose read behavior matched model 5-14 and three whose behavior matched model 5-16(a). The Micropolis disk did not appear to benefit from read ahead in this experiment, and the Barracuda disk showed the extreme behavior predicted by model 5-16(b). Overall the best possible response is one similar to model 5-16(a); the latency at any point is the lowest it can be. In model 5-14, some points at small step sizes have a higher latency. However, the result depends on how the disk policies interact with the system dependent *MinimumMediaTime*. A disk that gives a result like model 5-14 on one system may well give a result like model 5-16(a) on another system. A result like model 5-16(b), however, suggests a bad read ahead policy or a firmware bug.

Also, if we compare the SCSI and IDE disk results, we see that the IDE disks have lower *MBuffer* values than almost all the SCSI disks. This is not surprising, as the IDE disks also have much lower *MinimumMediaTime* values than the SCSI disks. The exception is the SCSI 9ZX disk, which has a *MBuffer* of 130 us, a factor of two lower than all the other disks.

5.8. Summary

Disks have always been difficult to measure because of the rotational effect. The rotational latency can add anywhere from zero to the full rotation time to any latency measurement. If we do not know what part of the latency is rotational, it is virtually impossible to determine other parameters like head switch time. This variability is why many benchmarks that work on other parts of computer systems, like memory [Saavedra92, McVoy96[, do not work well on disks. The linear stride technique actually takes advantage of the disk's rotational nature; the result curve shows very clearly what part of each measurement latency is rotational. It is possible to extend this technique to filter out the rotational effect in all kinds of disk measurements.

The Skippy benchmark strides across the disk, transferring one sector at a time and increasing the step size with each step. The resulting latency curve has a sawtooth form; the lowest points are the minimum latency to access drive media, and the highest points are when a full rotational miss occurs. Instances of head and cylinder switches stand out clearly, making it easy to determine switching times and the number of heads on the disk. This

single benchmark can extract all the disk geometry information and many useful mechanical latencies.

We explored the benchmark behavior for writes and reads and presented results for seven modern disk drives. We found that the write curves have the same shape for all disks, while the read curves can have several shapes depending on the disk's read ahead algorithms. Nevertheless, we were able to extract parameters from all the write cases and all but one of the read cases. The extracted parameters matched all the specification data we were able to find, with less than 3% error. One of the benchmark's strengths is that most parameters can be measured in more than one way. Therefore, even if the shape of the curve changes slightly between disks, we can still extract all the information we need.

In the next chapter, we explore extensions to the benchmark and presents a tool to automate the parameter extraction process.

6 Automatic Extraction

6.1. Introduction

Chapter 5 described the Skippy algorithm for extracting disk geometry details and mechanical latencies. The extracted information can be used by disk controllers, device drivers and file system layers to create drive specific performance enhancements [Horst99]. Even though the technique is simple and efficient, it cannot be incorporated into such a higher level system without a mechanism to automatically extract the parameters from the graphical result. This chapter describes such a mechanism.

The chapter is organized as follows. Section 6.2 describes the four phase approach used in the extraction algorithm for write graphs. Section 6.3 describes each phase in detail and illustrates the results on the IBM UltraStar XP disk drive. Once the technique has been explained, we extract the parameters of the other SCSI disks in Section 6.4. Section 6.5 explores ways to improve the accuracy of the extracted results. Section 6.6 discusses these results in more detail. Section 6.7 describes how the extraction techniques can be adapted to read graphs and Section 6. 8 concludes with a summary. All through the chapter, the SCSI disk results from Chapter 5 are used to test the extraction algorithms.

6.2. Approach

Figure 6-1 shows a sample write result. As Chapter 5 described, the disk parameters of interest are embedded in the linearly increasing segments of this graph. However, the saw-tooth nature of the graph makes it to hard access these segments directly. To isolate the linearly increasing segments, we first break the graph down into several pieces. In Figure 6-1, the graph is divided into two linearly increasing segments, S1 and S2, and two transition segments, T1 and T2. The height of a transition is the rotational latency.

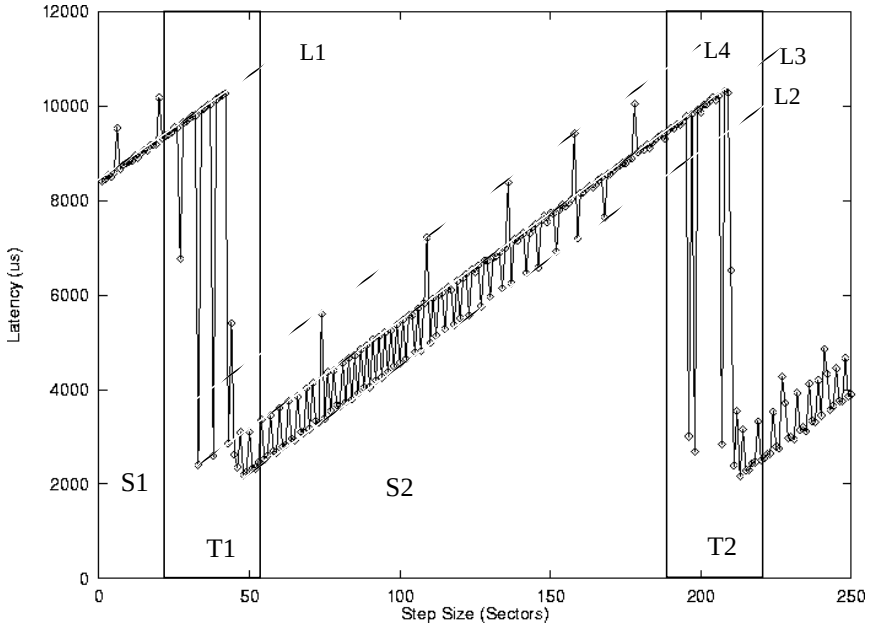

Figure 6-1. Classifications of Graph Regions

This figure shows how the data is classified during processing. The graph is broken down into sections S1, T1, S2, and T2. T1 and T2 are transition sections. The lines L1, L2, L3 and L4 have the same slope.

S1 and S2 contain points that fit on three lines; the first line, marked as L1 in S1 and L2 in S2, is called the base. The second line, marked as L3 in S2, contains head switches, and the third line, marked as L4 in S2, contains cylinder switches. Note that these lines all have the

same slope, and differ only in the offset. If we can separate the points that belong to each line, we can then use linear regression to find the slopes and offsets. The slope gives the Sectors/Track ratio, and the offsets between the lines gives the head and cylinder switch times.

The automated extraction process requires the following four phases of processing:

Phase I: Filtering the data: The upward and downward spikes caused by head and cylinder switches make it harder to isolate the transition regions. Therefore, phase I removes as many of these spikes as possible by filtering the data.

Phase II: Isolating the Transition Regions: The filtered data is used to isolate the transition regions T1 and T2. Once T1 and T2 are known, we can isolate S1 and S2. We also estimate the slope of the line L1 by applying linear regression on the filtered latency values in region S1.

Phase III: Extracting Head and Cylinder Switch Times: Now that the transition regions and the slope have been extracted from the filtered data, we return to the original data. We use the coordinates discovered in phase II to isolate S2 in the original data. Once this region is found, we can separate the base, head switch and cylinder switch points. Section 6.3 describes how these points are extracted.

Phase IV: Calculating Parameter Values. Once the base, head switch and cylinder switch points in a single linearly increasing segment have been identified, we can use the equations in chapter 5 to extract all necessary parameters.

6.3. Implementation Details

This section describes how each phase is implemented. Throughout the section, we use the UltraStar XP's graphical result to illustrate the processing steps. Some steps use techniques borrowed from other fields, in particular the Artificial Intelligence and Statistics communities. Therefore, in each phase, we describe the techniques used, define any necessary terms, and outline any trade-offs.

6.3.1. Phase I: Median Filter

The goal of phase I is to ease the detection of transition regions by removing as many spikes as possible from the data. A median filter is very useful for this task, as it removes sudden noise spikes without excessively distorting the surrounding data.

A median filter is a nonlinear filter commonly used in digital image processing to remove noise from images [Davies88, Pitas90, Russ95]. In the digital processing context, a median filter is a sliding window spatial filter that replaces each pixel with the median value of all the pixels surrounding it. The advantage of the median filter is that it removes Gaussian nose without affecting edges; a low pass filter, in contrast, will blur the image while reducing nose. Figure 6-2 shows a two dimensional median filter where the median is calculated from the 3x3 grid surrounding the image. The number of points used to find the median is the *window size*. In our context, we use a one dimensional version of the same idea. Figure 6-2 also shows a one dimensional filters with a window size of 5.

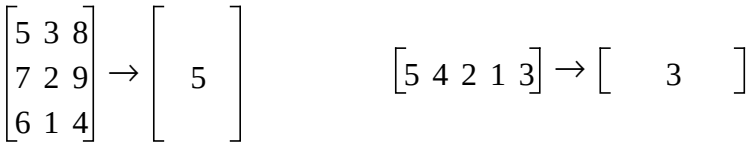

Figure 6-2. Examples of Median Filters

This figure shows a 3x3 window filter and a 5x1 median filter.

Figure 6-3 shows what happens when a median filter is applied to the benchmark result for the IBM UltraStar XP drive. The original benchmark result is in Figure 6-1. The median filter used here has window size 3; each latency value is replaced by the median of itself, the value immediately before, and the value immediately after. We discuss the effects of varying the window size later in the chapter. If we compare Figure 6-3 to Figure 6-1, we can see that the graph in Figure 6-3 is considerably smoother for small step sizes. As long as the step size is small, there are very few head and cylinder switches; once this region is filtered, all those spikes are removed. The filter also causes the sawtooth transition to be more clearly defined. At larger step sizes, there are too many head switches to be removed by the median filter. However, we see that the filter smooths out the early part of the graph and the first two transition regions quite well.

6.3.2. Phase II: Identifying the line slope and transition points

Now, we can use the filtered result to find the first two transition regions. Although the median filter does a good job of removing noise spikes, we cannot guarantee that there will be only one downward transition; therefore we identify transition *regions* in the graph. We define a transition region to be when the latency drops from the prior value by over 30%.

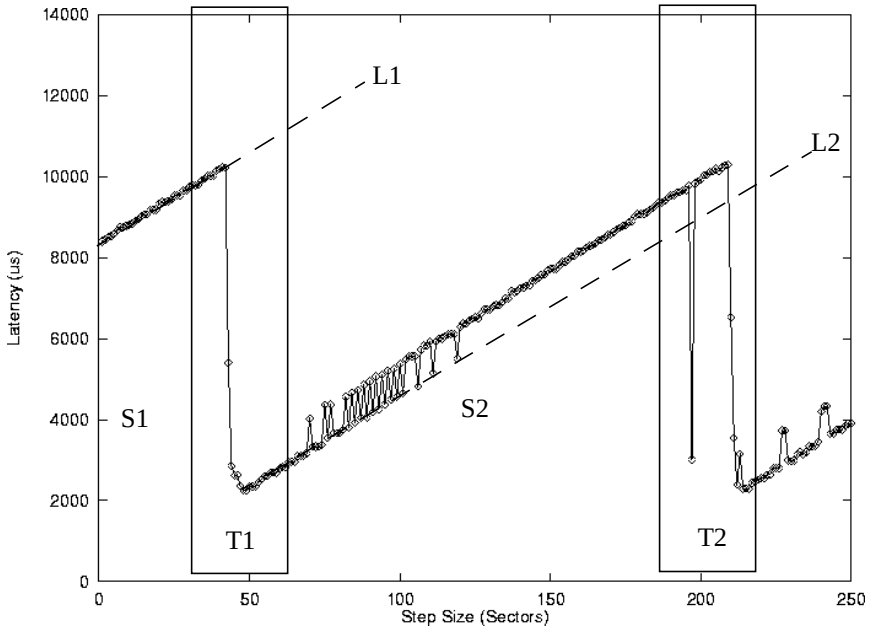

Figure 6-3. Median Filtered Graph

The IBM UltraStar XP result from Figure 6-1 after being processed with a median filter of window size 3

The 30% point was chosen because a drop that large was not likely to be the result of noise; the measurement variance is typically less than 10%. The transition region ends when three consecutive monotonically increasing latency values are detected. Once the transition regions are identified, the height of the transition is a good estimate of the full rotation time.

The area to the left of the first transition region is S1. Since there are very few head/cylinder switch spikes at small step values, the median filter does a very good job of removing noise in this region, What remains are the base points that fit on line L1. Therefore, linear regression on these filtered data points reveals the slope of L1. This is, in turn, a good estimate of the slope of L2, L3 and L4 in the original graph. For the UltraStar XP drive, this extracted slope value is 44.9 usec/sector.

6.3.3. Phase III: Identifying the head and cylinder switches

Next, we focus on the data segment between the two transition regions, region S2. We cannot use this region in the filtered graph, however, since the median filter has removed many cylinder and head switch points. Therefore, we analyze this region in the original data. The median filtered data is used only to find the slope, the full rotation time, and the transition regions.

Our goal is to classify each point in this region into one of three categories: base, head switch, and cylinder switch. This is hard to do, however, because the latency values are linearly increasing. So we begin by removing the linearly increasing portion of the latency. Since the full rotation time, *Rl*, is known, we can add it to each latency value in S2. This causes the entire segment to move up, as in Figure 6-4(a). The base line in segment S2 now becomes a continuation of line L1 from segment S1. Since we know the slope and offset of line L1, we can subtract the linearly increasing segment from all points in region S2. Once this is done, the data appears as in Figure 6-4(b); all the points in one category are now the same height and the base, head switch and cylinder switch points are easily distinguishable.

Now that all the points from each category have roughly the same Y value, we can use a clustering algorithm to separate the base, head switch and cylinder switch points. There is a slight complication, however. Excess noise and unexpected rotational misses can create points that don't belong in any of the three categories. If these points are included in one of the clusters, the outlying values will reduce the accuracy of the linear regression and the extracted mechanical latency values.

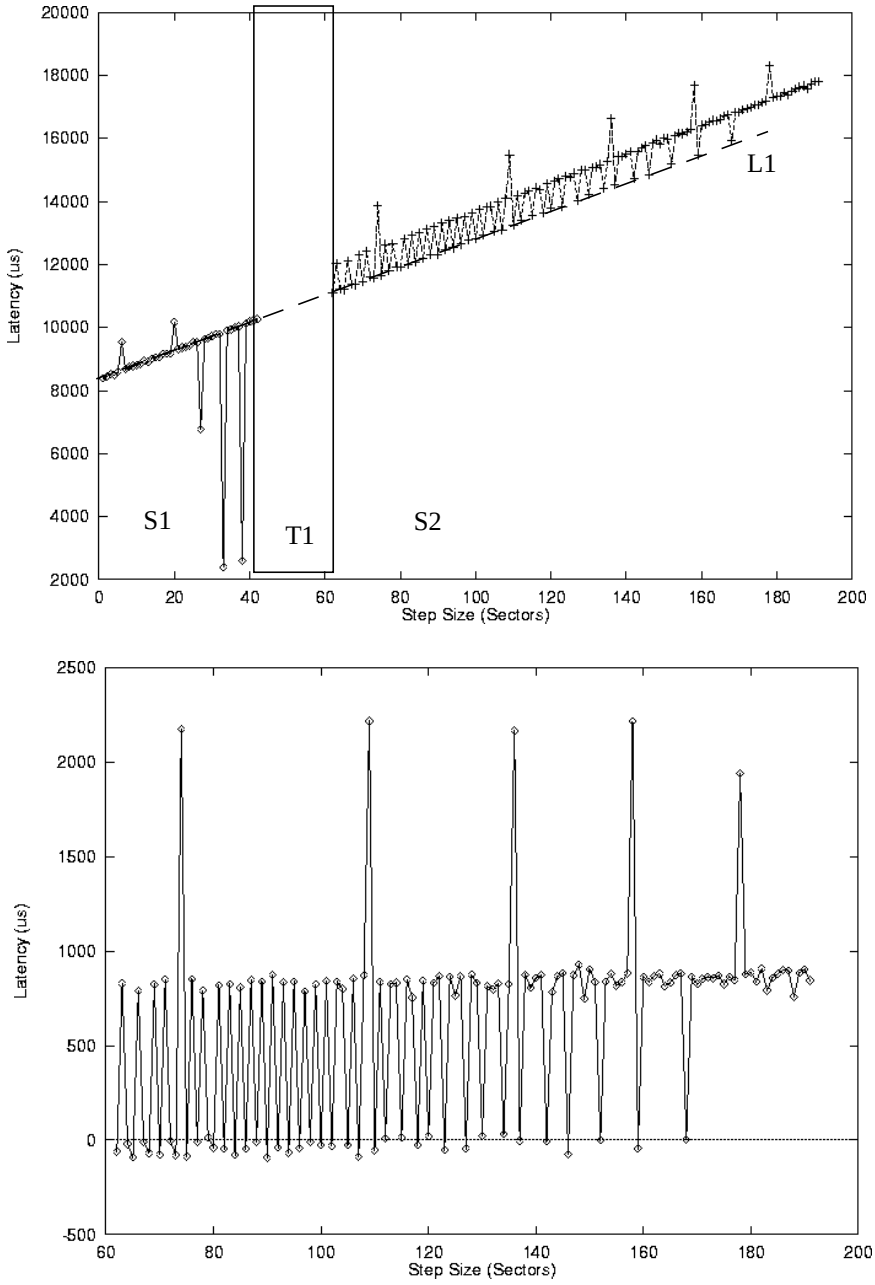

Figure 6-4. Removing the Linearly Increasing Offset

The first graph shows how segment S2 in Figure 6.3 can be moved up. The base line of segment S2, line L2, now becomes a continuation of line L1. The second graph shows the Base, Head Switch and Cylinder Switch points after the linearly increasing portion of the latency is removed from Figure 6.4(a). The category in which each data point belongs is clear from its Y value.

Our initial solution to this problem is as follows: the number of clusters is not set to three, we impose only a minimum distance between clusters. This way, outlier points will form clusters that will not be merged with the useful data points. Since we assume that there are more useful data points than outliers, the three clusters with the most points will be the data clusters. The key is choosing the right minimum distance so that head switch points and cluster switch points are not merged into the same cluster. For the moment, we set the distance between clusters to 0.2 ms. Although this constant works well for the UltraStar XP result, it is not a robust solution. Section 6.4 shows how well the constant works for other cases and Section 6.5 explores more robust techniques.

6.3.4. Phase IV: Parameter calculation

Once the three clusters of points are identified, we can apply linear regression (using the original latency values of each point), to calculate the head switch time *HeadSwitchTime* and the cylinder switch time *CylinderSwitchTime*. Since we already know the slope *FullRotationTime/SectorsPerTrack* and we have an estimate of *FullRotationTime,* we can calculate the Sectors/Track ratio. By counting the number of head switch data points between each cylinder switch data point, we can calculate the number of recording surfaces.

6.3.5. A Sample Result

Table 6-1 shows the manufacturer specified parameters for the UltraStar XP drive, along with the manually extracted and automatically extracted values.

Parameter	Manufacturer Data	Manually Extracted Values	Percentage Error (as compared to Manufacturer Data)	Automatically Extracted Values	Percentage Error (as compared to Manufacturer Data)
Sectors/Track	184	181.9	1.1%	184.2	0.1%
Full Rotation Time	8.33 ms	8.30 ms	0.4%	8.27 ms	0.7%
Minimum Media Time	-	2.19 ms	-	2.34 ms	-
Head Switch Time	0.85 ms	0.87 ms	2.3%	0.87 ms	2.3%
Cylinder Switch Time	2.17 ms	2.19 ms	0.9%	2.24 ms	3.2%

Table 6-1. Percentage Errors of Manual and Automatic Extraction

The table shows, for each parameter, the manufacturer specified value, the value manually extracted using Skippy, and the value automatically extracted using Skippy. For all parameters, both the automatically extracted and manually extracted values are close to the manufacturer value. The biggest disparity between manual and automatically extracted values occurs in the MinimumMediaTime parameter. This disparity is larger because this value is determined using one or two points, and is as such more prone to error than the other values.

The automatically extracted values are as follows. The full rotation time, measured as the height of the transition, is 8.27 ms. Compared to the manufacturer's specification, the error is 0.7%. The sectors/track ratio is 184.18; the error is less than 0.1%. The head and cylinder switch times are 0.87ms and 2.24ms respectively. The error rates here are 2.3% and 3.2%. We see that the extracted values are very close to the actual values. In all cases, the error is less than 5%. The table shows that the automatically extracted values differ slightly from the manually extracted values. Occasionally, as in the Sectors/Track measurement, the automatically extracted value is closer to the specified value than the manually extracted value.

6.4. Experiments

Next we apply this algorithm to the write results for the other SCSI disk drives presented in Chapter 5. Figure 6-5 shows, for each SCSI disk, the absolute relative error between the manually extracted values and those extracted by the algorithm. In all cases, the techniques described in section 6.3 were used, with the same constant values (30% drop required to determine transition in Phase II and 0.2 ms fixed distance between clusters in Phase III). As the figure shows, in most cases the error rate is less than 5%. In general, the error rates for the *Minimum Time to Media* are greater than the error rates for all other parameters. This happens because the *MinimumMediaTime* value is approximated as part of the transition detection process; the other parameter values are considerably more accurate since they are extracted from a larger number of points.

The only disk whose extracted values show a marked inaccuracy is the Micropolis drive. There are several reasons for this. First, as Figure 5.4 showed, the Micropolis disk result has more noise than the other SCSI disks' results. A single pass of a median filter does not remove all noise spikes. As a result, the rotational latency value and the slope values are less accurate. This inaccuracy affects all other results, since these quantities are used to calculate *SectorsPerTrack*, *HeadSwitchTime* and *CylinderSwitchTime*. Second, the transition region is considerably wider than in the other results, leading to a less accurate *MinimumMediaTime* measurement. Third, we discover that the clustering technique described in section 6.3 does not work well for the Micropolis drives. The clustering process terminates prematurely, since the constant separation distance of 0.2 ms is inappropriate for a result with as much noise as the Micropolis result. Although the clusters containing base and head

switch points are correct, the cluster that should contain cylinder switch points actually contains head switch points. This mix-up is why the relative error for the cylinder switch time is so high in Figure 6-5. The next section addresses these shortcomings.

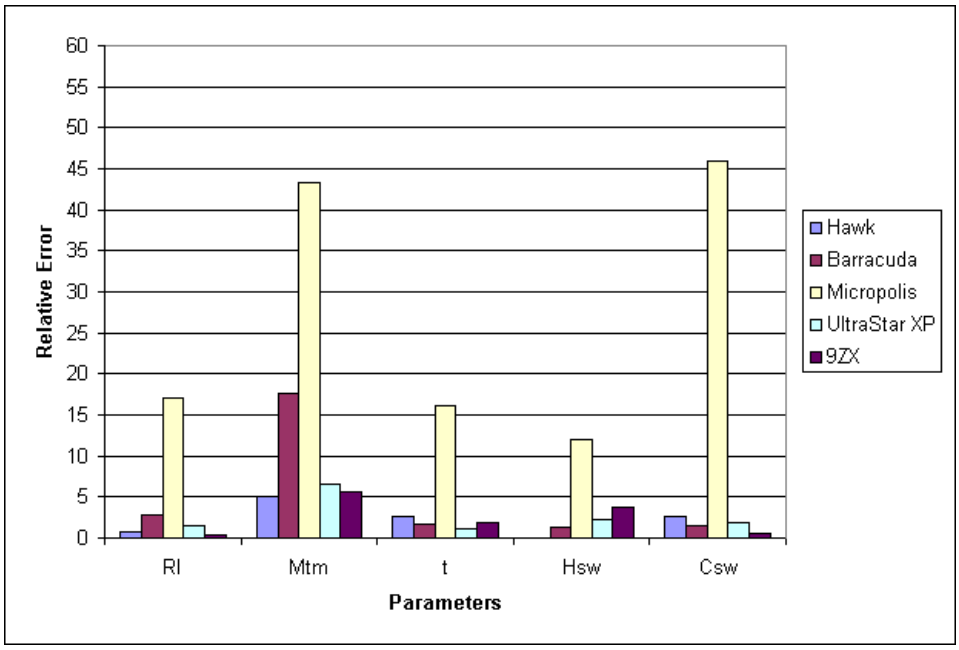

Figure 6-5. Extraction Accuracy

The absolute relative errors between the manually extracted and automatically extracted values. We calculate the absolute percentage relative error between two values y1 and y2 as the absolute difference between y1 and y2, divided by their average, or $AbsoluteRelativeError = \frac{|y1 - y2| \times 2}{y1 + y2}$

6.5. Optimizations

The prior results showed that the technique is in general very accurate. However, as the amount of noise in the graph increases, the results can become quite inaccurate. In particular, small inaccuracies in the estimation of the slope and rotational latency can lead to large errors in the estimation of the other parameters. In this section, we examine alterna-

tives to the basic algorithm that deal with some of these problems. We explore the following:

(i) Wider filters and multiple filter passes: The goal here is to reduce noise even further by using filters with larger window sizes or using multiple passes of a filter. The trade-off is that the data is further distorted.

(ii) Using an alternative clustering algorithm: The clustering algorithm used thus far attempted to avoid outlier points by limiting the distance between clusters. Here we explore alternative clustering algorithms.

(iii) Comparing multiple values of the same parameter for robustness checking: The rotational latency and slope values are embedded in more than one place in the graph. By comparing the values extracted from different points in the graph, we can make some estimate of the accuracy of the extraction process.

We examine each optimization in turn, focusing on how the alternatives affect the extraction accuracy for the five disks mentioned in Section 6.4. Finally, we combine some of the optimizations to create a better extraction algorithm.

6.5.1. Wider and Multiple Pass Filters

Figure 6-5 shows the extraction results when the data was filtered with one pass of a median filter with window size 3. Here we examine four alternative filters: a size 5 filter, a size 7 filter, two passes of a size 3 filter, and three passes of a size 3 filter. Intuitively, a filter with a smaller window distorts the data less than a filter with a larger window. At the same time,

a filter with a smaller window removes fewer spikes than a filter with a larger window. Multiple passes of a smaller window filter will remove more spikes than a single pass, while likely distorting the data less than a single pass of a filter with a larger window size.

Figure 6-6 shows the relative error rates for each parameter and each type of filter. In all cases, the accuracy is calculated by comparing with the manually extracted value. In each graph, the disks are labeled on the X-axis; each disk has a cluster of bars representing the error rate with each filter. The filter's are labeled on the legend, starting with the single pass, size 3 filter, and ending with the single pass, size 7 filter.

In almost all the cases, we see that using multiple passes of the size 3 filter does not increase the error. In the Micropolis case, where the errors are the highest and the data had the most noise, the multiple passes give a noticeably improvement in the error rate. For *MinimumMediaTime*, using two passes of the 3 filter reduces the error rate from over 40% to around 25%. For *FullRotationTime* and *Sectors/Track*, the improvement is even greater. The extra filtration does not help the accuracy of *HeadSwitchTime* and *CylinderSwitch-Time* as much. This is not surprising; the head and cylinder switch times are affected more by the clustering algorithm than the filtration process.

In most cases, using three passes of the 3 filter does not do damage, but also does not improve the accuracy further. On the Micropolis result, the triple pass of 3 filter does cause slightly higher error rates for *FullRotationTime*, *SectorsPerTrack*, *HeadSwitchTime* and *CylinderSwitchTime*. It is still however, a great improvement from the single pass 3 filter. The Barracuda is the only disk for which the three pass 3 filter seems to help; the error rates

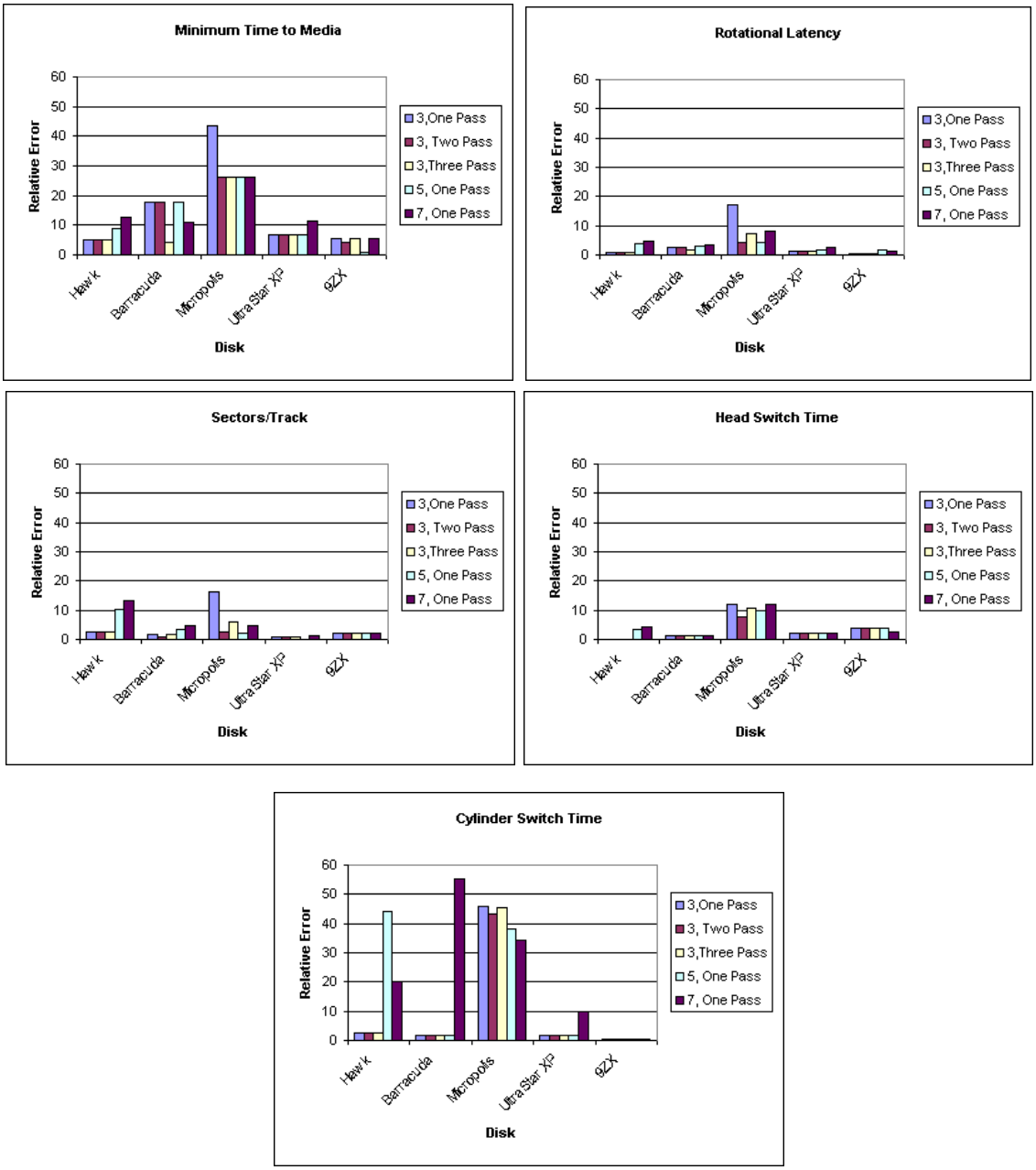

Figure 6-6. Using Wider Filters and Multiple Passes

Figures 6-6(a) and (b) show the error rates for the minimum time to media and rotational latency parameters. Figures 6-6(c) and (d) show the error rates for the sectors/track ratio and the head switch time parameters. Figure 6-6(e) shows the error rates for the cylinder switch time.

for *MinimumMediaTime* and *RotationalLatency* are considerably lower than in the case where two passes of the size 3 filter were used.

The remaining two filters, the size 5 filter and size 7 filter, perform considerably worse than the size 3 filters. In all cases but the Micropolis disk, these filters actually increase the error rate. On the Micropolis, they do reduce the error compared to a single pass of the size 3 filter, but never do any better than two passes of the size 3 filter. Multiple passes of size 3 filters are less intrusive to the data than the size 5 and size 7 filters. Since the filter works by replacing each value with the median of those around it, the size 5 and size 7 filters distort the data more than the size 3 filter. Our goal of removing point noise is better served with multiple passes of the size 3 filter than with single passes of wider filters. Thus we will use 2 passes of the size 3 filter as our baseline.

6.5.2. Using Alternative Cluster Algorithms

The clustering solution used so far in Phase III has been simple; points are grouped into clusters until a minimum distance between clusters is reached. Although only three clusters are expected, this technique stops noise points from joining the three clusters and affecting the regression results. The distance between clusters was set to 0.2 ms; this value worked well for all the graphs except the Micropolis disk. In that case, the algorithm stopped before all the head switch points could be joined into one cluster. As a result, the points identified by the algorithm to be cylinder switches were actually head switches. A better clustering algorithm, one that does not require a fixed distance between clusters, is clearly needed.

While looking for a better clustering algorithm, we explored and rejected several alternatives. We describe them briefly and explain why they did not work, but do not go into detail with each. The unsuccessful alternatives are listed below:

(i) The first alternative was to force all points into three clusters and then remove outliers from each cluster. This did not work because the values of the noise points were so different from the data values that they tended to form clusters on their own. As a result, the useful points were forced into a single cluster. The converse, removing the outlier points before clustering, also does not work. If there are no outliers, this process can remove cylinder switch data points.

(ii) The second alternative was to purposely place noise points that could attract other noise points into clusters. Later, these noise clusters (identified by the artificial points), could be removed. Here we're exploiting the fact that we can predict the values of some outlier points. Given the structure of the graph, we expect some outliers in the data with values of approximately plus and minus the rotational latency. This technique worked well for some results. However, it is not robust since it does not work when there are noise points with values far away from plus and minus the rotational latency.

In the ideal case, the clustering should continue until most of the useful data is in the three clusters, and stop before two of the useful clusters are merged into one. To effect this compromise, we used a hybrid technique. In the beginning, the clustering process proceeds until the three largest clusters contain some predetermined percentage, *p*, of the data. After this happens, we assume that each cluster has enough points that we can calculate its width (the width is defined as the average plus or minus three times its variance). From this point onwards, clusters are merged only when their widths overlap. The process stops once no more clusters can be merged.

Figures 6-7(a) and (b) show the extracted head and cylinder switch times using this hybrid optimization. Since the other parameters are extracted before the clustering phase, their values do not change. Each figure shows the extraction accuracy for the original clustering scheme and for the hybrid scheme for *p=90%* and *p=95%*. As the figures show, this technique does improve the accuracy of the extracted cylinder switch time for the Micropolis disk. The accuracy of the head switch time is slightly worse on the Micropolis disk, but the other disks' results appear unaffected.

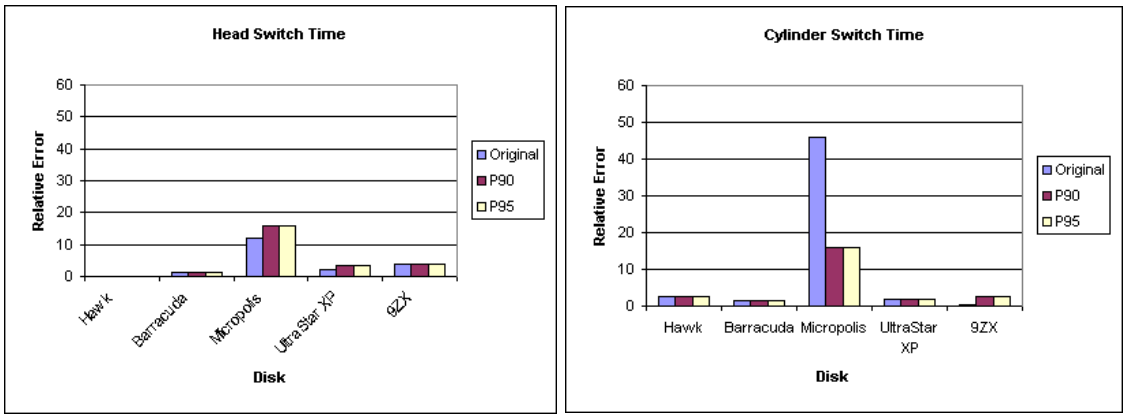

Figure 6-7. Using An Optimized Clustering Algorithm

Figures 6-7(a) and (b): Accuracy of head and cylinder switch values extracted using the new cluster extraction algorithms. As the figures show, the new algorithm causes the head switch error to increase slightly, but the cylinder switch error (for the Micropolis disk) improves dramatically.

6.5.3. Using multiple extractions for accuracy checking

Because of the symmetric nature of the benchmark result, there are several ways to calculate the *FullRotationTime*, and the *slope FullRotationTime/SectorsPerTrack.* In particular, the latency value at step size 0 should be approximately *FullRotationTime*. The slope value

is also available in more than one way. Once linear regression has been done on the base, head switch, and cluster switch points, the slope values should be approximately equal, and should also match the slope value extracted from the filtered graph. By comparing the values of these parameters, we can obtain some assurance of the accuracy of the parameters extracted by the algorithm.

6.5.4. Combining the optimizations: A better algorithm

This section combines the alternative filter and clustering options described above to create a better extraction algorithm. The new algorithm uses two passes of a size 3 median filter and the hybrid clustering algorithm described in section 6.5.2 with $p=90\%$. Figure 6-8 shows the error rates of the resulting algorithm. If we compare these results to those of the original extraction algorithm (in Figure 6-5), we see that the relative error rates of the optimized algorithm are considerably lower. Except for the *MinimumMediaTime* values of the Barracuda and Micropolis disk, and the *CylinderSwitchTime* value of the Micropolis disk, the relative errors of all other parameters are less than 10%. In fact, the relative error of most parameters is under 5%.

6.6. Discussion

Sections 6.4 and 6.5 show that an automated algorithm can successfully exact the critical parameters embedded in the benchmark's graphical result. In most cases, the automatically extracted parameter values were within 5% of their manually extracted counterparts. The

median filter approach is particularly useful in filtering the data, since it removes spikes without distorting the surrounding data. Although the values removed by these filters were not actual noise, they should be equally effective if the spikes were caused by noisy data points. Section 6.5.1 showed that, in most cases, using multiple passes of a small filter improved the extraction accuracy for the more noisy cases without adversely affecting the other cases.

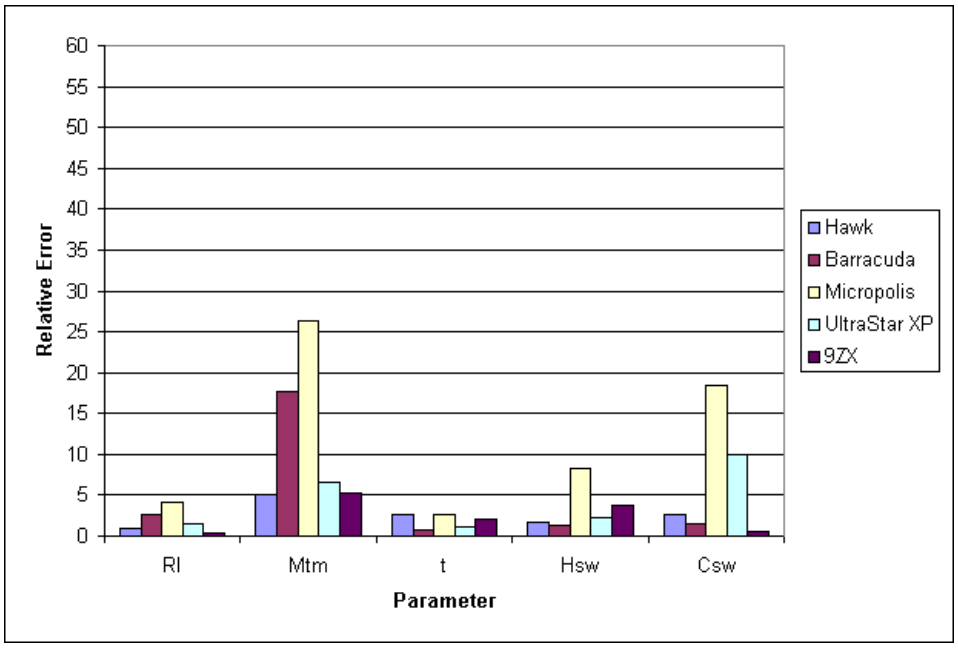

Figure 6-8. Relative Errors of Optimized Algorithm

The optimized algorithm used two passes of a size 3 filter in phase I and used the hybrid clustering algorithm, As a result, the accuracy of the extracted parameters is noticeably improved.

Although this chapter focused on extracting parameters from write graphs, these techniques are all applicable to the read graphs. The algorithm itself cannot be the same because the shape of the read graphs is different from the write graphs. However, since the read graphs have the same sawtooth form as the write graphs, they can also be broken down

into linearly increasing regions and transition regions. Since the head switch and cylinder switch points are embedded in the linearly increasing segments of the read graphs, the techniques described in section 6.3 and 6.5 should also work well for the read graphs.

6.7. Conclusion

This chapter outlined an algorithm for automatically extracting information embedded in the graphical output of the Skippy benchmark. The algorithm was tested on the write results of the five SCSI disks that were presented in Chapter 5. Several optimizations were explored; combining the optimizations led to a new version of the extraction algorithm whose results were in most cases within 5% of manual extraction.

7 Extensions

7.1. Introduction

The last two chapters presented the basic Skippy benchmark and a sample extraction tool. The technique used single sector accesses, started with a step of 0, and increased the step distance by one with each stride. This chapter describes extensions to this basic method. The extensions take two forms. First, two algorithms are presented that, combined with Skippy, extract a *global* picture of a disk drive by gathering information about recording zones and seek behavior. The second part of the chapter describes how the Skippy technique can be extended by changing the step size interval and the transfer size. This section also briefly introduces a backward stride technique that preserves the advantages of the read Skippy technique while removing some disadvantages.

The chapter is organized as follows. Section 7.2 describes the two algorithms for collecting zone and seek information and presents data for the disks described in Chapter 5. Section 7.3 describes how the basic technique can be extended with variable step size increments and transfer sizes. Section 7.4 discusses related issues and Section 7.5 concludes with a summary.

7.2. Extracting Global Disk Characteristics

The Skippy benchmark is *local* in nature; it provides a detailed picture of drive behavior in a small area. Two global pieces that are missing are the drive's recording zone characteristics and its seek behavior. The recording zone characteristics describe how the Sectors/Track ratio varies across different areas of the disk, and the seek behavior describes the latencies associated with moving the disk arm.

7.2.1. Recording Zones

We begin with *Zoned*, a micro-benchmark designed to extract a bandwidth profile across the different recording zones of the disk. The basic algorithm is depicted in Figure 7-1 and is quite straight-forward. The algorithm reads each sector of the disk, in fixed size units. The resulting graph of bandwidth vs. sector address shows the drive's recording zones. Note: it is possible to extract much the same information by sampling the bandwidth at various points in the disk drive. However, as the measurement results show, some disks are very finely zoned: a full sweep is necessary to capture all the recording zones.

Figure 7-2 shows the algorithm's result on the UltraStar XP disk drive. From the manufacturer specification, we learn that the disk has eight recording zones, with the Sectors/Track ratio ranging from 184 at the outermost zone to 120 at the innermost zone. The graph clearly shows the recording zones. Chapter 5 demonstrated how Skippy can extract Sectors/Track in the local area where it is run. By running Skippy in each zone defined by Figure 7-2, it is possible to extract Sectors/Track at each zone in the drive. Using this tech-

```
fd = open("raw disk device");
while (read(fd, buffer, LARGE_SIZE) == LARGE_SIZE) {
      transfer += LARGE_SIZE;    if (transfer >= REPORT_SIZE) {
      // output location and bandwidth achieved over region
      transfer = 0;
      }}
close(fd);
```

Figure 7-1. Pseudocode for Zoned Benchmark

The benchmark simply reads the disk sequentially, in blocks of size LARGE_SIZE. When a threshold amount has been read (REPORT_SIZE), the benchmark outputs the location as well as the bandwidth achieved over the region.

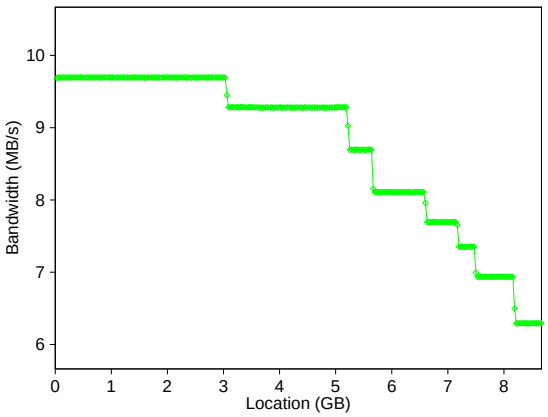

Figure 7-2. Zoned Result on IBM UltraStar XP

The figure shows the Zoned results for the IBM UltraStar XP disk drive. The graph clearly shows the eight recording zones on the drive.

nique, we learn that the first and largest zone has on average 187.36 sectors per track. The Sectors/Track values for all subsequent zones are 179.85, 167.66, 155.82, 147.76, 142.10, 134.14, and 120.39, respectively. All values match the specifications in [UltraStar96] to within 2%.

One also can observe the large difference in delivered bandwidth across the zones of the drive. In the outermost zone, bandwidth is roughly 9.68 MB/s, whereas the inner tracks deliver 6.29 MB/s, roughly a 54% increase from inner to outer tracks.

Figures 7-3(a) to 7-3(d) show the zoned results for the remaining SCSI disk drives. We can make two general observations from these results. First, the Seagate drives are noticeably more finely zoned than the IBM and Micropolis drives. Second, the overall difference between outer-track and inner-track bandwidth ranges from 50% up to 80%. An anomaly occurs with the Micropolis drive. The transfer rate at the outermost zones is lower than the transfer rate in the next innermost zone. This anomaly is one of many oddities seen on the Micropolis drive.

The most recent, comprehensive, discussion of disk drive zoning behavior was in [VanMeter97], which observed that the relationship between transfer rate and disk position was far better described with a linear function than a single value. After examining the zone results, we see that the curve is actually closer to parabolic than linear. The quadratic shape occurs partly because the outermost zone is often longer than the other zones. This feature is particularly obvious in the IBM drives and occurs because an internal data rate limit is reached and the drives cannot support a higher sectors per track ratio [Palmer99].

A quadratic function, of the form $ax^2 + b$ is a much better fit for the zone graph than the linear function. In fact, by fitting both linear and quadratic functions to the data (using standard linear regression techniques), we learned that the quadratic function has between a factor of 2 to a factor of 10 better error than the simple linear fit. The linear fit explored in [VanMeter97] had an extra advantage in that it only required the highest and lowest band-

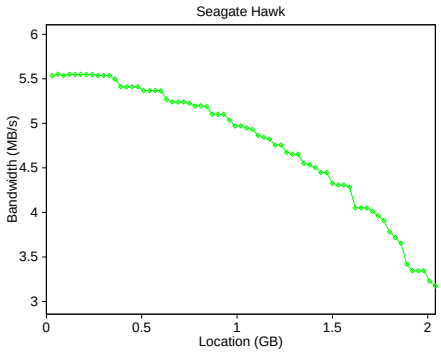

Figure 7-3(a)

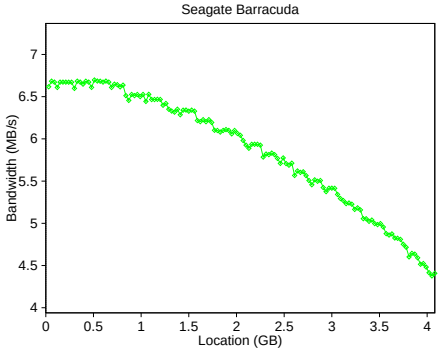

Figure 7-3(b)

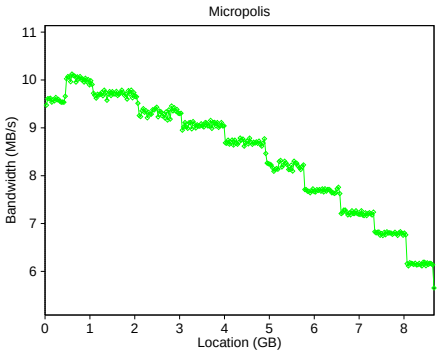

Figure 7-3(c)

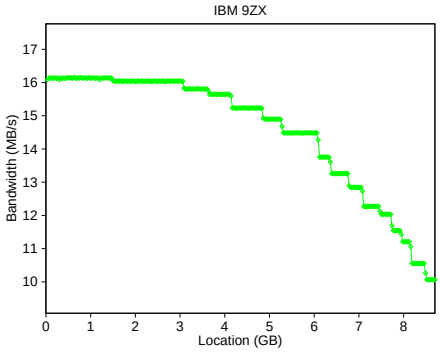

Figure 7-3(d)

Figure 7-3. Zoned Results for SCSI Disk Drives

The figures, numbered in row-major order, show the Zoned results for the remaining four SCSI disk drives. The drives are ordered in increasing RPM, starting with the 5400 RPM Hawk and ending with the 10000 RPM IBM 9ZX.

width values from the drive. However, we found that a quadratic fit using only these two values was still better (by a factor of 10 to 20!) than a linear fit using the same two values. Table 7-1 shows the SSE (Sum of Squared Errors) for each a linear fit using all points, a linear fit using only the first and last point, a quadratic fit using all points, and a quadratic fit using only the first and last point. As the table shows, in all cases but one, the quadratic fit with two values was better than a linear fit using all values, by a factor of 2 to 10. Figure

7-4 shows the four approximations to the recording zone graph of the IBM UltraStar XP drive.

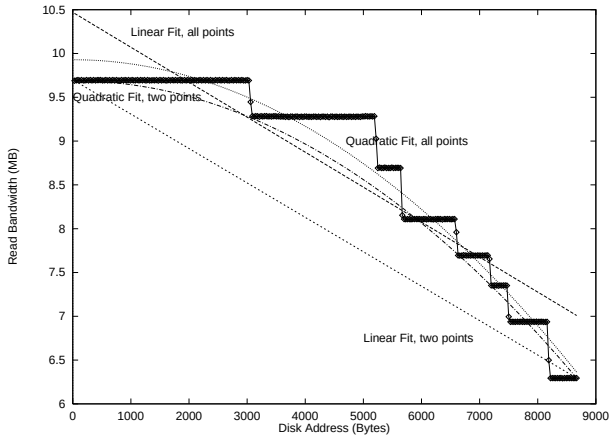

Figure 7-4. Linear and Quadratic Curve Fits for UltraStar XP Zoned Result

This figure shows the linear and quadratic approximations for the UltraStar XP recording zone graph. The quadratic fits are closer to the graph shape than the linear fit. In particular, even the quadratic fit using two points is better than the linear fit with all points

Thus, if a model must be employed, we recommend usage of a quadratic fit. It is as simple to construct as the linear model (requiring only two data points) and matches the profiles better than the linear fit. For disks with only a few zones, the exact step function should be utilized; at least one modern disk drive simulator [Ganger98] makes use of such an exact characterization. In fact, the quadratic fit showed the best results over the linear fit in the more finely zoned disks, where the zones are virtually impossible to identify. For the other disks, it is possible to generate a step function that is an exact match.

Drive	SSE (Linear Fit using all data points)	SSE(Linear Fit using only two data points)	SSE(Quadratic Fit using all data points)	SSE(Quadratic Fit using two data points)
Hawk	2.49	14.19	0.19	0.31
Barracuda	2.79	19.25	0.38	0.49
UltraStar XP	53.03	212.14	12.54	22.87
Micropolis	23.95	248.33	7.79	25.97
9ZX	156.88	795.05	30.72	99.67

Table 7-1. SSE for Linear and Quadratic Fits to Zoned Results

The table shows the Sum of Squared Errors for the linear and quadratic fits to the Zoned results. The quadratic fit has less error, by between a factor of 2 to 10, than the linear fit in all cases. For all results but the Micropolis result, the quadratic fit using only two points is still better, by factors of 2 to 10, than a linear fit using all data points.

7.2.2. Seek Profile

The second global disk characteristic missing is the seek profile. Fortunately, seek delays are based solely on the mechanical movements of the disk arm, and have been thoroughly explored in several prior studies [Worthington95, Ruemmler91]. We limit our discussion of seeks, therefore, to the following. First, we present a variant of Skippy that can be used to make seek experiments easier by factoring out the rotational latency component of the measured time. Second, we present seek curves as a function of sector distance, not cylinder distance.

Since Skippy is a local benchmark, it cannot be directly used to measure seek distances. If the stride size is large, the benchmark will overrun the drive boundary before enough steps are taken. Also, since the Sectors/Track ratio varies across different areas of the disk, the striding technique is not useful when the strides cross a large portion of the disk surface. However, we can utilize the technique to remove the rotational latency component of a seek measurement.

Figure 7-5(a) describes an algorithm for measuring seek times. Between each of the measurements, the algorithm writes to a fixed location at the beginning of the disk. This variant allows the same disk space to be reused, and creates a similar (although not identical) sawtooth wave whose minimum value can be used to estimate the seek time if the rotational latency is zero. By determining this minimum time for different seek distances, a seek profile can be created.

The algorithm depicted in Figure 7-5 (a) uses write accesses. The second write in each iteration can be replaced by a read, but the first write cannot. The reason is that the first write is always to the same disk location. If it were replaced by a read, the read may be cached, and the disk arm would not be moved to the starting location. Therefore, this algorithm relies upon the drive not doing write caching.

A more robust algorithm, the *Seeker* algorithm, is described in Figure 7-5(b). In this case, the disk accesses at each area of the disk are done with linear strides. This algorithm, in a sense, is an interleave of two Skippy runs on different areas of the drive. This technique is more robust since it works with reads as well as writes.

Figure 7-6 shows seek latency versus distance from sector 0 for the Seagate Barracuda. The shape of the curve is slightly different from most seek curves seen in papers and textbooks, since it is seek time versus *sectors* and not versus cylinders. Also note that the *Minimal Time to Media (Mtm)* is included in the values reported; the true seek values can be obtained by subtracting the *Minimum Time to Media* value derived by the Skippy benchmark.

```
fd = open("raw disk device");
for (base = 0; base < DISK_SIZE; base += LARGE_SIZE} {
     for (i = 0; i < measurements; i++) {
          lseek(fd, 0, SEEK_SET);
          write(fd, SINGLE_SECTOR);
          // time following sequence, output <location, time>
          lseek(fd, base + (i * SINGLE_SECTOR), SEEK_SET);
          write (fd, buffer, SINGLE_SECTOR);
     }
}
close(fd);
```

Figure 7-5(a)

```
fd = open("raw disk device");
for (base = 0; base < DISK_SIZE; base += LARGE_SIZE} {
     for (i = 0; i < measurements; i++) {
          lseek(fd, i*SINGLE_SECTOR, SEEK_SET);
          read(fd, SINGLE_SECTOR);
          // time following sequence, output <location, time>
          lseek(fd, base + (i * SINGLE_SECTOR), SEEK_SET);
          read (fd, buffer, SINGLE_SECTOR);
     }
}
close(fd);
```

Figure 7-5(b)

Figure 7-5. Seek Measurement Algorithms

In the first algorithm (Figure 7-5(a)), the benchmark jumps between the beginning of the disk and the target locale, writing a single sector each time. The time for the second write is timed. This is performed repeatedly for many parts of the disk, as shown by the outer loop. The SEEK_SET argument moves the file pointer to the absolute (not relative) location specified by the call. This algorithm has the disadvantage that it relies on write accesses.

The second algorithm (Figure 7-5(b)) is the algorithm used in the seek results presented in the rest of the chapter. This algorithm differs from the above in that the drive is accessed in linearly increasing strides in each local area and in that it uses reads. This algorithm is an interleave of two runs of Skippy, one run in each area of the disk drive. It is more robust than the previous algorithm since it works with both read and write accesses.

Figures 7-7(a) through 7-7(d) show the Seeker results for the remaining 4 SCSI disk drives. For seeks over one tenth of the disk, the seek latency appears to increase linearly with sector distance (much like the seek latency increases with larger numbers of cylinders).

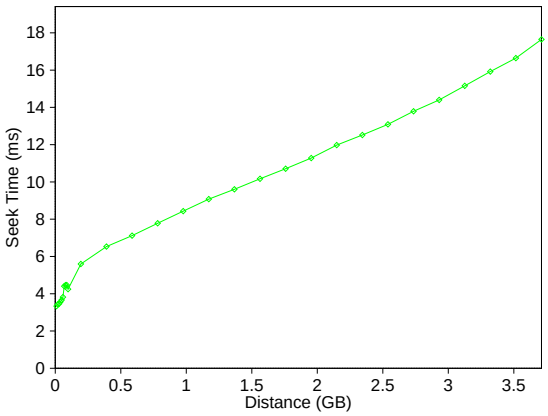

Figure 7-6. Seeker Result for Seagate Barracuda Drive

Close examination of the data reveals that, for seeks reaching the innermost zones, the latency increase is higher than linear. This increase is most observable in the IBM 9ZX seek result. The seek time increases more rapidly because the Sectors/Track ratio decreases more rapidly in this area, requiring more arm movement for the same sector distance.

7.3. Extending the Skippy Technique

This section discusses how the Skippy technique can be extended by varying step size intervals and transfer sizes. By increasing the step size interval, it is possible to extract all the parameters extracted by the original technique in less time, using less disk area. The trade-off, however, is that as the step size increment becomes larger, the result graph loses detail. By increasing the transfer size, it is possible to measure the transfer rate of the drive. Each extension is illustrated using the UltraStar XP disk drive.

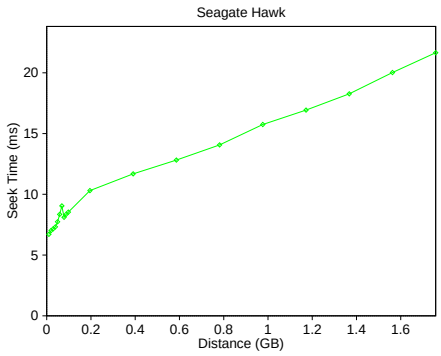

Figure 7-7 (a)

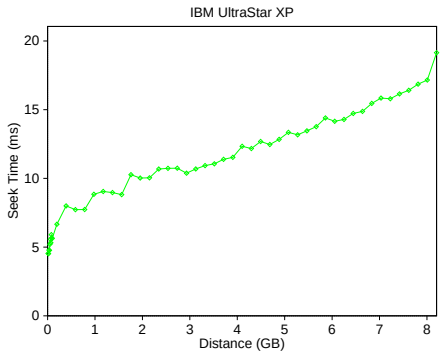

Figure 7-7(b)

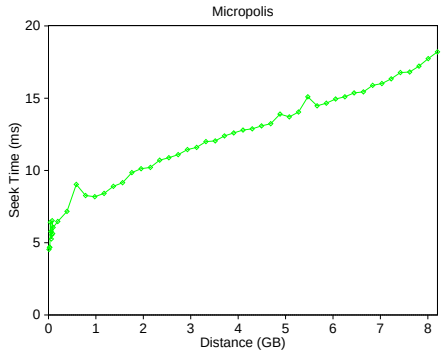

Figure 7-7 (c)

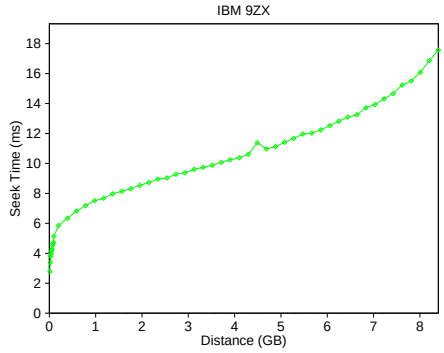

Figure 7-7(d)

Figure 7-7. Seeker Results for SCSI Disk Drives

7.3.1. Variable step size interval: Accuracy vs. Time Trade-off

The first variable is the step size interval. Varying this parameter creates a trade-off between result accuracy and benchmark execution time. There are two advantages to increasing the step size interval. First, we can obtain a result curve with two sawtooth transitions with fewer measurements and in less time. Second, since each step increases the disk surface exposed to the benchmark, increasing the step interval reduces the overall data space touched by the benchmark. The trade-off is that the result graph contains fewer

points, making the extracted values less accurate. Figures 7-8 (a) through (c) show the benchmark's write behavior for the IBM UltraStar XP disk, when the step size interval varies from 1 to 3.

When the step size increment is 2 (Figure 7-8(b)), we see that some of the detail is lost, but the graph retains all the important characteristics of Figure 7-8(a). Although there are fewer points in this graph, there is enough information to extract all the necessary parameters. By applying the automatic extraction technique, we get the following parameter values: the *Minimum Time To Media (Mtm)* is 2.32ms, the *FullRotationTime* is 8.36ms, the Sectors/ Track ratio is 183.24, the head switch time is 8.70ms, and the cylinder switch time is 2.08 ms. Except for the cylinder switch time, all values are within 1% of their counterparts that were extracted with step interval 1. The cylinder switch time value is within 7% of the original; this value is less accurate because there are fewer points to contribute to the cylinder switch time calculation. There are less head and cylinder switches overall, since the benchmark traverses less disk area. For this loss in accuracy, the gain is a reduced execution time. While a single iteration with step size interval 1 took 1.57 seconds, an iteration with step size interval 2 took 0.78 seconds.

If the step size interval is increased to 3, the graph deteriorates further. It is no longer possible to determine the cylinder switch time, since the benchmark does not travel across more than one cylinder during a single sawtooth. Therefore, it does not make sense to increase the step size interval beyond 2.

The main advantage to making the step size interval 2 is that the same parameters can be extracted as in the original benchmark, while touching half the disk area. Since the original

benchmark runs very fast, 1.5 seconds, in practice it may not be necessary to increase the step size increment for faster benchmarking.

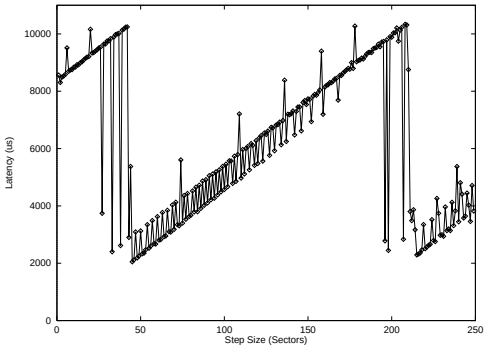

Figure 7-8(a)

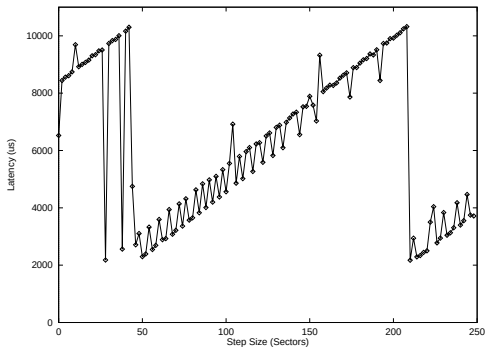

Figure 7-8(b)

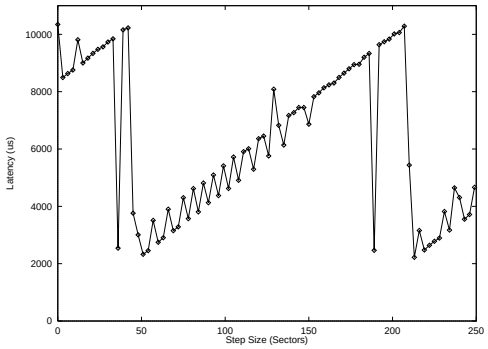

Figure 7-8(c)

Figure 7-8. Effect of Increasing Step Interval Size

Figures 7-8 (a), (b) and (c) (Numbered in clockwise order) shows the results of the write benchmark as the step interval is varied between 1 to 3. As the figures show, the general shape of the result is maintained, but some of the detail is lost with each increment.

7.3.2. Variable transfer size: Transfer Rate Measurement

Next we examine the effects of increasing the transfer size. After trying variable step size increments, the transfer size is the next parameter of the original Skippy algorithm that can be varied. Figure 7-9 shows the benchmark with 512 byte, 64KB and 128KB transfer sizes.

Note that the shape of the curve does not change; as the transfer size increases, the curve moves up. In each case, the low points in the curve show the possible transfer latency when there is no rotational delay. When the request size is 512 Bytes, this latency is primarily the overhead since the transfer time is nearly negligible. When the request size is 128KB, the rotational delay adds only a small increment to the overall latency.

By comparing the three curves in Figure 7-9, we can make several other observations. First, since the regions written are larger, for any given number of steps, the benchmark with the larger request size traverses more disk area than the benchmark with the smaller request size. Second, when the request size is large, it is quite likely for a head or cylinder switch to occur in the middle of a transfer. This effect, particularly, makes it harder to extract information like head switch time from the graph results for larger request sizes.

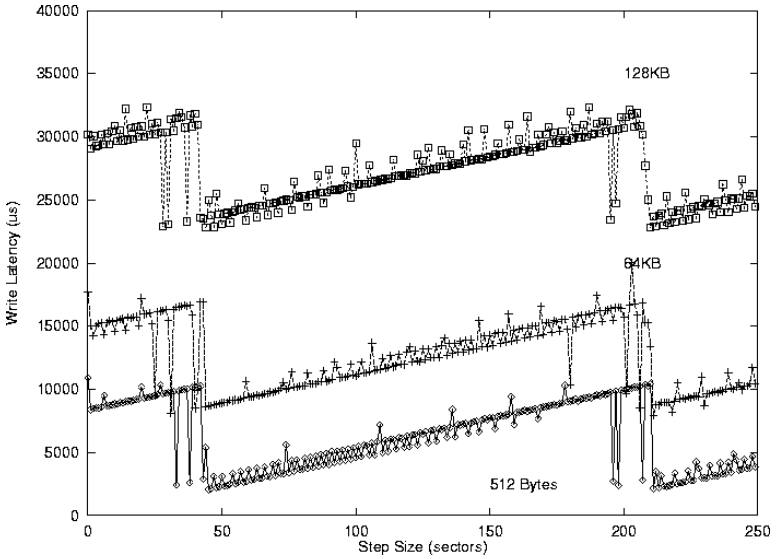

Figure 7-9. Effects of Increasing Transfer Size

The figure shows the results for the write benchmark under different transfer sizes. As the transfer size increases, the curve moves up by an amount representing the additional time needed to transfer the data. Other aspects of the graph remain relatively the same.

These graphs are useful, primarily, for determining bandwidth. The request size divided by the access latency gives the effective write bandwidth. Looking at the 128KB graph, we see that when there is no rotational latency or head switch delay, access latency is approximately 23 ms, and the effective write bandwidth is approximately 5.57MB/s. In practice however, a request will encounter some head switch delay and on average one half a full rotational delay. When these effects are taken into account, the effective write bandwidth becomes approximately 4.56MB/s. This value is close to the measured write bandwidth of the disk, approximately 4.30MB/s.

7.3.3. The Backwards Read Benchmark

The final extension is the *Backwards Read*. Figure 7-10 shows the pseudocode for this extension. Basically, the benchmark implements the Skippy technique in reverse, with read accesses. Overall, the benchmark interacts with the drive mechanism in much the same way that the forward benchmark does. At some point, the natural rotation between requests matches the stride size, and the sawtooth transition occurs. The advantage of the backwards read technique is that it maintains the advantages of read without the distortion of read ahead. The backwards pattern is also less like regular access patterns, making it less susceptible to drive optimizations. Figure 7-11 shows the backwards read result on the IBM UltraStar XP drive. The parameters extracted from this graph are also accurate, in all cases within 4% of manufacturer specification.

```
fd = open("raw disk device");
lseek(fd, TotalArea, SEEK_SET);
CurrentPosition = TotalArea;
for (i = 0; i < measurements; i++) {
      // time following sequence, output <location, time>
      lseek(fd, CurrentPosition - i * SINGLE_SECTOR, SEEK_SET);
      read (fd, buffer, SINGLE_SECTOR);
      CurrentPosition = CurrentPosition - i * SINGLE_SECTOR;
}
close(fd);
```

Figure 7-10. Pseudocode for Backwards Read Benchmark

The algorithm begins by seeking to the end of the region. Each subsequent step seeks backwards, using linearly increasing strides

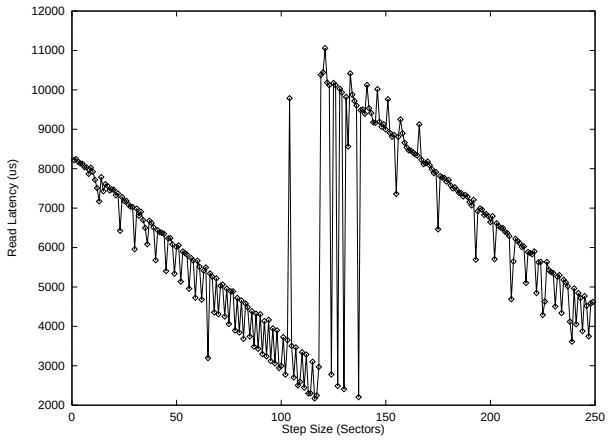

Figure 7-11. Backwards Read Result for IBM UltraStar XP Drive

As the figure shows, the backwards result is also a sawtooth wave. All the characteristics are reversed; head and cylinder switches appear as downward spikes rather than upward spikes.

7.4. Other Issues

7.4.1. Accuracy and Speed

The SKIPPY technique is local in nature; it provides a detailed picture of drive behavior in a small area. As a result, it is extremely fast. One iteration of the benchmark runs in less

than a second on faster drives, such as 10000 RPM or 7200RPM, and in 2 to 3 seconds on slower 5400 RPM drives. The accuracy of the extracted parameters is extremely good with one iteration. Since it is good practice to perform multiple iterations, the data presented here and in the last two chapters used 10 iterations of the benchmark. In practice, however, there is no noticeable difference in accuracy between a measurement with 1 iteration or 10 iterations.

7.4.2. Cache Effects

Modern disks are capable of both read and write caching. In most SCSI disk drives that are used in servers, write caching is disabled. Most IDE disk drives that are used in desktop environments, write caching is enabled. When write caching is enabled, the write version of SKIPPY does not work, since it is impossible to measure the latency of a write to disk media. However, the read forward and read backwards versions do work on such disk drives.

In the read cases, when Skippy uses forward strides, there is no need to flush the cache between strides. Even between iterations, we did not find it necessary to flush the disk buffer cache. By the time enough measurements are done in one iteration, the benchmark has traversed about 20MB of disk area, so the data read during the first few accesses has been flushed out of the cache.

The seek algorithms are far more sensitive to cache effects since they require the same disk area to be repeatedly accessed. The first seek algorithm, presented in Figure 7-5(a) was ineffective for this reason. The Seeker algorithm, presented in Figure 7-5(b), works despite disk caching because it is essentially two runs of the Skippy benchmark. Within each local

area, the caching effects are the same as for a single run of Skippy. The backwards read version can also be used in Seeker, resulting in yet a more robust seek algorithm.

7.5. Summary

This chapter described several extensions of the Skippy technique. The first half of the chapter described Zoned and Seeker, two algorithms that can be used to extract global disk drive characteristics. Zoned extracts the disk's recording zones; the Sectors/Track ratio in each zone can be found by running Skippy within the zone. Seeker measures the seek time between two disk locations, using the linear stride technique to factor out the rotational latency component. Automatic extraction would be useful for the Zoned result, to create a table listing the starting and ending positions of each zone. The median filter technique is also useful in this instance, for removing n oise. After the graph is filtered, it may be possible to isolate step transitions by determining gradient values within a small sliding window. We leave such an endeavor to future work.

The second half of the chapter described how Skippy can be used with different step size increments and different transfer sizes. The advantage of increasing the step size increment is that the same parameters can be extracted using less measurements, covering less disk area, in less time. Experimentation showed that step increments of 2 are practical; the automated extraction algorithm can still extract the required parameters. Some accuracy is lost, however, since there are fewer data points available. When the step size increment is raised to 3, the resulting graph does not have enough information to extract all the required

parameters, although some values can still be extracted. When the transfer size is increased, the result curve moves up. The base of the curve can be used to calculate the drive's transfer rate. The chapter also presented the Backwards Read technique that preserves the advantages of reads and eliminates interaction with read ahead.

8 Conclusion

8.1. Summary

This dissertation characterized two factors that contribute to storage system variability, error behavior and disk drive heterogeneity. The study led to the following two main research contributions.

8.1.1. Characterizing Soft Error Behavior

The thesis described a large storage system prototype. This prototype was ideal for the study of soft error behavior for several reasons. First, it contained a large number of data disk drives and supporting infrastructure such as SCSI and network hardware. Second, all components used were commodity hardware. Third, the operating system had open source, making it possible to trace the cause of error messages, and hence better understand the nature of the system's error behavior.

System logs and maintenance data from the prototype were used to characterize soft error behavior. The analysis revealed some interesting insights. The data disks drives were among the most reliable components in the system. Even though they were the most

numerous component, they experienced the lowest failure rate. Also, the study found that all the errors observed in six months can divided into eleven categories, comprising disk errors, network errors and SCSI errors. The same errors occurred repeatedly, supporting the observation, made in a prior study [Tsao83], that errors seen in a short time period are representative of the types of errors seen over a system's lifetime.

The log data was also used to study failure cases. The data supports the notion that disk and SCSI failures are predictable, and suggests that partially failed SCSI devices can severely degrade performance. A failure prediction algorithm, the Dispersion Frame Technique [Lin90], was evaluated. The evaluation suggested that this technique, and others that predict failures by detecting increasing intensity of error messages, are more useful in detecting cases where human intervention is needed than cases where replacement is needed. The types of messages generated can sometimes be used to separate absolute failures from transient errors.

8.1.2. Disk Drive Heterogeneity

In the area of addressing disk drive heterogeneity, the primary contribution of this dissertation is the development of the linear stride technique for extracting important parameters from disk drives. The Skippy benchmark utilizes this technique to extract parameters from SCSI and IDE drives. The linear stride technique is an excellent match to the rotational nature of a disk drive, a feature that most disk benchmarks try to defeat, rather than take advantage of. As a result, the technique is portable across drive interfaces, working on both

SCSI and IDE drives, requires no prior knowledge of the drive's internals, and delivers extremely accurate results with a few seconds.

The thesis also describes an automated technique for extracting parameter values from the graphical benchmark result. These techniques make it possible to use the linear stride technique, not merely as a stand-alone benchmark, but also has part of a larger adaptive storage system. In such a system, the parameters of a new disk drive can be determined automatically and used in disk specific optimizations or load balancing algorithms.

8.2. Future Directions

The results presented suggest future directions in both of the explored areas. The possible future directions fall into two categories: ways to refine the characterization techniques, and ways to make use of them in adaptive storage systems.

8.2.1. Understanding Error Behavior

In this dissertation, the analysis of soft error behavior was done by compiling statistics on each type of observed error, understanding its cause by tracing the path of the error through the operating system code, and by isolating failure cases and studying them in depth. Although these techniques revealed many useful insights, there are several areas that deserve further exploration:

(i) The logs provided empirical evidence that disk failures affect the performance of neighboring disk drives. It would be useful to quantify the extent to which performance of neighboring drives deteriorates. This data will help determine how to trade-off maintenance time for system performance.

(ii) The logs showed evidence of correlations between events. For instance, network errors were heavily correlated. It may be possible to apply data mining techniques to the system log data to automatic detect interesting correlations.

(iii) The study of failure cases suggested that failure prediction algorithms are useful for detecting cases where human intervention is required. The type of message can indicate whether the failure is absolute or transient. A useful task for future work will be to determine how these two techniques can be combined in a failure detection and diagnostic system.

8.2.2. Understanding Disk Drive Heterogeneity

This dissertation showed how linearly increasing strides can be used for extracting disk drive parameters via operating system level measurements. This technique can be explored further in the following ways:

(i) Chapter 7 presented initial work on the Backwards Read benchmark. This variant is interesting because it retains the advantages of a read experiment without interference from the drive's read ahead mechanism. Further exploration of this variant would be useful.

(ii) Extending the linear stride technique to arrays of disk drives. Extracting critical parameters from disks in a striped array is also a useful exercise. A direction for future work would be to see how these techniques could be extended to work over striped arrays, to extract information about each disk in the array.

(iii) Finally, the ultimate goal would be to incorporate such a technique into an adaptive storage system. This would require developing algorithms that can take advantage of the underlying disk parameters to improve performance. Several such algorithms exist [Horst99] [Worthington94]. Making use of them in an adaptive storage system is an interesting direction for future research.

8.3. Conclusion

This thesis presented evidence variability in storage systems. The data showed that large storage systems can display considerably variability, either from degraded behavior or from device heterogeneity. An essential part of an adaptive storage solution will be to understand and react correctly to such variability. The contributions of this dissertation should assist such a task.

Bibliography

[Asami98] Asami, S. “GridPix: A Method for Presenting Large Image Files Over the Internet”. http://now.cs.berkeley.edu/Td/Papers/.

[Asami99] Asami, S. Talagala, N. Patterson, D. “Design of a Self Maintaining Storage System”. In *Proceedings of the 1999 IEEE Symposium on Mass Storage Systems*. pages 222-234. March 1999.

[Burkhard93] Burkhard, W. Menon, J. “Disk Array Storage System Reliability.” In *Proceedings of the 23rd International Symposium on Fault Tolerant Computing*, June 1993.

[BSD96] McKusik, M.K. *The Design and Implementation of the 4.4BSD Operating System*. Addison-Wesley, 1996.

[Davies88] Davies, E.R. “On the Noise Suppression and Image Enhancement Characteristics of the Median, Truncated Median, and Mode Filters.” In *Pattern Recognition Letters*. Vol 7. Pages 87-97, 1988.

[FreeBSD97] FreeBSD Library Functions Manual, Version 2.2

[Ganger98] Ganger, G. Worthington, B. Patt, Y. “The DiskSim Simulation Environment Version 1.0 Reference Manual”. Technical Report CSE-TR-358-98. Department of Electrical Engineering and Computer Science, University of Michigan, February 1998.

[Gibson92] Gibson, G. *Redundant Disk Arrays: Reliable, Parallel, Secondary Storage*. The MIT Press, Cambridge Massachusetts, 1992.

[Gray90] Gray, J. “A Census of Tandem System Availability Between 1985 and 1990.” In *IEEE Transactions on Reliability*. Vol 39. No 4. October 1990.

[Grochowski96] Grochowski, E. Hoyt, R. “Trends in Modern Disk Drives”. *IEEE Transactions on Magnetics*. vol.32, (no.3, pt.2) pages 1850-1854, May 1996.

[Horst99] Horst, B. MacDonald, J. Alessi, B. “Beyond RAID: An Architecture for Improving PC Fault Tolerance and Performance.” In *Digest of Fast Abstracts, Proceedings of the 29th International Symposium on Fault Tolerant Computing*.

[IBM99] IBM Disk Drive Specifications, available at http:// www.storage.ibm.com/.

[IDEMA97] Frank, B. “Rigid Disk Drive Price Trends.” *IDEMA Insight*. August 1997.

[Kodak97] Flashpix White Paper. Kodak Corporation. http://www.kodak.com/ country/US/en/digital/flashPix/.

[Lin90] Lin, T-T., Siewiorek, D. “Error Log Analysis: Statistical Modeling and Heuristic Trend Analysis.” In *IEEE Transactions on Reliability.* Vol 39. No 4. October 1990.

[Manley97] Manley, S., Seltzer, M. “Web Facts and Fantasy” In *Proceedings of the 1997 USENIX Symposium on Internet Technologies and Systems,* December 1997.

[McVoy96] McVoy, L. Staelin, C. “lmbench: Portable Tools for Performance Analysis.” In *Proceedings of the 1996 Winter USENIX Symposium.* January 1996.

[Merry98] Merry, K. FreeBSD SCSI Group. *Personal Communication*.

[Ng94] Ng, S. Crosshatch Disk Array for Improved Reliability and Performance. In *Proceedings of the 21st International Symposium on Computer Architecture.* Pages 225-264. April 1994.

{Palmer99] Palmer, J. IBM Almaden Research. *Personal Communication.*

[PFA99] Predictive Failure Analysis. IBM Corporation. http:// www.storage.ibm.com/storage/oem/tech/pfa.html.

[Pitas90] Pitas, I, Venetsanopoulos, A.N. *Nonlinear Digital Filters: Principles and Applications.* Kluwer academic publishers 1990.

[Quantum99] Quantum Disk Drive Specifications, available at http:// www.quantum.com/.

[Ruemmler91] Ruemmler, C., Wilkes, J. An Introduction to Disk Drive Modeling. In *IEEE Computer*. March 1991.

[Russ95] Russ, J.C. *The Image Processing Handbook, 2nd Edition.* CRC Press 1995.

[Saavedra92] Saavedra-Barrera, R. *CPU Performance Evaluation Using Narrow Spectrum Benchmarking.* Ph.D Thesis, U.C. Berkeley, February 1992.

[Saavedra94] Saavedra, R. Gaines, S. Carlton, M. “Characterizing the Performance Space of Shared Memory Machines Using Micro-Benchmarks”, *In Hot Interconnects 1994.* August 1994.

[SCSI2] The SCSI-2 Interface Specification.

[Schwarderer96] Schwarderer, D., Wilson, D. *Understanding I/O Subsystems*. Adaptec Press, January 1996.

[Schulze88] Schulze, M.E. “Considerations in the Design of a RAID Prototype.” Technical Report UCB/CSD 88/448. Computer Science Division, University of California at Berkeley, 1988.

[Seagate99] Seagate Disk Drive Specifications, available at http:// www.seagate.com.

[Sigma97] “SA-H381 Environmental Sensing Communications Specification.” Trimm Technologies, 1997.

[SMART99] “Self Monitoring, Analysis and Reporting Technology, Frequently Asked Questions.” Seagate Technology. http://www.seagate.com/ support/disc/faq/smart.shtml

[Smith98] Smith, M. FreeBSD SCSI Group. *Personal Communication*.

[Talagala96] Talagala, N. Asami, S., Patterson, D. "A Comparison of PC Operating Systems for Storage Support." Technical Report UCB// CSD-98-1018. Computer Science Division, University of California at Berkeley.

[Talagala99] Talagala, N. Asami, S., Patterson, D. "Usage Patterns of a Web Based Image Collection", In *Proceedings of the 1999 IEEE Symposium on Mass Storage Systems*. March 1999.

[Tsao83] Tsao, M. “Trend Analysis and Fault Prediction.” PhD. Dissertation, Technical Report CMU-CS 83/130, Computer Science Division, Carnegie Mellon University, 1983.

[UltraStar96] “Ultrastar 2XP Hardware/Functional Specification: 4.55 GB and 8.22 GB Models, 7200 RPM, Version 5.03.” Document Number AS05-0087-45. IBM Storage Products Division. June 1996.

[VanMeter97] VanMeter, R. “Observing the effects of Multizone Disks.” In *Proceedings of the 1997 USENIX Conference*, January 1997.

[Worthington94] Worthington, B.L., Ganger, G, Patt, Y. “Scheduling Algorithms For Modern Disk Drives.” In *1994 International Conference on the Measurement and Modeling of Computer Systems.* Pages 241-151. May 1994.

[Worthington95] Worthington, B.L., Ganger, G.R., Patt, Y.N., Wilkes, J. “On-line Extraction of SCSI Disk Drive Parameters.” In *1995 Joint International Conference on Measurement and Modeling of Computer Systems*.

[Yoshikawa97] Yoshikawa, C. Chun, B. Eastham, P. Vahdat, A. Anderson, T. Culler, D. “Using Smart Clients to Build Scalable Services”. In *Proceedings of the 1997 USENIX symposium.*

Appendix A: Skippy Code

The code for the Skippy benchmark is listed below. If writes are used, the benchmark first reads in all the data that will be touched on disk. This data is in turn written back during the measurement phase. As such, the data on disk is not modified.

```
void main(int argc, char * argv[])
{
int bufferSize = 512;                          /* Buffersize in Bytes  */
int totalIterations = 1;          /* Number of iterations */
int readWrite=0;            /* Writes                */
int numSteps=250;           /* Stride size up to 250*/
int sectorSize=512;
int stepInterval=1;          /* Stride Size Increment*/

struct timeval startTime, endTime;
struct timezone timeZone;

char  *buffer, *originalData;
int fd;
double *sumLatency, *sumLatencySquares;
char *deviceName;

double accessLatency;
int stepSize;
int iteration;
int stepNumber;
int i;

      buffer = (char *) malloc(bufferSize*sizeof(char));
      if (Writes == 1) {
        /* Create structure to hold the read info */
        originalData = (char *)
            malloc(numSteps*bufferSize*sizeof(char));
      }
      sumLatencySquares = (double *)malloc(numSteps*sizeof(double));
      sumLatency = (double *) malloc(numSteps*sizeof(double));
      bzero(sumLatencySquares, numSteps*sizeof(double));
      bzero(sumLatency, numSteps*sizeof(double));
```

```
    /* open device file */
    if(readWrite == 0)
      fd = open(deviceName, O_RDONLY, 666);
    else
      fd = open(deviceName, O_RDWR, 666);
  fprintf(stderr, "Running benchmark on %s for %d steps and %d it
          erations\n", deviceName, numSteps, totalIterations);
  /* The meat of the benchmark */
  /* If we are doing writes, read the data in first */
  lseek(fd, 0, SEEK_SET);
  if (readWrite == 1) {
    stepSize =0;
    for (stepNumber =0; stepNumber < numSteps; stepNumber++){
      lseek(fd, stepSize*sectorSize, SEEK_CUR);
      if(read(fd, buffer, bufferSize)!= bufferSize) {
      fprintf(stderr,"Error during initial read phase\n");
      exit(3);
      }
      bcopy(buffer, originalData+bufferSize*stepNumber, bufferSize);
      stepSize += stepInterval;
    }}
    /* Now do the benchmark */
  for (iteration=0; iteration <totalIterations; iteration++) {
    lseek(fd,0,SEEK_SET);
    stepSize =0;
    for (stepNumber=0; stepNumber<numSteps; stepNumber++) {
      lseek(fd, stepSize*sectorSize, SEEK_CUR);
      gettimeofday(&startTime, &timeZone);
      if (readWrite == 1) {
      if(write(fd,originalData+bufferSize*stepNumber, bufferSize) !=
                              bufferSize) {
        fprintf(stderr, "%s %d: Write error at step %d. Exiting..\n",
                  argv[0], bufferSize, stepSize);
        exit(2);
      }} else {
      if (read(fd, buffer, bufferSize) != bufferSize) {
        fprintf(stderr, "%s %d: Read error at step %d. Exiting..\n",
                  argv[0],bufferSize, stepSize);
        exit(2);
      }}
      gettimeofday(&endTime, &timeZone);

     accessLatency = (double) (endTime.tv_sec*1000000.0 + endTime.tv_usec
            - startTime.tv_sec*1000000.0 - startTime.tv_usec);
      sumLatency[stepNumber] +=accessLatency;
      sumLatencySquares[stepNumber] += accessLatency*accessLatency;
      stepSize += stepInterval;
    }}

  /* Now report results */
for (stepNumber=1; stepNumber<numSteps; stepNumber++)
    printf("%d\t%lf\n", stepNumber*stepInterval, (double)
            sumLatency[stepNumber]/totalIterations );
```

```
/* Clean up and exit */
close (fd);
exit(0);
}
```